PURDUE UNIVERSITY
GRADUATE SCHOOL
Thesis/Dissertation Acceptance

This is to certify that the thesis/dissertation prepared

By Yifan Ge

Entitled
INVESTIGATING SPATIAL DISTRIBUTION AND DYNAMICS OF MEMBRANE PROTEINS IN POLYMER-TETHERED LIPID BILAYER SYSTEMS USING SINGLE MOLECULE-SENSITIVE IMAGING TECHNIQUES

For the degree of   Doctor of Philosophy

Is approved by the final examining committee:

Christoph A. Naumann
Chair

Eric C. Long

Shelley A. Claridge

Chirstine A. Hrycyna

To the best of my knowledge and as understood by the student in the Thesis/Dissertation Agreement, Publication Delay, and Certification Disclaimer (Graduate School Form 32), this thesis/dissertation adheres to the provisions of Purdue University's "Policy of Integrity in Research" and the use of copyright material.

Approved by Major Professor(s): Christoph A. Naumann

Approved by: Eric C. Long   12/8/2016
            Head of the Departmental Graduate Program   Date

INVESTIGATING SPATIAL DISTRIBUTION AND DYNAMICS OF MEMBRANE

PROTEINS IN POLYMER-TETHERED LIPID BILAYER SYSTEMS USING SINGLE

MOLECULE-SENSITIVE IMAGING TECHNIQUES

A Dissertation

Submitted to the Faculty

of

Purdue University

by

Yifan Ge

In Partial Fulfillment of the

Requirements for the Degree

of

Doctor of Philosophy

December 2016

Purdue University

Indianapolis, Indiana

To my parents.

Mr. Jianhua Ge and Ms. Runsheng Wang

ACKNOWLEDGMENTS

Looking back into these five years, I would have never thought of what a colorful journey I would have during my Ph.D. studies. Tremendous thanks to Prof. Christoph Naumann for being such a wonderful supervisor, who guided me into the field, taught me what I need and what I want to know, gave all the thoughtful suggestions and great support through my Ph.D. studies. I am also really grateful for having an excellent crew of coworkers. Thanks to Dr. Amanda Siegel for teaching me how to do PCH, for all the revealing discussion and wise advice over the last four years, for helping me editing my thesis. Thanks to Dr. Noor Hussain and Dr. Yu-Hung Lin for teaching me the techniques including lipid bilayer fabrication, membrane protein reconstitution, and cell culturing. Dr. Yu-Hung Lin also provided me results, presented as Fig. 4.34.A and Fig. 4.37.A. My research would not work out so smoothly without the help of Mr. Jiayun (Eric) Gao, who has done a lot of model membrane fabrication in my thesis work, and also provided me results presented as Fig. 4.13. I would also like to thank Mr. Kent Shilts for his selfless help in proof-reading my thesis, and all the helpful discussions in the working of cell mechanics. Many thanks to Dr. Dan Minner for all the helpful discussions on my cell-based work. Thanks to Prof. Presse for all the help with mathematic models, I have learned a lot from him. Additionally, I would like to express my gratitude to my committee members, Prof. Eric Long, Prof. Christine Hrycyna and Prof. Shelley Claridge for the helpful discussions.

I would take this chance to thank my family and friends. Thanks to my husband, Mr. Chenyao Tang, for being patient with me and supporting me to get through all the crazy times. Chenyao also helped me to produce the 3D schematic presented in this dissertation as Fig. 4.30. I am grateful to have met and know a group of friends here in Indianapolis. Especially Dr. Jingwen Yan and Dr. Jing Liu, who are like family to me and gave me lots of support and helpful discussion on my work and study. Special thanks to Dr. Jingwen Yan

TABLE OF CONTENTS

LIST OF FIGURES

SYMBOLS

$\delta F(t)$	Fluorescence fluctuation
ε	Photonphysical properties
γ	Ratio of the norminal and effective radius in FRAP analysis
ω	Radius of the volume element
τ	Absolute infinitely short-time interval
τ_D	Diffusion time
A	Assignment matrix
$\hat{A}$	Matrix with minimize the sum of costs
$C(x, y, t)$	Concentration of fluorescent probes
C_i	Prebleach fluorophore concentration
D	Diffusion coefficient
E_{raft}	Raftophilic excess
$G(\tau)$	Fluorescence autocorrelation function
M_f	Mobile fraction
N	Number of fluorescent particles
$PCH(k; N_{avg}, \varepsilon)$	Solutions to the PCH algorithm for k
q	Quantum yield of fluorophores (for FRAP)
r_e	Effective radius of a postbleach profile
X_{dimer}	Dimerization ratio
$X_{migrate}$	Mole fraction migrating

ABBREVIATIONS

3D	Three dimensional
AFP	Atomic force microscopy
AJ	Adherens junction
APD	Avalanche photodiode
CCD	Charge coupled device
CHOL	Cholesterol
Cryo-EM	Cryo-electron miscroscopy
CS-XY	Confocal spectroscopy XY scan
DEPC	1,2-dierucoyl-sn-glycero-3-phosphocholine
DGS-NTA Ni	1,2-dioleoyl-sn-glycero-3-[(N-(5-amino-1-carboxypentyl)iminodiacetic acid) succinyl] (nickel salt)
DIC	Differential interference contrast
$diC_{18}M_{50}$	1,2-dioctateclysn-glycero-2-N-poly (2- methyl-2-oxazoline)50
DiD	1,1-dioctadecyl-3,3,3,3-tetramethylindodicarbocyanine,4-chlorobenzenesulfonate Salt
DMEM	Dulbeccos Modified Eagle Medium
DOPC	1,2-dioleoyl-sn-glycero-3-phosphocholine
DPPC	1,2-dipalmitoyl-sn-glycero-3-phosphocholine
DPPE	1,2-dipalmitoyl-sn-glycero-3-phosphoethanolamine
DPTE	1,2-dihexadecanoyl-sn-glycero-3-phosphothioethanol (sodium salt)
DSPE-PEG2000	1,2-distearoyl-sn-glycero-3-phosphoethanolamine-N-[methoxy (polyethylene glycol) -2000] (ammonium salt)
ECM	Extra cellular matrix
EGFR	epidermal growth factor receptor

EPI	Epifluorescent microscopy
EPR	Electron paramagnetic resonance
FA	Focal adhesion
FCS	Fluorescence correlation spectroscopy
FN	Fibronectin
FRAP	Fluorescence recovery after photo bleaching
FRET	Foster resonance transer
GM_1	Monosialotetrahexosylganglioside
GM_3	Monosialodihexosylganglioside
GPCR	G-protein coupled receptor
GPI-AP	Glycosylphosphatidylinositol-anchored protein
GPI	Glycosylphosphatidylinositol
GPMV	Giant plasma membrane vesicle
GUV	Giant unilamellar lipid vesicles
l_d	Liquid disorder
l_o	Liquid order
LaB	Latrunculin B
LAP	Linear assignment problem
LB	Langmuir-Blodgett
LC	Liquid-condensed phase
LE	Liquid-expanded phase
LS	Langmuir-Schaefer
LUV	Large unilamellar vesicles
MAb	Monoclonal antibody
MHT	Multiple-hypothesis tracking
MLV	Multilamellar lipid vesicles
NA	Numberic aperture
NBD-DHPE	N-(7-nitrobenz-2-oxa-1,3-diazoly-4-yl)1,2-diahexadec-anoyl-sn-glycero-2-phosphoethanolame, triethylammonium salt

NMR	Nuclear magnetic resonance spectroscopy
OG	n-octyl-glucopyranoside
PBS	Phosphate buffer saline
PCH	Photon counting histogram
PEG2000-maleimide	1,2-distearoyl-sn-glycero-3-phosphoethanolamine-N-[maleimide(polyethylene-glycol) 2000]
PMT	Photonmultiplier
POPC	1-palmitoyl-2-oleoyl-sn-glycero-3-phosphocholine
PSF	Point spread function
R6G	Rodamine-6-G
ROI	Area region of interest
SLB	Solid-supported lipid bilayers
SPT	Single particle tracking
SUV	Small unilamellar vesicles
T_m	Transition temperature
TR-DHPE	Texas Red-1,2-dihexadecanoyl-sn-glycero-3-phosphoethanolamine
TRITC-DHPE	N-(6-tetramethyl-rhodamine-thiocarbamoyl)-1,2-dihexadecanoyl-sn-glycero-3-phosphoethanolamine
uPAR	Urokinase plasminogen activator receptor
VN	Vitronectin
ZDC	Z drift compensation module

ABSTRACT

Ge, Yifan. Ph.D., Purdue University, December 2016. Investigating Spatial Distribution and Dynamics of Membrane Proteins in Polymer-Tethered Lipid Bilayer Systems using Single Molecule-Sensitive Imaging Techniques. Major Professor: Christoph A. Naumann.

Plasma membranes are complex supramolecular assemblies comprised of lipids and membrane proteins. Both types of membrane constituents are organized in highly dynamic patches with profound impact on membrane functionality, illustrating the functional importance of plasma membrane fluidity. Exemplary, dynamic processes of membrane protein oligomerization and distribution are of physiological and pathological importance. However, due to the complexity of the plasma membrane, the underlying regulatory mechanisms of membrane protein organization and distribution remain elusive. To address this shortcoming, in this thesis work, different mechanisms of dynamic membrane protein assembly and distribution are examined in a polymer-tethered lipid bilayer system using complementary confocal optical detection techniques, including 2D confocal imaging and single molecule-sensitive confocal fluorescence intensity analysis methods [fluorescence correlation spectroscopy (FCS) autocorrelation analysis and photon counting histogram (PCH) method]. Specifically, this complementary methodology was applied to investigate mechanisms of membrane protein assembly and distribution, which are of significance in the areas of membrane biophysics and cellular mechanics.

From the membrane biophysics perspective, the role of lipid heterogeneities in the distribution and function of membrane proteins in the plasma membrane has been a long-standing problem. One of the most well-known membrane heterogeneities are known as lipid rafts, which are domains enriched in sphingolipids and cholesterol (CHOL). A hallmark of lipid rafts is that they are important regulators of membrane protein distribution and function in the plasma membrane. Unfortunately, progress in deciphering the mech-

anisms of raft-mediated regulation of membrane protein distribution has been sluggish, largely due to the small size and transient nature of raft domains in cellular membranes. To overcome this challenge, the current thesis explored the distribution and oligomerization of membrane proteins in raft-mimicking lipid mixtures, which form stable coexisting CHOL-enriched and CHOL-deficient lipid domains of micron-size, which can easily be visualized using optical microscopy techniques. In particular, model membrane experiments were designed, which provided insight into the role of membrane CHOL level versus binding of native ligands on the oligomerization state and distribution of GPI-anchored urokinase plasminogen activator receptor (uPAR) and the transmembrane protein $\alpha_v\beta_3$ integrin. Experiments on uPAR showed that receptor oligomerization and raft sequestration are predominantly influenced by the binding of natural ligands, but are largely independent of CHOL level changes. In contrast, through a presumably different mechanism, the sequestration of $\alpha_v\beta_3$ integrin in raft-mimicking lipid mixtures is dependent on both ligand binding and CHOL content changes without altering protein oligomerization state. In addition, the significance of membrane-embedded ligands as regulators of integrin sequestration in raft-mimicking lipid mixtures was explored. One set of experiments showed that ganglioside GM_3 induces dimerization of $\alpha_5\beta_1$ integrins in a CHOL-free lipid bilayer, while addition of CHOL suppresses such a dimerization process. Furthermore, GM_3 was found to recruit $\alpha_5\beta_1$ integrin into CHOL-enriched domains, illustrating the potential significance of GM_3 as a membrane-associated ligand of $\alpha_5\beta_1$ integrin. Similarly, uPAR was observed to form complexes with $\alpha_v\beta_3$ integrin in a CHOL dependent manner, thereby causing the translocation of the complex into CHOL-enriched domains. Moreover, using a newly developed dual color FCS and PCH assay, the composition of uPAR and integrin within complexes was determined for the first time.

From the perspective of cell mechanics, the characterization of the dynamic assembly of membrane proteins during formation of cell adhesions represents an important scientific problem. Cell adhesions play an important role as force transducers of cellular contractile forces. They may be formed between cell and extracellular matrix, through integrin-based focal adhesions, as well as between different cells, through cadherin-based adherens

junctions (AJs). Importantly, both types of cell adhesions act as sensitive force sensors, which change their size and shape in response to external mechanical signals. Traditionally, the correlation between adhesion linker assembly and external mechanical cues was investigated by employing polymeric substrates of adjustable substrate stiffness containing covalently attached linkers. Such systems are well suited to mimic the mechanosensitive assembly of focal adhesions (FAs), but fail to replicate the rich dynamics of cell-cell linkages, such as treadmilling of adherens junctions, during cellular force sensing. To overcome this limitation, the 2D confocal imaging methodology was applied to investigate the dynamic assembly of N-cadherin-chimera on the surface of a polymer-tethered lipid multi-bilayer in the presence of plated cells. Here, the N-cadherin chimera-functionalized polymer-tethered lipid bilayer acts as a cell surface-mimicking cell substrate, which: (i) allows the adjustment of substrate stiffness by changing the degree of bilayer stacking and (ii) enables the free assembly of N-cadherin chimera linkers into clusters underneath migrating cells, thereby forming highly dynamic cell-substrate linkages with remarkable parallels to adherens junctions. By applying the confocal methodology, the dynamic assembly of dye-labeled N-cadherin chimera into clusters was monitored underneath adhered cells. Moreover, the long-range mobility of N-cadherin chimera clusters was analyzed by tracking the cluster positions over time using a MATLAB-based multiple-particle tracking method. Disruption of the cytoskeleton organization of plated cells confirmed the disassembly of N-cadherin chimera clusters, emphasizing the important role of the cytoskeleton of migrating cells during formation of cadherin-based cell-substrate linkages. Size and dynamics of N-cadherin chimera clusters were also analyzed as a function of substrate stiffness.

1. INTRODUCTION

1.1 Rationale and Objective

Plasma membranes are fascinating assemblies that separate cell interior structures from the external environment and contain highly dynamic and complex structures. One hallmark of this dynamic, complex property of the plasma membrane is the lateral mobility of embedded membrane proteins, which is one of the most important regulatory factors for membrane protein functionality. The major goal of this dissertation is to elucidate potential mechanisms of membrane protein dynamics by investigating distribution and oligomerization of membrane proteins. This goal will be achieved through analyzing membrane protein dynamics using the model platform of polymer-tethered lipid bilayers from two aspects with four different objectives. The first section of my dissertation, including the first three objectives, focuses on factors that regulate lipid-protein, protein homo-complexes and protein hetero-complexes processes in model membranes. The second section of my dissertation, associated with the last objective of this thesis work, focuses on analyzing the dynamic assembly of cell-cell adhesion proteins that function as menchanosensors by using a model platform that mimics the cell-cell interface. Together, this research demonstrates the significant role of biophysical processes that can be understood through model membrane systems that incorporate important properties of cell membranes.

The bilayer structure of the cell membrane is comprised of hundreds of different types of lipid molecules [1, 2] that vary in composition depending on the organelle [3] and on pathological [1, 4] and physiological states of the cell [5]. Furthermore, the lateral mixing of these lipid components is highly non-uniform and dynamic [6–8]. Enrichment of lipids is observed in different leaflets of the membrane [2], while transient domain structures form and disappear on a microsecond scale in both leaflets [8]. In addition to the incredible heterogeneity displayed by lipids, typically 50% of the cell membrane is composed of mem-

brane proteins that are encoded by one-third of typical eukaryotic genomes [9]. Combined, the structure of a cell membrane is a highly complex, crowded assembly of fascinating dynamic properties. One hypothesis posits that this heterogeneous structure is required for the proper structure and assembly of membrane proteins, which is critical to cellular activities such as signal transduction and cell migration [10]. In fact, cellular membrane functions are mostly achieved through proper structure and dynamics of membrane proteins, which is essential in both physiological and pathological processes. Currently, about 60% of existing drug targets are aimed at membrane proteins and their assemblies [11]. Therefore, improving our understanding of the link between membrane heterogeneity and membrane protein functionality will be essential to reveal fundamental mechanisms in diseases such as cancer and neurodegenerative diseases and will assist the development of novel therapeutic strategies [12].

The most prominent membrane heterogeneity, known as lipid rafts, plays a significant role in the functionality of plasma membranes. Lipid raft structures are proposed to be nanosized structures enriched with saturated lipids including cholesterol, glycosphingolipids, and sphingomyelin, therefore they are more rigid compared to other areas of the cellular membrane [13–15]. This particular lipid environment appears to recruit certain membrane proteins with relatively confined diffusivity. Such a protein sorting effect, through both physical and chemical mechanisms, enables proteins to form functional centers during several important cell physiology events, including signal transduction [16, 17], cell adhesion, division and migration [18–20]. Such assemblies are also crucial in processes such as pathogen infection [21, 22].

A hallmark of lipid rafts is that they are remarkably dynamic and transient membrane structures [10, 23]. In other words, lipid rafts are constantly assembling and disassembling as a result of complex lipid mixing behavior in the plasma membrane [8], as well as protein-protein, protein-lipid interaction, and cytoskeletal polymerization [10]. Due to this transient and dynamic nature of such membrane heterogeneities, investigating the impact of lipid heterogeneity on membrane protein functionality remains extremely challenging. Previously utilized biochemical methods of raft characterization, such as the cholesterol

(CHOL) depletion assay, was later shown to cause disruption of other lipid components including glycolipids [24]. Therefore, plenty of uncertainties about the role of membrane heterogeneities on membrane protein functionality remain unsolved as a result of the limitations in applicable investigative methods.

According to the raft hypothesis, the raft affinity of membrane proteins can be attributed to several molecular motifs, one of which is glycosylphosphatidylinositol (GPI) anchors [13]. GPI-anchored proteins (GPI-AP) constitute about 0.5% of all cellular proteins [25], and they function as important membrane receptors. Representative GPI-AP includes human CD59 [26] and urokinase plasminogen activator receptor (uPAR) [27, 28]. The overall localization of GPI-AP in the plasma membrane indicates that these proteins are transported and sorted to fulfill their function [25]. These processes are believed to be raft associated [7, 13, 29]. In addition, GPI-APs often fulfill their function through dimerization or oligomerization. This process, is also proposed to be related to the structure of lipid rafts [7, 14, 29, 30]. Nevertheless, the mechanisms of sorting GPI-AP and the regulation of GPI-AP clustering remain obscure. It has been suggested that several factors, including CHOL content and ligand binding can work as potential regulatory factors during these processes [25]. For example, Paladino et.al reported that not only apical sorting but also oligomerization states of GPI-AP interfered during the process of CHOL depletion, suggesting a role for CHOL and lipid rafts in the sorting and oligomerization of GPI-AP [31]. Additionally, Caiolfa et.al reported a ligand dominated mechanism for the regulation of GPI-anchored uPAR oligomerization states in different regions of the cell [32]. Together, these findings suggest a critical functional relationship among GPI-AP oligomerization, CHOL content, and sorting of GPI-AP.

In the case of transmembrane proteins, lipid raft structures, as well as CHOL content in the membrane, work as important regulatory factors for membrane protein functionality. For instance, CHOL in the membrane is important because it regulates integrin-mediated functional complex formation as well as integrin clustering [19, 33]. Furthermore, integrin clustering at cellular focal adhesions (FAs) are found to be dependent on the structure of lipid rafts and CHOL content [19, 34]. In addition to the self-clustering effects, integrin can

also associate with other components embedded in plasma membranes such as ganglio-sides and uPAR to form complexes. Such complexes are of physiological and pathological importance. For example, integrin-uPAR complex formation is one of the key mechanisms during cancer cell migration [35, 36]. Another example is integrin-ganglioside complexa-tion, which is essential for the formation of glycosynaptic domains. These glycosynaptic structures are critical in carbohydrate-mediated cell migration [37] and are especially im-portant for neuron function. Intriguingly, previous research has indicated that both of these integrin-associated complexes are related to the CHOL levels of the cell membrane [38,39]. However, there are still uncertainties about the models and mechanisms of such integrin-mediated complexes. Furthermore, the role of lipid environments during this protein com-plex formation largely remained unclear.

To overcome the challenges of characterizing lipid heterogeneities in cell membranes, model membranes with relatively large lipid phase separations have been widely applied to investigate the influence of membrane heterogeneity on membrane protein sequestration and oligomerization [40–45]. These model membranes, such as solid-supported lipid bi-layers (SLBs) [40, 41], giant unilamellar lipid vesicles (GUVs) [42, 43], and giant plasma membrane vesicles (GPMVs) [44, 45] have provided extensive information on membrane phase transition, lipid dynamics under highly mixed environments [44, 46], and membrane protein diffusion sequestration and oligomerization [41, 45, 47, 48] . These relatively sim-ple lipid mixtures with coexisting liquid-ordered (l_o), liquid-disordered (l_d) lipid domains hold similar phase properties as cellular membranes [8, 44, 45, 49, 50]. Additionally, these lipid mixtures are prepared with a well-defined composition, and therefore allow system-atic characterization of the lipid mixing behavior in varying membrane environments. For instance, Schwille's group has established the difference in such lipid mixtures in response to variation of CHOL content [51], whereas the phase diagram and hydrophobic thickness of different domains in such lipid mixtures were revealed by Keller's group [46, 52, 53]. This information provides valuable insights into lipid mixing behavior in the model mem-brane that allows systematic investigation of membrane protein sequestration according to changes in lipid environment.

Taking advantage of the intriguing opportunity to use model membranes, the primary goal of this dissertation is to explore the role of CHOL, a key compound of lipid rafts, and ligand binding in the assembly and distribution of membrane proteins. In the previous work of our group, polymer-tethered raft-mimicking lipid mixtures were adapted for the investigation of integrin sequestration. Using a combination of confocal based fluorescent quantitative analyses, we not only established the raft-affinity of integrin upon ligand activation without altering the integrin oligomerization, but also illustrated the significance of bilayer asymmetry on integrin sequestration [54, 55]. In this dissertation, this platform was adapted and further developed with the goal of gaining a better understanding of the influence of lipid environment, specifically CHOL content, on membrane protein dimerization, dynamics, distribution, and protein hetero-complex formation. In particular, this goal will be achieved through the following set of objectives:

The first objective was to explore the role of CHOL and ligand binding in the dimerization and sequestration of GPI-anchored urokinase plasminogen activator receptor (uPAR), to provide insight into the mechanism of functional sorting and clustering of GPI-AP.

The second objective was to investigate the influence of CHOL and ligand binding in the distribution of integrin by systematically changing the CHOL level in raft-mimicking lipid mixtures. We investigated integrin sequestration and oligomerization with and without natural ligands.

The third objective was to investigate the role of CHOL in the assembly of complexes between integrin and other membrane embedded ligands. Specifically, two integrin-containing complexes, namely integrin-monosialodihexosylganglioside (GM_3) and integrin-uPAR were investigated. To achieve this objective, a new fluorescent assay was introduced to provide information on the dynamics, oligomerization states, and composition of membrane protein in the protein hetero-complex. Furthermore, the influence of membrane CHOL content on complex formation was also investigated.

The second section of this dissertation is focused on the assembly and dynamics of adhesion linkers underneath migrating cells. Cellular adhesions, including focal adhesions (FAs) [56] and intercellular adhesions [57], are remarkably complex protein assemblies,

which change their size, shape, and dynamics in response to the cytoskeleton-induced contractile forces of adhering/migrating cells. Importantly, cellular adhesions are also sensitive mechanosensors, which probe external mechanical cues, such as substrate stiffness [58,59]. For example, by changing the crosslinking density of polymer gels, the stiffness of polymer substrates can be varied systematically, causing a change in cellular properties, such as spreading area and cytoskeletal organization. This artificial substrate works well to replicate the interaction between cell and extracellular matrix (ECM) [60,61]. However, such polymer-based substrates with chemically conjugated linkers fail to mimic the rich dynamics of cadherin-based cellular adhesions, which exhibit long-range movements at cell-cell interfaces [62,63].

Previous work from our group introduced polymer-tethered lipid bilayers as novel cell surface-mimicking substrates for the analysis of cellular mechanosensitivity [64,65]. Polymer-tethered lipid bilayers have an interesting property: the diffusion of membrane compositions is closely related to the concentration of lipopolymers, which act as diffusion obstacles [66]. If the size of the interested target is substantially smaller than tether distance, free planar diffusion in the membrane can be observed. However, if the tracking target is around the same size or larger than the distance between lipopolymer tethers, obstructed diffusion or immobilization will occur [64]. In addition, we have established a novel polymer-tethered multi-bilayer, in which the number of bilayers in the multi-bilayer stack determine substrate stiffness, thus influencing properties of cellular mechanosensing including cell spreading area, migration speed, and cellular traction forces [65].

The final objective of this thesis work, building on the previous work mentioned above, was to analyze the assembly and dynamics of N-cadherin linkages on polymer-tethered lipid bilayers underneath migrating cells. Additionally, the influence of bilayer stacking and cytoskeletal organization on the assembly of cadherin linker clusters and their dynamics is investigated.

The objectives were fulfilled by building on the expertise in characterization of membrane proteins in planar model membranes that were developed in the first section of this dissertation, using biophysical detection and analysis techniques at the single molecular

level. In this case, techniques such as fluorescence correlation spectroscopy (FCS), photon counting histogram (PCH), and particle tracking were applied to study the objectives described in the four listed Objectives. By developing combined dual-color FCS and PCH, new methodology was introduces as part of this thesis that enables the characterization of dynamic assemblies of membrane proteins with unprecedented accuracy.

1.2 Organization

This dissertation includes five different chapters. The first chapter describes the rationale and objectives of this study and introduces the structure of the dissertation. The second chapter provides information about methods and instrumentation used in this research. This chapter also includes the scientific background of the topics related to the dissertation. The third chapter covers experimental materials and detailed experimental procedures. It also contains details related to data analysis as well as algorithms and equations applied in FRAP, PCH, and cluster tracking. The fourth chapter includes results of experiments and detailed discussion. The fifth chapter includes conclusions and possible trends of the future work related to the objectives discussed in the dissertation.

2. METHODOLOGY AND BACKGROUND

2.1 Methodology

2.1.1 Fabrication of Polymer-Tethered Lipid Bilayers

Planar-supported lipid bilayers have been widely applied as biomembrane mimicking systems [67, 68], biosensing platforms [69], and cellular substrates [64, 65, 70] for studies of membrane structure and biophysical processes. Even though the support substrate of the bilayer varies from glass, silica, polymer cushion [68, 71, 72] to a recently developed carbon graphene substrate [73], the principles of fabricating planar supported lipid bilayers are largely the same. Commonly applied methods, including Langmuir-Blodgett (LB) dipping combined with Langmuir-Schaefer (LS) transfer technique (LB-LS), and vesicle fusion, have been developed for reconstituting a bilayer over a planar substrate. Polymer-tethered lipid bilayers have been fabricated by conjugating polymer chains with planar-supported lipid bilayers [68]. This polymer-tethering strategy enables the bilayer to be lifted up from the solid support, improving mobility of incorporated proteins and altering the mechanical properties of planar bilayer system [68].

2.1.1.1 Langmuir-Blodgett (LB) / Langmuir-Schaefer (LS) Method

In 1917, Irving Langmuir systematically described monolayer formation of amphiphilic molecules at the air-water interface and was the first to introduce the modern concept of molecular conformation [74]. In his pioneering work, the surface pressure-molecular packing relation was investigated through an instrument, later known as a Langmuir trough. Typically, when a certain amount of an amphiphilic solution is deposited on the water surface, the solution spreads to cover the whole surface area. With the evaporation of the spreading solvent, a monolayer of amphiphilic molecules (Langmuir film) is formed. The

modern design of a Langmuir trough is in combination with a Wilhelmy plate to monitor the surface tension and a surface arm, enabling variation in total surface area of the trough. The plate and arm are coupled to a feedback system that allows precise detection and control of the surface pressure through an actuator system. In this way, the surface pressure isotherm can be studied (Fig. 2.1); moreover, by controlling and varying the surface pressure during monolayer fabrication, it is possible to build monolayers of the same molecule with different physical properties.
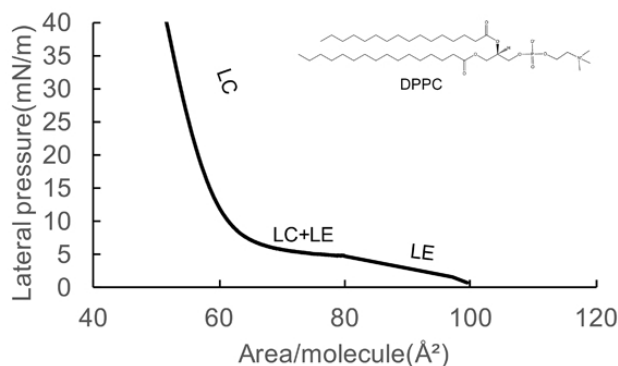
Fig. 2.1. Typical pressure-area isotherm of DPPC at 22.5°C exhibiting liquid-expanded phase (LE), liquid-condensed phase (LC) and a mixed phase of liquid-expanded and liquid condensed phases.

In 1919, Langmuir indicated that a monolayer at the air-water interface could be transferred to a solid substrate. Later, Blodgett extensively studied the vertical dipping process to transfer a monolayer onto a solid substrate [75]; meanwhile Schaefer invented the technique of horizontal transfer [76]. Specifically, prior to the dipping and transfer processes, monolayers should be kept at liquid crystalline phase, using a Langmuir trough to maintain a well-controlled surface pressure. As a solid substrate, such as a glass slide with hydrophilic surface, is dipped through the Langmuir film, a monolayer is deposited on the substrate, while sustaining a constant surface tension of the remaining Langmuir film at the air-water interface (Fig. 2.2.A). This process, later referred to as Langmuir-Blodgett (LB) dipping process, could preserve the monolayer orientation and the crystalline packing. The key aspects of a successful LB dipping process are the meniscus and the dipping

speed, and well-chosen conditions for surface pressure and substrate are also critical. If the dipping speed is too high, the crystalline structure is changed or broken. In this case, the monolayer would not be correctly transferred to the substrate. The other transfer method, known as Langmuir-Schaefer (LS) transfer techniques, describes the horizontal transfer of the Langmuir film at the horizontal orientation. This process requires the solid substrate approaching the Langmuir film with relatively slow speed until contacting the monolayer (Fig. 2.2.B).

To date, LB dipping and LS transfer have been applied as a combination for the fabrication of supported bilayers. The LB/LS method is extensively used in this dissertation for the fabrication of polymer-tethered lipid bilayers. Specifically, the first leaflet containing lipopolymer and phospholipids are transferred to the glass substrate using LB dipping process where hydrophilic headgroups are close to the solid substrate with the hydrophobic tail pointing away from substrates (Fig. 2.2.A). In this way, lipopolymers, which contain a hydrophilic polymer group at the head of the phospholipid are physisorbed to the substrate, creating a cushion underneath the lipid monolayer. The bilayer is completed by transferring the substrate with the first monolayer through the second monolayer using the LS transfer methods (Fig. 2.2.B). This leaflet-by-leaflet assembly strategy enables fabrication of a bilayer with a different lipid composition in the top and bottom leaflets, which is quite useful in the fabrication of polymer-tethered lipid bilayers.
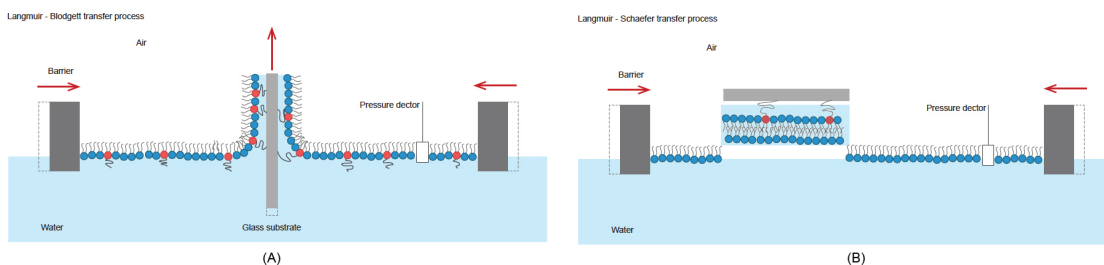
Fig. 2.2. Fabrication of polymer-tethered lipid bilayers using LB/LS method. Lipopolymers are shown as red lipids with black hydrophilic polymers. (A) exhibits the LB dipping process of polymer tethered lipid monolayer onto solid substrate, (B) shows LS transfer of the second leaflet to form a complete polymer-tethered lipid bilayer.

2.1.1.2 Planar Lipid Bilayer Assembly by Vesicle Fusion and Multi-Bilayer Stacking

Lipid vesicles are lipid assemblies that encapsulate a relatively small aqueous chamber. They are usually prepared from diluted lamellar dispersions in combination with different methods that introduce mechanical (sonication or extrusion), chemical (change of solubility conditions or incorporation of other chemicals) or electrochemical (change of ionic strength or pH) energy [77]. As a result of different preparation techniques, lipid vesicles display variation in size and structure that can be obtained (Fig. 2.3), including mutilamellar lipid vesicles (MLVs), giant unilamellar vesicles (GUVs), large unilamellar vesicles (LUVs) and small unilamellar vesicles (SUVs) [78].
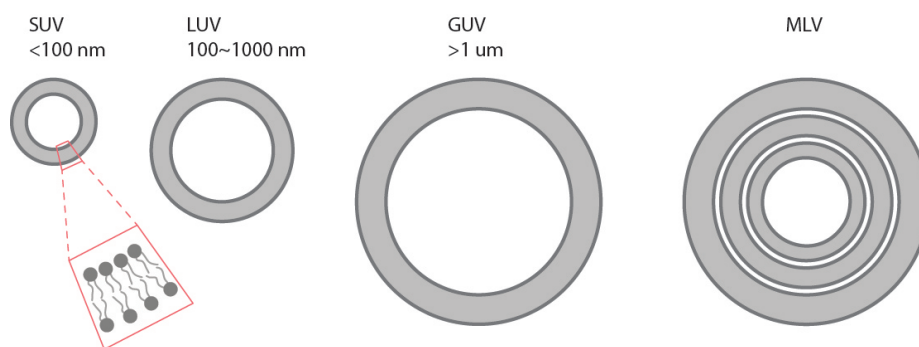
Fig. 2.3. Size and structure of the different types of lipid vesicles.

In the past decades, lipid vesicles have been widely used as biomimetic systems for the study of membrane phase behavior, membrane fusion, cell adhesion and membrane trafficking [79]. However, the major drawback for the vesicle system is the potential aging over time, which decreases the stability and causes aggregation of lipid vesicles [80].

Other than using lipid vesicles as a biomimetic model, lipid vesicles have been extensively applied for the preparation of SLBs or polymer-tethered lipid bilayers [40]. This method is commonly known as vesicle fusion. Specifically, to prepare planar lipid bilayers, suspensions of unilamellar lipid vesicles are added to a clean hydrophilic substrate or supported lipid monolayer [40]. Then the vesicles cover and adsorb to the surface of the substrate. Driven by the substrate-induced bilayer deformation, the adsorbed vesicles rupture spontaneously. This rupturing effect, in cooperation with fusion between neighboring

vesicles, will lead to the formation of a planar lipid bilayer [81]. It has been indicated that the quality control of planar lipid bilayers fabricated through vesicle fusion is particularly complicated [81]. Factors such as substrate properties, lipid vesicle properties, and buffer solution play key roles in vesicle fusion process, thus influencing formation of a planar lipid bilayer [81]. It is essential to use hydrophilic substrates with relatively smooth surfaces and appropriate surface charge under applicable buffer environment during vesicle fusion, to produce planar lipid bilayers with good homogeneity and mobility [71, 82, 83]. Other factors such as application of divalent cations, especially calcium at mmol/L level or below, have been shown to be favorable to induce vesicle rupture and therefore help improve the quality of resulting planar lipid bilayers [84, 85].

Though the vesicle fusion methods have some shortcomings compared to LB-LS, there are several advantages of using lipid vesicles for the preparation of SLBs in comparison to the fabrication via dipping techniques. First, vesicle fusion is not restrained by a specific instrument. Secondly, planar lipid bilayers can be built on substrates with different geometry including curved and even round supports via vesicle fusion, whereas they can only be built on flat and relatively smooth surfaces if LB-LS is adopted. Therefore, vesicle fusion has been applied for the preparation of polymer-supported bilayers and used as a fabrication method for multiple-bilayer stacking [86].

Multilamellar structures are present in living systems with biological importance [87, 88], and have been widely built as a mimetic model. Building a multiple planar bilayer stack could be achieved through electrostatic attraction [89] between two bilayers or using coupling chemistry [90]. In this dissertation, coupling chemistry between maleimide and sufhydryl groups existing in adjacent bilayers will be adopted as the linking mechanism to form a stable stack of multiple polymer-tethered lipid bilayer (Fig. 2.4). In this dissertation, the application of multi-bialyer stacking, through the fusion of GUVs, will be employed to fabricate artificial cell substrates of adjustable stiffness for the analysis of cellular mechanosensitivity.
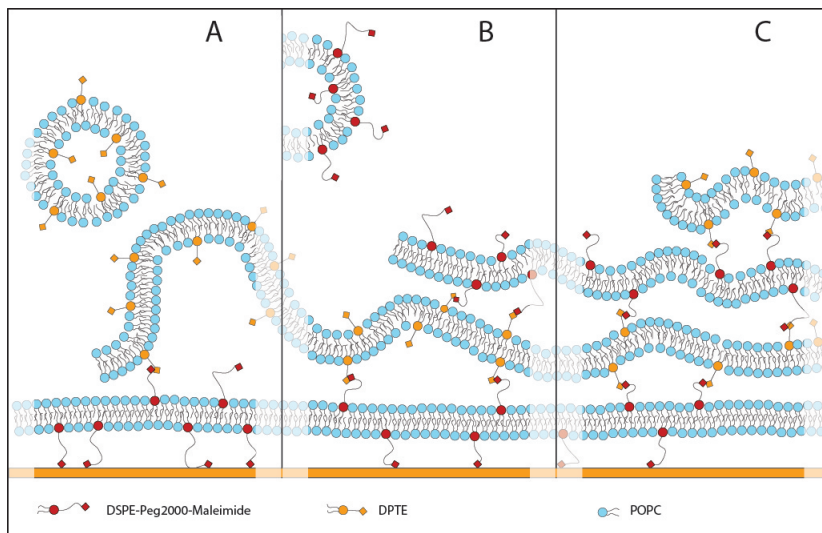
Fig. 2.4. Schematice of layer-by-layer assembly of polymer-tethered multibilayer stack through maleimide-thiol coupling chemistry using GUV fusion. Double bilayer (A), triple bilayer (B), and quadruple bilayer systems (C) were formed through this process [86].

2.1.2 Epifluorescence microscopy (EPI)

Epifluorescence has been applied as the major optical setup for almost every fluorescence microscope. Specifically, in an EPI microscope, the excitation and emission light are both on the same side of the observed specimen. In this way, the fluorescent specimen can excited by an excitation beam at a specific wavelength and a dichroic mirror assures that only emission signal generated from the fluorescent specimen will be observed. The key element of EPI microscopy is a dichroic mirror that separates the emission and excitation beams. In wide-field fluorescence microscopy, the excitation source, normally a mercury discharge arc lamp, passes through a beamsplitter, such as a dichroic filter or an acusto-optical filter, and then reaches the sample specimen. Fluorescent emission of the sample also passes through a narrow band emission filter so that only specific red-shifted photons are collected by a charge coupled device (CCD) camera, which transfers excited photons into voltage and digital output is reported at a working station (Fig. 2.5).

CCD CAMERA

WORK STATION

OCULAR

EMISSION FILTER

DICHROIC MIRROR

EXCITATION FILTER

LIGHT SOURCE

OBJECTIVE

SPECIMEN
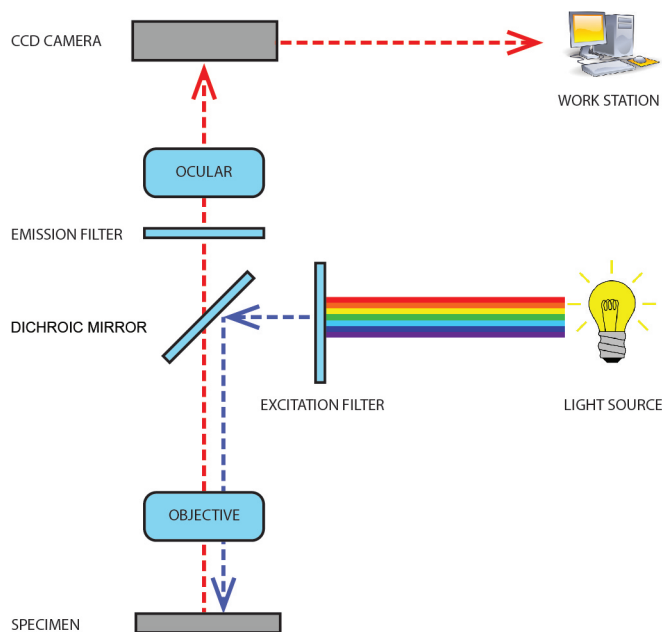
Fig. 2.5. Schematic of a simple EPI fluorescent microscope. Key elements include light source, filter sets, objective, dichroic mirror as well as a CCD camera as a detector.

2.1.3 Confocal Methodology and Quantitative Analysis of Confocal Data

Confocal microscopy, also referred as laser scanning confocal microscopy, is currently the most commonly applied optical imaging technique in life science research and industry. Developed 60 years ago, this microscopic technique became the most powerful tool to take fluorescent images in living systems with high optical resolution and with the ability to provide three-dimensional (3D) images, by introducing spatial pinhole apertures in the traditional epifluorescent microscope system. With a combination of different analysis methods or with the application of specific optical apertures, the confocal microscopy platform is able to provide extensive quantitative information in living systems.

2.1.3.1 Image Acquisition using Laser Scanning Confocal Microscope

The unique property of confocal microscopy compared to traditional wide-field epifluorescence microscopy is its ability to only process the signals from the focal plane. As a consequence, confocal microscopic methods are able to provide more structural details. A laser light source is often adapted to achieve the goal of point scanning, together with pinhole apertures in front of the photon detector to exclude the out-of-focus information (Fig. 2.6). In particular, a laser beam, with a well-defined wavelength, passes through the first pinhole and is adjusted to fill the rear aperture of the objective. The beam will be further focused by the objective lens at the desired focal plane as a diffraction-limited spot, which is also known as the scanning point. This point scans in the X and Y direction in the raster pattern. This procedure, known as point scanning, is applied in most commercially available confocal systems. However, according to the requirements of a specific experiment, other scanning models, such as tornado scanning, might also be applied.

Following the laser excitation, the emitted light from the fluorescent specimen goes through the beam splitter and reaches the detector pinhole and is then analyzed by the photonmultiplier (PMT) detector that renders a digital image. By application of multiple laser sources and PMT detectors, the modern confocal microscope allows simultaneous imaging from multiple channels. Moreover, the adoption of a scanning stage enables image stacking at different confocal planes to produce a 3D image using laser scanning confocal microscope.

Image quality obtained from a confocal microscope is usually considered by analyzing aspects of spatial resolution, dynamic range of light intensity, signal-to-noise ratio, and temporal resolution. All four factors can be adjusted through application of different hardware, as well as software, adjustment of certain aperture functions to optimize conditions according to each experimental requirement. Here, the spatial resolution that describes the smallest resolvable distance between two points in acquired images is determined by the point spread function (PSF) [91]. This function, usually characterized as a Gaussian function, describes the 3D diffraction pattern of light emitted from a point source
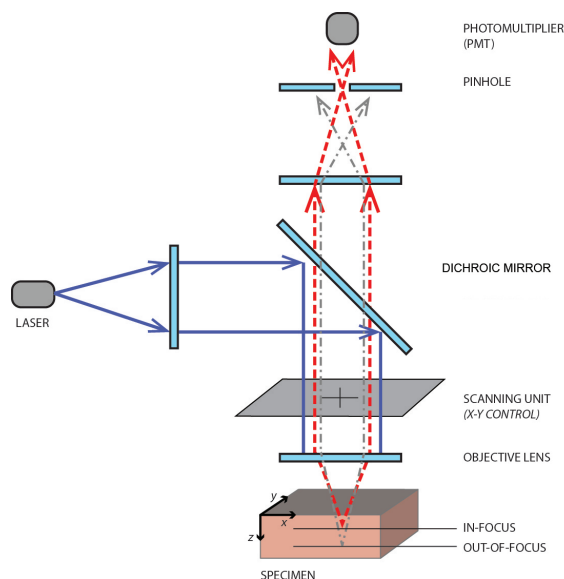
Fig. 2.6. Schematic of a laser scanning confocal microscope. The adoption of a laser light source, as well as the pinhole aperture, excludes out-of-focus signal and allows 3D image acquisition.

and transmitted to the image plane. For a confocal microscope, the PSF is influenced by the numerical aperture (NA) of the applied objective lens, excitation and emission wavelength, and the size of the pinhole aperture. Moreover, software controlled parameters including zoom factor, gain and offset of the intensity dynamic rate, and the laser scan rate will also influence the resulting resolution of the obtained image. However, enhancement of image resolution might sacrifice other aspects, such as response time during image acquisition. In that sense, different combinations of microscope adjustments should be used according to image requirements.

2.1.3.2 Fluorescence Correlation Spectroscopy (FCS)

First introduced in the 1970s as a tool for the study of chemical dynamics during a chemical reaction [92], fluorescence correlation spectroscopy (FCS) has not been extensively used until the last two decades, when confocal optical principles were adopted in the FCS detection. The application of the confocal principle to FCS solved the issue of

poor signal-to-noise when FCS was first introduced, and transformed the method to one of the most sensitive techniques in terms of spatial and temporal resolution available today. Nowadays, FCS is one of the most commonly applied methods for the study of biological molecule dynamics under different conditions with single molecule sensitivity [93–95].

Rather than only recording the absolute fluorescence intensity, the measurement of FCS is based on spontaneous fluorescence intensity fluctuations. These fluctuations are mostly driven by deviations of the system from thermal equilibrium. Therefore, FCS is able to provide information on almost all physical parameters that influence the fluorescence fluctuation signal, such as sample concentration, target fluorescent bio-molecular brightness, diffusion properties of the target molecules, intermolecular and intramolecular interactions, and reactions of the fluorescently labeled biomolecules.

The typical optical setup of a FCS system is similar to that of a regular confocal microscope. The detectors applied in FCS systems are usually an avalanche photodiode (APD) detector or a PMT detector with single photon sensitivity [96]. On the other hand, the objectives used for FCS are usually water immersion objectives with high NA so the diffraction of light is relatively limited. In addition, to reach higher signal-to-noise, proper usage of filter systems and laser sources is essential.

Once the fluorescent signal is received, fluctuations in the fluorescent signal are analyzed by temporally autocorrelating the recorded intensity signal. It has been noted that the temporal average of particle number should be adjusted between 0.1 to 1000 at one time, particle number is related to sample concentration, which can range from below nano-molecular up to micromolecular level. Fluctuation of the fluorescence emitted by molecules is mathematically determined as:

$$\delta F(t) = F(t) - \langle F(t) \rangle \tag{2.1}$$

where,

$$\langle F(t) \rangle = \frac{1}{T} \int_0^T F(t) dt \tag{2.2}$$

In the case where a constant intensity of excitation is applied, the autocorrelation function $G(\tau)$ is given as [94]:

$$G(\tau) = F(t) \cdot \langle F(t) \rangle = \lim_{T \to \infty} \frac{1}{2T} \int_{-T}^{T} \langle F(t) \cdot F(t + \tau) \rangle dt \tag{2.3}$$

where τ presents an infinitely short-time interval, and t is any arbitrary time. Since the excitation is constant, one can assume the average fluorescent intensity at the confocal volume is constant. Then, equation (2.2) could be transferred as [94]:

$$\langle F \rangle = \langle F(t) \rangle = \frac{1}{T} \int_{0}^{T} F(t)dt \tag{2.4}$$

Therefore, the autocorrelation function $G(\tau)$ could be further transformed as [94]:

$$G(\tau) = \langle F \rangle^2 + \langle \delta F(t)\delta F(t + \tau) \rangle \tag{2.5}$$

This function contains a constant part of the average fluorescent intensity, $\langle F \rangle^2$, and a time-dependent part, which provides information about the kinetics of the system. It can be normalized as [94]:

$$G'(\tau) = 1 + \frac{\langle \delta F(t)\delta F(t + \tau) \rangle}{\langle F \rangle^2} \tag{2.6}$$

Herein, the temporal information of the fluorescent intensity can be analyzed together with the total amount of fluorophores. To obtain diffusion information of the target molecules, the PSF of the microscope needs to be considered for the confocal volume of the FCS system. The number of fluorophores within the confocal volume follows the Possion-distributed statistics, and the relation between the number of molecules (N) and fluorescent is [94]:

$$\frac{\lim_{\tau \to 0} \langle \delta F(t)\delta F(t + \tau) \rangle}{F^2} = \frac{1}{N} \tag{2.7}$$

Suppose the radius of the volume element in XY direction is ω_1 whereas half of the length of the volume element in Z direction is ω_2. Under the condition that fluorescence decay time $<<$ diffusion time (τ_D), then the diffusion coefficient of the target molecule is [94]:

$$D = \frac{\omega_1^2}{4\tau_D} \tag{2.8}$$

Taking equations (2.6), (2.7), (2.8) together, the normalized autocorrelation curve can be transformed as [94]:

$$G'(\tau) = 1 + \frac{1}{N} \cdot \frac{1}{1 + \frac{4D\tau}{\omega_1^2}} \cdot \left\{ \frac{1}{1 + \frac{4D\tau}{\omega_2^2}} \right\} \tag{2.9}$$

Therefore, by fitting autocorrelation curves obtained from FCS experiments, information including numbers of fluorescent molecules, and the diffusion coefficient of fluorescent molecules can be extracted.

Nowadays, FCS methods are no longer limited to single photon excitation and single color analysis. Advanced protocols including two photon excitation, dual color FCS, and fluorescence cross-correlation spectroscopy have been widely applied for different purposes [94].

2.1.3.3 Photon Counting Histogram Analysis (PCH)

As mentioned in the previous section, the FCS analysis provides temporal behavior of fluctuations through autocorrelation analysis. However, the amplitude of fluorescence fluctuations is largely dependent on the probability distribution of detecting a certain number of photons for a given sampling time. The analysis of this probability distribution can be experimentally analyzed by using the histogram of the detected photons; this is known as photon counting histogram (PCH) analysis [97]. Unlike FCS, which distinguishes species mostly according to different diffusion coeffeicients, PCH analysis distinguishes different species according to the brightness and therefore provides direct information about aggregation state of fluorophores, a parameter which is only indirectly accessible using FCS autocorrelation analysis.

In the case where single photon excitation is applied, the confocal excitation volume (v_0) can be described by 3D Gaussian approximation. Suppose the v_0 is large enough to allow diffusion of a single fluorescent particle for a long enough observation time. The

particle might appear in any position of within v_0. In this case the probability of detecting k photons that have been emitted by the particle can be described as [97]:

$$p^{(1)} = \frac{1}{v_0} \int \text{Poisson}[k, \varepsilon \cdot W(\vec{r})] d(\vec{r}) \qquad (2.10)$$

where $W(\vec{r})$ is the observed volume information profile, which can be commonly replaced by the PSF of the optical system, and ε which characterizes the photophysical properties of a certain fluorescent species under specific experimental setup.

Therefore, the probability of observing N particles is described by the Nth convolution of the Poisson function [97].

$$p^{(N)} = p^{(1)} \otimes p^{(2)} \otimes p^{(3)} \otimes \cdots \otimes p^{(N)}(k; v_0, \varepsilon) \qquad (2.11)$$

For an average concentration, the number of actual particles inside the volume fluctuates. This fluctuation can also be established as a poission distribution of the average number of particles N_{avg}.

$$\text{PCH}(k; N_{avg}, \varepsilon) = \sum_0^\infty p^{(N)}(k; v_0, \varepsilon) \cdot \text{Poisson}(N, N_{avg}, \frac{v_0}{v}) \qquad (2.12)$$

Under experimental conditions, the volume information is usually approximated by measuring the Gaussian function of the microscopic system, and photophysical properties can be characterized by comparison with a fluorescent standard having known photophysical properties. Therefore, the number of particles with specific brightness will be obtained by deconvoluting the Poisson function. The oligomerization states of individual molecules will be determined by exploiting the concept that dimers are twice as bright as monomers. Therefore, by adding a second layer of deconvolution (Eq. 2.13), the number of dimers and ratio of dimerization will be solved.

$$\text{PCH}(k; N_1, \varepsilon_1, N_2, \varepsilon_2) = \text{PCH}(k; N_1, \varepsilon_1) \otimes \text{PCH}(k; N_2, \varepsilon_2) \qquad (2.13)$$

where,

$$\varepsilon_2 = 2\varepsilon_1 \qquad (2.14)$$

2.1.3.4 Fluorescence Recovery after Photo Bleaching (FRAP)

As one of the most well-established techniques, fluorescence recovery after photobleaching (FRAP) has been widely applied for the quantitative analysis of molecular species in living systems to provide information about mobility and interaction [15]. As illustrated in Fig. 2.7, FRAP experiments are fulfilled by quickly illuminating a relatively small area (region of interest, ROI) on a sample with homogeneously distributed fluorescent probes, to photobleach the dye molecules in the ROI. If the sample contains a mobile fraction, the fluorescent intensity of the ROI will generally be recovered. The rate of fluorescence recovery can be used to determine the diffusion coefficient, while the ratio of immobile fraction can be determined by comparing the original and final fluorescent intensity in the FRAP process (Fig. 2.7).
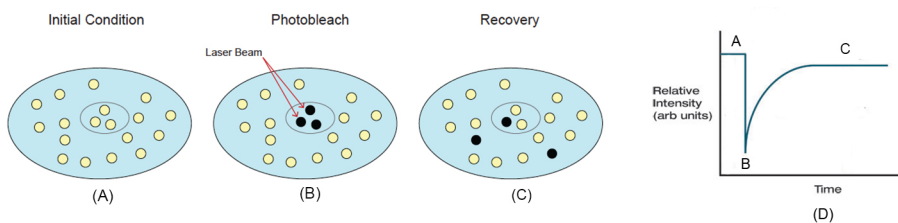
Fig. 2.7. Principle of FRAP experiment (A,B,C) and resulting FRAP curve (D). A small area of a sample with homogeneously distributed fluorescent probes (A) were photobleached within a small time period using a laser beam, causing the photobleaching of fluorescent probes in the laser excited area (nonfluorescent) (B). After photobleaching, fluorescence recovery occures if the fluorescently labeled molecules are mobile (C). The fluorescence intensity within the spot is recorded through the whole process and graphed (D).

Unlike FCS and PCH analysis, which is only able to provide information on the mobile fraction of the sample, FRAP analysis provides information about both the immobile and mobile fractions. Therefore, FRAP experiments has have been widely adopted in various studies for measuring the lateral diffusion of components on plasma membranes as well

as model membranes [15]. Furthermore,FRAP has been established as a useful tool for the analysis of interactions and binding kinetics of molecules in live cells [98]. In this thesis, FRAP data are analyzed using the elegant math model developed by the Kenworthy group, published previously [98]. Specifically, assuming that the bleach spot size is small compared to the sample size, the intensity profiles of the bleaching lasers in the infinite sample plane are described as a Gaussian:

$$I_{(r_n)}(x, y) = \frac{2I_0}{\pi r^2} \exp(-\frac{2(x^2 + y^2)}{r_n^2}) \tag{2.15}$$

If the concentration of fluorescent probes $C(x, y, t)$ meets the diffusion equation

$$C_t = D\Delta C \tag{2.16}$$

where D is the diffusion coefficient and $\Delta = \frac{\partial^2}{\partial x^2} + \frac{\partial^2}{\partial y^2}$, therefore $C(x, y, t)$ can be reformatted as:

$$C(x, y, t) = \iint C(x - x', y - y', 0)\varphi_{Dt}(x', y')dx'dy' \tag{2.17}$$

with

$$\varphi_{Dt}(x, y) = \frac{1}{4\pi Dt} \exp(-\frac{x^2 + y^2}{4Dt}) \tag{2.18}$$

The fluorescent intensity from the bleached area can be calculated using the equation

$$F(t) = q \iint \varepsilon I_{(r_n)}(x, y)C(x, y, t)dxdy \tag{2.19}$$

where q is the quantum yield of fluorophores.

The confocal postbleach profile can also be described as a simple Gaussian function

$$C(x, y, 0) = C_i(1 - K\exp(-\frac{2(x^2 + y^2)}{r_e^2})) \tag{2.20}$$

where C_i is the prebleach fluorophore concentration and r_e is the effective radius of the postbleach profile.

To find the diffusion coefficient, the following equation can be applied:

$$F(t) = F_i \left\{ 1 - \frac{K}{1 + r^2 + \frac{2t}{\tau_D}} \right\} M_f + (1 - M_f)F_0 \tag{2.21}$$

where, $\tau_D = \frac{r_e^2}{4D}$ and γ is the ratio of the nominal and effective radius. M_f is the mobile fraction which defined as:

$$M_f = \frac{F_\infty - F_0}{F_i - F_0} \qquad (2.22)$$

and K could be resolved from pre-bleaching fluorescent intensity, F_i, and intensity at t = 0, (F_0).

$$K = \frac{F_i - F_0}{2} M_f + F_0 \qquad (2.23)$$

Combining equations 2.20, 2.21, 2.22, and 2.23, the diffusion coefficient can be written as:

$$D_{confocal} = \frac{r_e^2 + r_n^2}{\tau_{\frac{1}{2}}} \qquad (2.24)$$

If the bleaching is instantaneous, $r_e = r_n$, then

$$D = 0.25 \frac{r_n^2}{\tau_{\frac{1}{2}}} \qquad (2.25)$$

Therefore, the diffusion coefficient can be found by measuring bleaching area and the diffusion time $\tau_{\frac{1}{2}}$.

Though FRAP has been shown to be a powerful tool, there are several limitations of this technique for the investigation of protein dynamics. For example, to obtain reasonable results, fluorescent tagged molecules should be homogeneously distributed. Furthermore, FRAP analysis is only applicable for the target molecules with diffusion coefficients ranging from 0.1 to $100\mu m^2$/s [15].

2.1.3.5 Single Particle Tracking and Cluster Tracking

The single particle tracking (SPT) method has long been used for the analysis of molecular dynamics on cell surfaces, as well as in model membranes [29]. Though the ideal temporal and spatio resolution of SPT is similar to that of FRAP, SPT provides the specificity in motion measurements of single or very few molecules [99], whereas, FRAP is based on average information from a substantial number of diffusing fluorescent molecules. Due to the fact that SPT provides specific motion information, SPT may provide further information that explains the findings from FRAP. Furthermore, the spatial resolution of SPT is

much higher than FRAP analysis, therefore with sufficient time resolution, motion modes of target molecules can be resolved [99].

SPT is usually fulfilled by the following procedures. First, the general input of SPT experiments are a series of time-lapse images of particles obtained by a microscopic technique. Following the data acquisition process, quantitative assessment of the dynamic properties of the imaged particles are analyzed by applying various mathematic modes that usually combines two steps. First, time-lapse of particles will be localized to distinct points, using Gaussian functions that are related to the PSF of the microscope. Secondly, following the localization process, tracking analysis will then be done by linking the positions of detected particles to generate trajectories. These trajectories can be further applied to group and analyze different types of movement of the particles analyzed [99, 100].

There are various methods that determine tracking trajectories. The most accurate method is known as multiple-hypothesis tracking (MHT), through which the tracking trajectories are found by considering all particle paths within the bounds of expected particle behavior through the entire time-lapse series and the non-conflicting ensemble of paths (given each particle has a unique tracking path) is selected as the final solution. However, this approach has a large computational cost when multiple particles are tracked, due to the nature of this algorithm that it requires the calculation of tremendous possibilities for each particle during tracking, making MHT almost impossible to use with current techniques. There are several SPT algorithms based on simplified MHT tracking methods. These algorithms are usually limited in precision, in order to reach a reasonable amount of computational cost [100].

A particle tracking method based on the mathematical framework of the linear assignment problem (LAP) was first introduced by Jaqaman et al. in 2008 [101]. Unlike MHT, LAP-based particle tracking is fulfilled by first linking particles between frames followed by close gaps of undetected tracks to capture merging and splitting events between the initial track segment at the lowest mathematical cost. This segment assignment is optimized from both temporal and spatial aspects and provides precise analysis that is close to MHT methods at low computational cost. Moreover, this LAP based tracking method is also

highly versatile and applicable to tracking tasks in live cell images, where tracking objects can change their size during the tracking process. This idea is fulfilled by using a comet detection algorithm [102]. In this algorithm, differences of two Gaussian transformations were calculated with standard deviation adjusted to enhance the signal associated with potential clusters. This process creates size thresholds for the detected clusters. The detected signals will further be adjusted using a unimodel threshold to exclude the background information. The individual object is generated by connecting labeled component that satisfies the set threshold of Gaussian function.

The tracking trajectory is acquired through three steps in the LAP algorithm. Following the initial step of particle detection, every step afterward including particle linking and tracking segment linking will be considered as a potential assignment. The cost of these assignments will be considered through a cost, C . The LAP will be solved by finding the combination of assignments with the minimal sum of cost:

$$\hat{A}_{arg_{min}} = \sum_{i=1}^{number of rows} \sum_{i=1}^{number of columns} A_{ij}C_{ij} \tag{2.26}$$

Where A is any assignment matrix with 1 (link) and 0 (no link) and, $\hat{A}$ is the matrix that minimizes the sum of costs. The conditions on A and $\hat{A}$ will be furthered controlled by a secondary condition that

$$\sum_{i=1}^{number of columns} A_{ij} = 1, \quad \sum_{i=1}^{number of rows} A_{ij} = 1 \tag{2.27}$$

to ensure the the assignment is exclusive, therefore no particle or tracks will be included in more than one tracking trajectory.

Gap closing will be considered when certain tracking objectives might potentially go out of focus or where the end of a track segment might be able to link to the start of another track segment. Cost will be determined during the merge of the segments. The gap as well as the cutoffs during each procedure will need to be adjusted in consideration to the experimental requirements, which will be described in section 3.2.11.

2.2 Background

2.2.1 Lipid Rafts

Cell membranes are crowded two-dimensional amphipathic solutions containing membrane proteins in a lipid solvent [10]. Importantly, the structure of the cell membrane is asymmetric, thereby displaying a heterogeneous distribution of both lipids and membrane proteins. This heterogeneous nature of the plasma membrane is essential for both cellular function and structure [10]. It is believed that heterogeneously distributed lipids and proteins in the plasma membrane assemble into transiently-stabilized structures known as lipid rafts [13]. The concept of lipid rafts overcomes the classical view of the plasma membrane, in which membrane proteins float in the homogeneously organized lipid bilayer [103]. Lipid rafts are now widely accepted as an important regulatory platform in multiple biological processes including cancer development [104, 105], virus infection [12, 106] and T-cell antigen receptor activation [16, 30]. However, the argument of whether lipid rafts exist or not has been under debate during the last 20 years [24, 107]. This is majorly due to the fact that the early concepts of lipid rafts are based on surfactant extraction experiments. Such surfactant extraction experiments were later found to introduce defects by aggregating specific lipid components before the extraction process [107], leading to a misunderstanding of the membrane structure. Nevertheless, the concept of lipid rafts emphasizes the importance of lipid environment for membrane protein distribution, dynamics, and function. This concept also promotes the idea that lipids and proteins are not passively organized, but actively interact with each other to regulate the functionality of cell membranes.

2.2.1.1 Lipid Mixing and Phase Separation in Lipid Membranes

Lipid bilayers in biological membranes are not just solvents that provide simple amphiphilic environments which allow membrane proteins to float around in the membrane. Instead, cellular lipidomics comprises over 1000 different lipids with different head groups

and carbon-hydrated chains [1]. This extensive diversity of lipid molecules in biological membrane results in a complex lipid environment.

Phospholipid molecules with different saturated and unsaturated acyl chains have intrinsic differences in thermodynamic properties such as transition temperature (T_m). Therefore, when mixing lipids into one lipid bilayer, it is possible that such mixtures exhibit different phase behaviors according to the variation of lipid composition and temperature. For example, in 1975, Wu et.al [108] reported that the DOPC-DPPE mixture exhibits two different liquid phases which coexists with a solid phase, whereas DEPC-DPPE lipid mixtures show an additional immiscible liquid phase. Those findings provided initial insight into the role of length and saturation states of acyl chains on lipid mixing behavior and the significance of mixing thermodynamics therein.

Other than phospholipids, sterols, especially CHOL, play key roles in the structure and organization of lipid bilayers in the cell membrane. Mainly embedded in the hydrophobic region, CHOL influences bilayer thickness, lipid packing of the lipid bilayer and potentially promotes phase separation between lipids with low T_m and lipids with high T_m at an intermediate temperature [109–111]. This specific function of CHOL enables phase separation at a temperature that phospholipids are not able to perform intrinsic phase separation. As a consequence, CHOL may induce two coexisiting liquid phases in lipid mixtures: liquid ordered (l_o) phase, enriched with CHOL and lipids with high T_m, and liquid disordered (l_d) phase enriched with lipids characterized by a lower T_m [109]. These two liquid phases show different physical properties. In particular, l_o phases are more densely packed than l_d phases. Therefore, distinct lipid diffusion in l_o and l_d phases are observed [51]. Furthermore, as confirmed by atomic force microscopy(AFM) [53, 112] the hydrophobic thickness of the l_o phase is usually larger than that of the l_d phase whem mixing two lipids of comparable chain length.

The phase behavior of ternary lipid mixtures of high T_m lipid/ low T_m lipid/ CHOL has been described by ternary phase diagrams, which were obtained using methods including detergent extraction, FRET [46], FCS [51], AFM [53, 112], NMR [46] and electron paramagnetic resonance (EPR) [113]. The phase diagram of several ternary lipid mixtures

such as DOPC/ sphingomyelin/ CHOL [114] and DOPC/ DPPC/ CHOL [46,52] have been reported. For example, Veatch et al. mapped the phase morphology of DOPC/ DPPC/ CHOL(Fig. 2.8) and described the relationship between temperature, lipid composition, phase mixing behavior, and estimated logical tie-lines of the phase diagram. Their results provide relevant information about the line tension of mixtures as a function of lipid composition. Furthermore, the resulting shape of tie-lines indicates that CHOL is more equally distributed than DPPC in different phases. Other interesting results established by
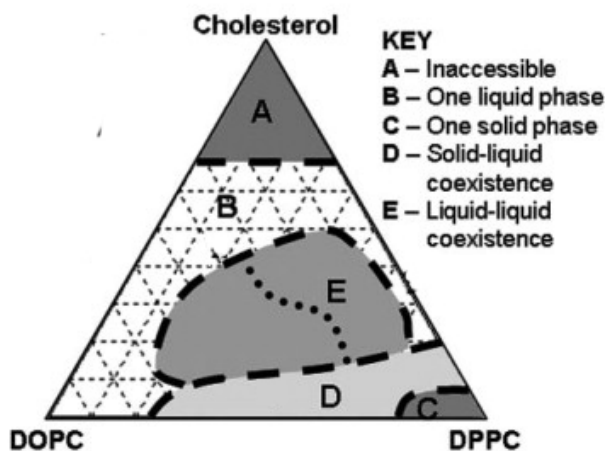
Fig. 2.8. A typical DOPC/DPPC/CHOL phase diagram revealed by a GUV based assay [46].

Scherfeld et al. [51] illustrate lipid dynamic information in DOPC/ DPPC/ CHOL mixtures by FCS analysis, indicating important lipid packing information within these lipid mixtures. All these significant features of ternary raft-mimicking lipid mixtures make them promising model membrane platforms for the analysis of lipid mediated membrane protein sequestration processes.

Lipid mixing behavior is more complicated in real cellular membranes with more complex lipid compositions [1]. According to a recent computational simulation experiment, in which 63 different lipid species combining 14 types of head groups and 11 types of tails were asymmetrically assembled across two leaflets, a heterogeneous distribution of CHOL can be observed in such system that highly mimics real cell membranes. Interest-

ingly, transient l_o phase domains were found in such system, which have a lifetime on the microsecond scale [8]. Furthermore, GPMV-based assays indicated that without embedded membrane proteins, lipid bilayers in plasma membrane exhibit similar lipid mixing behavior as ternary raft-mimicking lipid mixtures, which display macroscopic l_o-l_d phase coexistence [44, 45, 49]. These findings, illustrate that complex lipid mixtures and simple lipid mixtures share common physical-chemical properties regarding the mixing behavior.

2.2.1.2 Lipid Raft Hypothesis

The concept of lipid rafts was first proposed in the late 1990s [13]. According to the lipid raft hypothesis, lipid rafts were considered to be l_o-phase-like domains floating in a sea of lipids forming a liquid disorder phase. Raft domains were considered to be enriched in CHOL, sphingolipids, and specific membrane proteins such as GPI-anchored proteins. It is believed that the formation of lipid rafts is partially driven by the lipid mixing behavior in the plasma membrane [7, 115]. Importantly, the heterogeneous membrane structure of lipid rafts has the ability to work as a sorting platform of membrane protein, thereby regulating membrane protein functionality [7]. In other words, the lipid raft model emphasizes the role of lipid environment in regulating membrane protein distribution and corresponding membrane protein functionality.

During the last two decades, thanks to the development of optical imaging techniques, such as super-resolution microscopic methods [116], the concept of lipid rafts evolved [7, 10, 115]. Lipid rafts are currently considered as nanosized transient membrane structures enriched with sterol, sphingolipids, and certain membrane proteins that assemble and disassemble as reaction centers during biological processes [7, 10, 29, 115]. Several factors have been considered, which regulate the size of lipid rafts. For instance, the growth of these raft domains could be suppressed by the actin-based cytoskeleton organization, which responds to extracellular mechanical and chemical signals [29, 50]. On the other hand, lipid-lipid, protein-protein and protein-lipid interactions may further induce clustering of raft-associated molecules and form larger platforms with little energy costs [23, 117, 118].

The modern concept of lipid rafts is widely accepted to be one of the major principles of plasma membrane organization of functional importance [7]. The raft structure is closely related to the formation of protein oligomers and larger complexes between membrane-associated proteins and lipids [23]. For instance, it has been observed that raft-based lipid interactions would facilitate oligomerization of GPI-anchored protein. These homo-oligomers further assist the stabilization of raft structures thereby forming "receptor cluster rafts" [29, 119, 120]. Such a receptor oligomerization mechanism has been considered to be important during signal transduction as it mediates cluster-induced actin polymerization that has been suggested to play a key role in processes including cell apoptosis and cancer development [29]. Another interesting example can be seen in the association of transmembrane integrins to rafts. In particular, it has been observed through CHOL depletion assays, that upon activation, integrins are recruited to lipid raft-like domains [121]. This raft association effect is considered to be important in the process of integrin crosstalk which is deemed to be essential in the function of T-cell antigen recognition and cell spreading [122].

In general, the Lipid raft hypothesis provides a possible explanation to how the membrane is organized as a gatekeeper to fulfill the function of biological membranes at the lowest energy cost [7]. At the core of this hypothesis is the assembly of dynamic, nanoscale heterogeneities enriched in sphingolipid and CHOL in the cell membrane. Importantly, this hypothesis suggests the relationship between lipid environment and membrane protein assembly. Overall, considering the proposed close correlation between lipid rafts and cellular function, it will be essential to elucidate the role of lipid rafts in membrane protein functional sequestration and oligomerization.

2.2.1.3 Raft-mimicking Model Systems

Due to the transient nature and small size (nm scale) of lipid rafts, the investigation of rafts using cell-based assays is extremely challenging. The most commonly applied assays, including CHOL depletion and application of crosslinking agents, have inherent drawbacks of introducing other effects that potentially interrupt membrane protein distribution and

oligomerization [7, 24]. As discussed in section 2.2.1.1, cell membranes with complex lipid composition and model lipid mixtures exhibit similar physicochemical properties in phase separation [8]. In other words, rather than dampening the collective behavior of the complex lipid mixtures in plasma membrane, only demixing of two phases has been reported in the thermodynamical equilibrium in cell membranes with extremely complex lipid components [44, 45, 49, 50]. This finding provides a rationale for using simplified lipid ternary mixtures with defined composition and relatively large lipid phase separations (µm scale) as a model membrane to investigate the influence of membrane environment on membrane protein functional sequestration and oligomerization without the potential influence of the cytoskeleton [49].

Model membranes with raft-mimicking lipid mixtures have been widely used as models for lipid rafts [40, 115] and have provided extensive information on lipid mixing behavior and interaction between CHOL and phospholipids as described in section 2.2.1.2. Additionally, the underlying mechanisms of protein association to lipid rafts have also been investigated through model membrane platforms including GUVs, solid supported lipid bilayers and polymer-tethered lipid bilayers [40, 123]. For example, Winter and coworkers have investigated the distribution of N-Ras and K-Ras in GUV and solid supported bilayer models and demonstrated that palmitoylation of N-Ras causes l_d phases association [124]. Moreover, transmembrane proteins such as SNAREs have also been investigated using GUV based assays [125]. Compared to the GUV and solid supported bilayer model membrane, polymer-tethered lipid bilayers hold advantages for the investigation of membrane protein sequestration in the presence of lipid rafts as it allows the analysis of both transmembrane and lipid-anchored proteins in their functional orientations [54]. Additionally, using layer-by-layer assembly, bilayers with different phase behavior in opposing leaflets can be built. Therefore, influences of bilayer asymmetry on membrane protein sequestration has been investigated [55, 126]. For example, in previous experiments of our group, integrins were functionally reconstituted into polymer-tethered lipid mixtures, and integrin sequestration and oligomerization in the absence and presence of native ligands was investigated in both symmetric and asymmetric raft mimicking mixtures [54, 55].

2.2.2 Interaction Between Lipids and Membrane Proteins

As the primary barrier between living systems and the outer lifeless world, plasma membranes achieve their function primarily through the proper fulfillment of membrane protein and lipid interactions. Destabilization, misfolding, and perturbations in membrane protein structure are major causes of reduced or loss of membrane protein function [127]. Furthermore, abnormal membrane protein function is possibly reflected by unusual lipid-membrane protein complex formation since lipids are usually required as regulatory factors to promote function and sustain the structure of membrane proteins [128].

According to the various modes of intramembrane protein-lipid interactions in cellular membranes, membrane lipids can be distinguished as regulators of membrane protein functionality from both physical and chemical perspectives. Specifically, lipids that display a low level of interaction with the transmembrane region of membrane proteins are considered as bulk lipids, whereas annular lipids form shells surrounding particular membrane proteins and show a lower level of exchange rates with lipids in proximity. Lipids serve as solvents to a membrane protein and influence membrane protein functionality by regulating the lipid environment surrounding membrane proteins. In addition, there are specific lipid molecules that are able to interact with specific amino acid sequences of membrane proteins thereby serving as ligands to membrane proteins. These lipid molecules exhibit strongest interactions with membrane proteins and influence the structure through direct biochemical interactions [128]. Taken together, membrane lipids, indlucing sterols, may influence membrane protein functionality through a variety of lipid-protein interactions.

2.2.2.1 Lipids as Ligands for Membrane Proteins

The understanding of protein-lipid complex formation has been significantly improved thanks to the increasing availability of high-resolution protein structures solved by X-ray crystallography. Through this method, lipids tightly bound to transmembrane domains have been observed in some of the structures. Those bonds are mostly stabilized by at least two polar interactions between the phosphodiester group and a set of molecules containing

a positive charge and a polar amino acid. Those observed binding domains are usually nonlinear and consist of amino acids in several subunits. [128, 129] . Other than those specific binding sites, certain amino acid residues at the interface of the membrane protein, including most of the aromatic amino acids, play a role in stabilizing and interacting with lipid molecules [130].

The interactions between membrane proteins and nonannular lipids are functionally important. Until now, lipids such as phosphatidylglycerol (PG), phosphatidyliositol (PI), anionic phospholipids, CHOL, and cardiolipin (CL), have been proven to be important as chaperones in processes such as protein folding [131], complex stability [132, 133], ion transduction [134] and regulation of other ligand binding [135]. Moreover, lipid molecules residing within membrane protein oligomers play a role as molecular glue and promote the formation of functional oligomers. For example, CHOL can promote the oligomerization of caveolin-1 subunits in microsomes by binding to caveolin-1 at 1:1 ratio [136]. Similar effects have been indicated as one of the possible mechanisms of the formation of glycosynaptic microdomains that are significant for cellular adhesion. In this case, gangliosides could interact with integrin and possibly other membrane proteins, thereby promoting the function of integrins during cell migration [137]. On the other hand, this strong interaction between lipids and membrane proteins influences membrane lipid composition, not only due to the low exchange rate between the bound lipids and the adjacent lipid molecules, but also due to the functional activation of some specific proteins [128]. For example, the binding and interaction between CHOL and Peripheral-type benzodiazepine receptor induces CHOL transportation and compartmentalization and substantially affects cellular membrane organization [138].

2.2.2.2 Biophysical Lipid-Protein Interactions

While specific lipid-protein complex formation plays a significant role in protein function, most lipid molecules do not bind to membrane proteins through biochemical interactions, but are rather considered as solvents for membrane proteins. These general

bilayer-protein interactions are also essential in modulating membrane protein conformational transition, diffusion, and distribution in response to energetic and kinetic regulatory factors [139, 140].

It is widely accepted that when a soluble protein is distributed in the water-based solution, single molecules are covered by a shell of water molecules also known as hydration layer. Those water molecules are purturbed by interaction with the protein molecule and show distinct dynamic properties in comparison to bulk water. A similar concept applies to the distribution of membrane proteins by lipid molecules, where lipid shells were observed through several different methods including EPR [141], electron microscopy [142], X-ray diffraction [142], and fluorescence assays [143]. Those lipids, in comparison to lipids that chemically interact with membrane proteins, exhibit a substantially faster exchange rate with outer bulk lipids. Although annular lipids are less sticky to the membrane protein, the exchange rate between annular lipids and bulk lipids is still two times slower in comparison the exchange rate of lipids in bulk bilayers [143].

The interaction between annular lipid molecules and membrane proteins are non-specific and mediated through weak interactions such as van der Waals, hydrogen bonding, and electrostatic interactions. These subtle interactions might substantially change the membrane protein activity through cooperative effects. For example, it has been shown that the activity of Ca^{2+}-ATPase is influenced by both the headgroup and the chain length of the surrounding lipid environment. Changes in lipid composition are not sufficient to cause a significant change in Ca^{2+}-ATPase conformation, but will effect the additive binding of many sites and substantially modify the activity of the protein [144]. Furthermore, alteration of the length of fatty acyl chain length changes the thickness of the hydrophobic core of the lipid bilayer. Through the mechanism of hydrophobic matching, membrane proteins might compensate for a change in acyl change length by distorting their structure, influencing protein activities [140].

It is relatively well understood that the local lipid environment, determined by the composition of annular and non-annular lipids, influences membrane protein functionality by introducing changes in membrane protein structure, and folding, thus regulating membrane

protein binding sites directly. The influence of bulk lipids on membrane protein function is more complicated and relatively poorly understood. Since plasma membranes are highly dynamic assemblies, important physical properties including bilayer thickness, bilayer fluidity, lipid packing stress, bilayer stiffness, intrinsic lipid curvature have significant impacts for diffusivity and distribution of membrane proteins. Those factors are largely subject to the composition of bulk lipids, and regulate membrane protein dynamic and distribution through thermodynamic mechanisms. Membrane proteins with similar preference tend to move into or assist in forming distinct microenvironments such as lipid rafts in the plasma membrane, and therefore induce further function of membrane proteins [3, 4, 10, 23, 139].

Of all the lipid components found in the plasma membrane, CHOL is one of the most important co-solvents of membrane proteins. Its modulation of the dynamics of bulk membranes has been well documented [139, 141, 145]. It has been described in the previous section that CHOL addition promotes lipid phase separation. Particularly, CHOL influences membrane structure in two ways. First, due to structural properties of CHOL, the interaction between CHOL and more rigid saturated acyl chains is more entropically favorable compared to its interaction with lipids with unsaturated acyl chains. Therefore, CHOL has a relatively high propensity to condense with itself and saturated lipids, resulting in a relatively more rigidly-packed bilayer region. On the other hand, protein functions are sensitive to the CHOL contents of the membrane. For example, higher content of CHOL reduces the free volume available for molecular motion in the hydrophobic core of the bilayer, which influences the volume-dependent transition between signal-inactive metarhodopsin-I and signal-active metarhodopsin-II [145]. Moreover, it has been suggested that CHOL may modulate the dynamics of the bulk membrane with implications on the folding and stability of membrane proteins, as well as the energetics of protein oligomerization [145]. However, due to the limitations of existing assays that allow systematic variation of CHOL, little experimental evidence is avaiable to date on these issues. Another important feature of CHOL is its ability to alternate the thickness of the lipid bilayer by an increase in the length of the phosphatidylcholine (PC). For example, in a C16:0/C18:1 phosphatidylcholine bilayer, the addition of CHOL expands the bilayer thickness from 35Å to 40Å where its

hydrophobic core increases from 26Å to 30Å [146]. Interestingly, the impact of CHOL in a sphingomyelin-enriched lipid bilayer is relatively moderate. The thickness of a C18:0 sphingomyelin lipid bilayer is 46-47Å both with and without CHOL [147]. This effect of CHOL has a profound impact on the distribution of membrane proteins especially trans-membrane proteins. CHOL may play an important role in the process of protein sorting and potentially crucial roles in the processes of protein-protein interaction which is essential in process such as signal transduction. The functional significance of CHOL is illustrated by the fact that elevated levels of CHOL have been observed in cancer cells [104, 148] and models of neurodegenerative disease [149]. Therefore, it has been suggested that the effect of CHOL on membrane protein is closely related to protein function and disease development.

Intriguingly, the specific impacts of non-annular, annular lipids, and bulk lipids are often unclear. Consequently, the fundamental question of how lipid environments regulating membrane proteins remain unanswered. Additionally, the role of lipid environments in the biochemical interaction between non-annular lipids and membrane proteins remain a topic of open debate. Therefore, it is essential to gain a better understanding of membrane protein-lipid interactions and the regulatory effects of lipid environment on membrane protein dynamic distribution and functional oligomerization.

2.2.3 Membrane Protein Complex Assembly and Dynamics

Many vital cellular processes are dependent on protein oligomerization and protein-protein interactions within the membrane. For instance, in Ras-mediated signaling, it is found that signaling is more accurate when Ras functions as a dimer versus monomeric Ras [150]. Abnormal clustering or oligomerization of membrane proteins are related to development of disease states, including cancer and amyloidal diseases [151]. It is widely accepted that during the processes of signal transduction, ligand binding to membrane proteins often introduce structure changes, which trigger functional membrane protein redistri-

bution and oligomerization. Additional factors that affect membrane protein complexation are dynamics and structure of lipid bilayers, as well as cytoskeletal organization [152].

2.2.3.1 Formation and Regulation of Membrane Protein Homo-oligomers

As discussed in previous sections, the core of lipid bilayers in biological membranes is hydrophobic with a low dielectric constant. To stabilize membrane proteins that contain polar amino acids in the transmembrane region, formation of stable dimers may be triggered to overcome the energetically unfavorable situation [153, 154]. Additionally some receptors, such as GPI anchored uPAR are known to form homo-oligomers or clusters to achieve their functionality [32].

GPI-AP play important roles in signal transduction and cell adhesion. It has been observed that functional oligomers of GPI-AP are mostly formed during transportation to the apical domain of the plasma membrane, and therefore the oligomerization of GPI-APs has been proposed to be important in apical sorting signal transduction [32, 155]. Moreover, GPI-APs are observed to be associated with lipid rafts, and the formed oligomers are considered to further stabilize due to their raft-association [26, 119, 120]. Exemplary, such processes can be seen during the apical sorting processes of uPAR. This membrane protein, which contains three domains, works as an important regulator of ECM proteolysis [36]. Intriguingly, uPAR is often over expressed in cancer cells and has been proposed to be related to cancer invasion [28]. It has been suggested that the dimerization of uPAR regulates its function and related signal cascade through interaction with native ligands, including urokinase plasminogen activator (uPA) and VN [32].Interestingly, uPAR exhibits a dimer-oligomer equilibrium at the apical and basal side of epithelial cells, possibly due to its interaction with VN (Fig. 2.9). However, the relationship between GPI-AP sorting, lipid environment and oligomerization remains obscure. Several factors, including ligand binding, lipid environment, lipid-protein interaction and protein-protein interaction, have been considered to be responsible for the sorting and clustering of GPI-AP [26, 119, 120]. However, the formation of GPI-AP oligomers appears to be protein specific. On the other
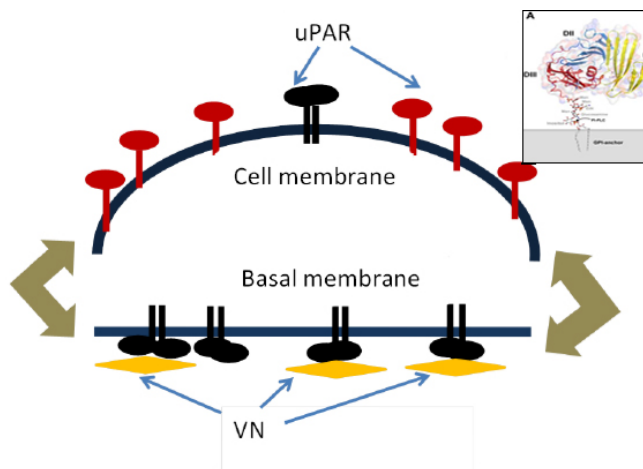
Fig. 2.9. Schematic uPAR dimer-oligomer transition as apical and basal side of epithelial cells [32]. The crystal structure of uPAR is shown as insert (A) in the figure [156].

hand, cellular experiments have lead to contradictory results about the regulation of GPI-AP oligomerization. For example, CHOL content has been indicated to be related to GPI-AP oligomerization, which has been considered to be one element of the lipid raft hypothesis [12]. Additionally, it has been proposed that GPI-AP oligomerization was dependent on lipid rafts. On the other hand, earlier research of uPAR dimerization suggested that CHOL depletion does not influence GPI-AP oligomers [157].

2.2.3.2 Formation and Regulation of Membrane Protein Hetero-complexes

Most membrane proteins are believed to exist in complexes that enable functionality. According to the Protein Data Base, most of the identified membrane protein structures are monomeric or form homo-oligomers. Multi-subunit membrane-protein complexes are extremely challenging to investigate using traditional structural biology methods [158]. Traditional biochemical and structural biology methods, such as immunoprecipitation and X-ray crystallography usually require relatively large amounts of membrane protein. Therefore, to investigate membrane protein complexes, membrane proteins within such a complex have to be coexpressed, purified and stabilized in order to analyze membrane protein

heterocomplexes [158]. This process is first limited by co-transformation of several plasmids with single or multiple expression cassettes, which has a drawback that the copy numbers of the respective plasmids can vary significantly [158]. In addition, the stabilization and purification of membrane protein complexes is extremely challenging due to the limitation of applicable detergents for multiple membrane proteins [158]. The recent advances in cryo-electron microscopy (cyro-EM) allows analysis of very large assemlies with relatively small amount of proteins, but the nature of cryo-EM prevents it from obtaining information about the dynamics of such complexes [159].

Nevertheless, among the 84 structures that have been identified, membrane protein heterocomplexes are believed to play important roles in processes, such as signal transduction and cellular adhesion [158]. For example, the activation of G-protein coupled receptor (GPCR) involves the association and disassociation of the complex among transmembranal GPCR, palmitoylated Gα-subunit and GPI-anchored G$\beta\gamma$-subunit [160].

The structure of lipid bilayers in the plasma membrane has been proposed to be important in processes such as signal transduction by regulating membrane protein oligomerization [161]. A study based on transmembrane peptides in a model membrane platform indicates that mismatching of transmembrane peptides of different length with bilayers of different thickness influences the clustering of transmembrane peptides. Furthermore, CHOL strictly constrains structural adaption at the peptide-lipid interface and therefore constrains the lateral segregation of peptides and lipids according to hydrophobic thickness [162].

There are several transmembrane proteins that have been widely studied in respect to functional oligomer formation. One of the most investigated examples is the family of integrins [163, 164]. Identified as essential adhesion receptors, integrin regulates cell migration and extracellular matrix assembly by binding to ECM ligands including vitronectin (VN) and fibronectin (FN), hence playing a critical role in processes such as tissue development, wound healing, immunity, and cancer development [165, 166]. Integrins by themselves are heterodimers substituted with α and β subunits and are capable of forming oligomers based on the GXXG motifs present within the transmembrane domain [167]. Upon activation by

natural ligands, the structure of integrins switched from a bent, low-affinity conformation to an extended conformation with closed head to reach its intermediate affinity [164]. This intermediate structure will be further developed into an extended conformation with open head to achieve the highest affinity by additional activation of external ligands [164] (Fig. 2.10).
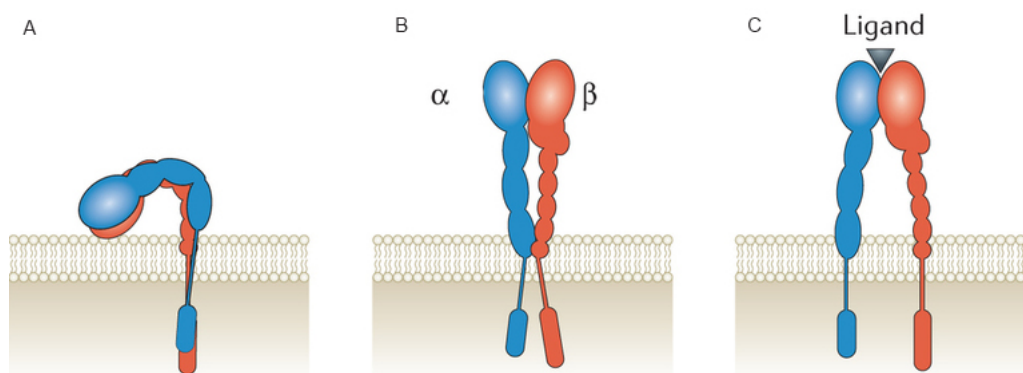
Fig. 2.10. Schematic of integrin at bent (A), extended (B), and extended-open (C) conformations. The αsubunit is shown in blue while β subunit is shown in red. In specific, at low affinity, integrin exists as bent structure, while extended structure is with intermediate conformation. Moreover, ligand activation promotes the conformational change further to open extended conformation [164].

These series of structure changes alternate the length of the transmembrane helix of the protein and lead to a dissociation of the transmembrane domain [164, 168]. As a consequence, integrins might be recruited to another region of the plasma membrane to lower their overall energy to maintain the structure. On the other hand, it has been proposed that the activated structures have a higher tendency to form homodimers [168]. Moreover, it has been suggested that ligand binding by itself facilitates the targeting process of focal contacts, and induces a higher-level of integrin clustering for further signal cascades. Intriguingly, it has been suggested that lipid composition, especially CHOL content in the membrane, has a profound influence on the ligand binding process [33, 169]. In this case, higher CHOL levels in the plasma membrane increase the possibility of forming integrin oligomers [169]. In addition, there is a proposed hypothesis suggesting that inte-

grins might be activated even without ligand binding, but solely dependent on membrane composition. However, there is no research that indicates any specific binding sites of CHOL in the transmembrane domain of integrin, suggesting a possible biophysical role of membrane composition in regulating integrin clustering. Another lipid that might influence integrin homo-oligomer formation are glycosphingolipids, such as monosialotetrahexosyl-ganglioside (GM_1) and monosialodihexosylganglioside (GM_3) [137], which influence integrin functionality through direct interaction between the carbohydrate groups in integrin and sugar moiety of gangliosides [170].

Higher levels of hetero-complex formation can also be observed in the plasma membrane. For example, integrins have also been identified as members of uPAR interactome [171], and potentially assist uPAR-mediated signaling by working as a lateral partner with the GPI-AP. It has been suggested that the regulation of such complex formation is highly dependent on ligand binding processes [172]. However, there is also evidence that lipid bilayer composition and membrane structure may play an essential role in hetero-complex formation between membrane proteins. For instance, cellular studies indicate that uPAR acts as a ligand to various species of the integrin family, causing their to raft domains and mediates cell-cell adhesions [38]. The process of complex formation is proposed to impact the structure of transmembrane domain of integrin [35]. Notably,CHOL depletion assays demonstrate the CHOL dependence of this process [38]. This uPAR-integrin complex and its influence on protein sequestration and oligomerization will be discussed in more detail in Chapter 4.

2.2.3.3   Assembly and Regulation of Cellular Adhesion Junctions

Most tissue cells are anchorage-dependent. Those cells probe the outer mechanical cues of the surrounding environment as they anchor and pull to spread and migrate. During these processes cells generate contractile forces by cross-bridging interactions of actin and myosin filaments, and partially transmit the force to the ECM [60]. In turn, cells are able to respond to the resistance of the substrate by adjusting adhesions, cytoskeleton or-

ganization and state [58, 60]. Such process are closely dependent on the organization of cellular adhesions such as FAs and AJs. These cellular adhesions are protein complexes that associate with cytoskeleton networks and function as mechanosensors. In other words, cellular adhesions change their shape, size, and dynamics according to the surrounding mechanical signals [60]. The formation of cellular adhesion complexes and regulation of their dynamics are critical for morphogenesis, embryogenesis, immune cell function, tissue repairing, and maintenance of tissue integrity [173–175]. On the other hand, those membrane protein-associate complexes also contribute to the development of diseases including cancer metastasis and invasion, as well as immune disorders [58, 175–177].

Thanks to the development of polymer-based cellular substrates, assembly of focal adhesions and their response to outer mechanical properties, such as substrate stiffness, have been extensively studied. Polymer substrates, coated with immobile ECM ligands, are well suited to mimic cell-ECM interactions, therefore revealing abundant information about the mechanosensitive assembly and regulation of FAs [60, 61]. In contrast, cell-cell adhesions, such as cadherin based AJs, can be highly dynamic. As a result, long range movement and treadmilling motion has been observed [62, 178]. This dynamic nature of the cell-cell interface cannot be mimicked by the traditional polymer-based substrates. Therefore, little is known about the correlation between the dynamics of cell-cell adhesions and external mechanical signals. Nevertheless, increasing evidence indicates that the interplay between mechanical signals and adhesion protein dynamics at cell-cell interfaces is a major factor in regulating morphogenetic processes in embryos and within organs [179–182]. These findings reveal the importance of understanding the assembly and dynamics of cellular AJs in response to mechanical signals.

Cadherins are a family of adhesion molecules that constitute Ca^{2+}- dependent homophilic cell-cell junctions of all solid tissues [57, 183]. Cadherins mediate cell-cell adhesion processes by recognizing specific types of cadherins expressed in different cell types. The classical types of cadherins include those ubiquitously expressed in epithelial cells (E-cadherin, P-cadherin), endothelial cells (VE-cadherin) and all other non-epithelial cells expressing N-cadherin [184, 185]. Moreover, through the association of cytoskeleton, cad-

herins act as mechanical sensors that promote changes in cell morphology and migration in response to outer mechanical signals [186].

During the previous decades, the role of cadherin in the process of mechanosensing and the underlying mechanism was partially revealed [57, 187]. As a transmembrane receptor, both extracellular and intercellular domains of cadherin are essential to cadherin functionalization. The extracellular domain of cadherin is responsible for the interaction with cadherin expressed at the nascent cell and promotes the assembly cluster formation during cell adhesion [57, 187]. The intracellular domain, on the other hand, forms complexes with the catenin family proteins p120-catenin and β-catenin that assemble onto the cytoplasm domain of cadherin [184, 186]. While p120-catenin stabilized the cadherin-catenin complex, β-catenin assembles with α-catenin and form a heterodimer. This cadherin-catenin complex further associates with the actin cytoskeleton through a connection between α-catenin and actin filaments(Fig. 2.11) [184–186]. Further studies based on cadherin-coated poly-
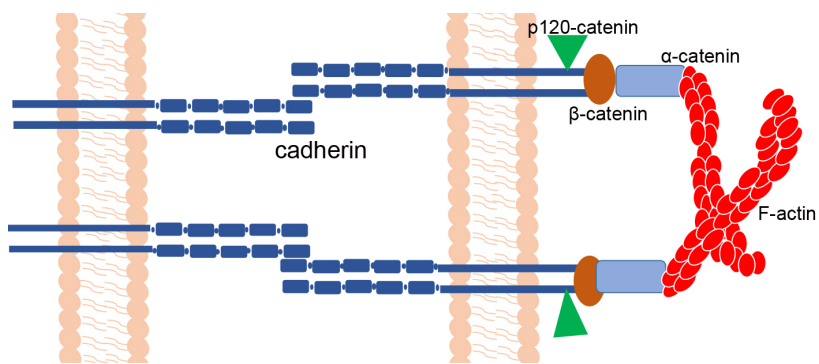
Fig. 2.11. Schematic of cadherin based cellular junctions.

mer substrates with adjustable stiffness indicates that cadherin-based adhesions transmit and adapt to mechanical loads using both traction force assay and FRET-based molecular tension sensor [188]. This statement could also be demonstrated through artificially stretching cell doublets where cadherin clusters are under tension modulated by contractile shear force [189]. Furthermore, the molecular mechanism of cadherin-based mechanosensing was in part established. α-catenin is proposed to undergo force-dependent conformational changes that regulate the amount of actin bound to cadherin-catenin complexes through

complex formation between α-catenin and vinculin [190, 191]. Moreover, binding of vinculin to catenins, especially α-actin has been reported to be dependent on myosin activity [192, 193].

However, due to the dynamic nature of cadherin mediated adhesions at cell-cell interfaces and the limitation in applicable materials to mimic such interfaces, one fundamental question of how AJs are able to maintain strong adhesion to maintain tissue cohesion while allowing cellular rearrangement in response to mechanical signals, and/or during cell migration remain largely unanswered. As collective migration of cell clusters is involved in morphogenesis, tissue renewal, wound healing, and tumor spreading, it is essential to get a better understanding of the dynamic cadherin-cadherin assembly and cluster movement in response to mechanical forces and cytoskeletal organization.

3. MATERIALS AND EXPERIMENTAL PROCEDURES

3.1   Materials

3.1.1   Materials for the Preparation of Polymer Tethered Lipid Bilayers

The phospholipids including 1,2- dioleoyl-sn-glycro-3-phosphocholine (DOPC) 1,2-diapalmitoyl- sn- glycero-2- phosphocholine (DPPC), 1- palmitoyl- 2- oleoyl-sn- glycero-3- phosphocholine (POPC)and 1,2- dipalmitoyl- sn- glycero- 3- phosphothioethanol (DPTE) as well as Cholesterol (CHOL), Ni- chelating lipid, 1,2- dioleoyl- sn- glycero- 3- [(N-(5- amino- 1- carboxypentyl) iminodiacetic acid)succinyl] (nickel salt) (DGS-NTA Ni) and monosialodihexosylganglioside (GM_3) were purchased from Avanti Polar Lipids (Alabaster, AL). Lipopolymer 1,2- dioctatecly -sn- glycero- 2-N- poly(2-methyl- 2- oxazoline)50 ($diC_{18}M_{50}$) was synthesized by Jordan group as previously reported [194]. Lipopolymers 1,2 - distearoyl - sn - glycero - 3 - phospho- ethanolamine - N- [methoxy (polyethylene glycol)- 2000](ammonium salt), (PEG-2000) and 1,2- distearoyl- sn- glycero-3- phospho-ethanolamine- N- [maleimide (poly- ethyleneglycol) 2000](ammonium salt) (PEG2000- maleimide) were purchased from Avanti Polar Lipids (Alabaster, AL). The dye-labeled phospholipids N- (7 -nitrobenz- 2- oxa- 1,3- diazoly- 4-yl) 1,2-diahexadecanoyl- sn- glycero- 2- phosphoethanolame, triethylammonium salt (NBD-DHPE), N- (6-tetramethyl- rhodamine-thio-carbamoyl)- 1,2- dihexadecanoyl- sn- glycero- 3- phospho-ethanolamine (TRITC-DHPE), 1,1'- dioctadecyl- 3,3,3',3'- tetra-methylindodicarbocyanine, 4-chloro- benzenesulfonate Salt (DiD), and Texas Red- 1,2-dihexa-decanoyl- sn- glycero-3- phosphoethanolamine (TR-DHPE) were obtained from Invitrogen (Carlsbad, CA).

Ultrapure water (Milli-Q, pH 5.5, 18 MU-cm resistivity) was prepared via a Millipore Water Purification System (Milford, MA). Glass coverslips (No.1, 40 x24 mm) were purchased from Fisher Scientific (Hampton, NH). To prepare the cover slips, they were baked

in a furnace at 515 °C oven for 40mins for EPI and laser scanning confocal microscopy experiments, or 1.5hrs for FCS and PCH analyses. The baked sildes were cooled down to room temperature and further sonicated in a sequence of solutions beginning with 1% SDS, then NaOH-saturated methanol, and lastly 0.1% HCl. Each sonicating step was timed at 30mins (EPI and confocal imaging) or 45mins (FCS and PCH analysis) with a thorough rinse by MilliQ water in between. All chemicals applied in the cleaning process were reagent level purchased from Fisher Scientific (Hampton, NH).

3.1.2 Membrane Protein and Chemicals for Protein Reconstitution and Labeling

Purified human integrin $\alpha_v\beta_3$ and $\alpha_5\beta_1$, as well as anti-integrin β_3, monoclonal antibody and anti-integrin β_1 monoclonal antibody(MAb), were purchased from EMD Millipore (Billerica, MA). Human recombinant urokinase plasminogen activator receptor (uPAR) and anti-DDK antibody were both obtained from Origene Technologies (Rockville, MD). Purified vitronectin (VN) and purified urokinase plasminogen activator (uPA) were purchased from EMD Millipore (Billerica, MA). His-tagged N-cadherin chimera and polyclonal uPAR antibody(N-terminal Domain1 specific) was purchased from R&D Systems, (Minneapolis, MN). Antibodies and N-cadherin chimera are labeled using Alexa 555 or Alexa 488 antibody labeling kits (Invitrogen, Carlsbad, CA) according to the standard protocol provided by the vendor. Fluorescent standard molecules, Rodamine-6-G(R6G) and fluorescein were purchased from Sigma-Aldrich (St. Louis, MO).

The surfactant n-octyl-glucopyranoside (OG) was obtained from Fisher BioReagents (Fairlawn, NJ). SM-2 Bio-Beads were purchased from Bio-Rad (Hercules, CA). HPLC grade Chloroform (Fisher Scientific, Hampton, NH) was used as the spreading solvent of lipid monolayers at the air-water interface. Lipid mixtures with reconstituted protein were kept in Phosphate Buffered Saline(PBS) (1X solution), diluted from 10X solution (Thermo Fisher Scientific, Waltham, MA).

3.1.3 Cell Culture Materials

C2C12 myoblast cell line was obtained from ATCC (Manassas, VA) and was cultured in phenol red free Dulbecco's Modified Eagle Medium(DMEM) with 10% fetal bovine serum, 1% Glutamate, and 100U/ml Penicillin. Cells were incubated at 37°C in humidified atmosphere with 5% CO_2 (Prixar Air). Trypsin was used and incubated for 10 mins. Residues of cells were rinsed off by PBS. All sterilized cell culture reagents, as well as tissue culture flasks and aspirator pipettes, were purchased from Thermo Fisher Scientific (Waltham, MA). Micropipettes were also obtained from Thermo Fisher Scientific (Waltham, MA) and were sterilized by autoclave (Primus Sterilze Co. Omaha, NE) prior to usage. Latrunculin B (LaB) was purchased from Sigma-Aldrich (St. Louis, MO).

3.2 Experimental Procedures

3.2.1 Preparation of Single Polymer-Tethered Raft-mimicking Mixtures

Single Polymer-tethered lipid bilayers were prepared layer-by-layer using LB-LS procedures described in section 2.1.1.1. A Langmuir trough (KSV-NIMA, Biolin Scientific) was applied in this process. To form the first monolayer, a chloroform solution of lipid mixtures containing 5% lipopolymers was spread at the air-water interface. The second monolayer was produced by spreading a lipopolymer-free chloroform solution of lipids at the air water interface. After complete evaporation of chloroform, the surface pressure of the lipid monolayer was adjusted to 30mN/m prior to the LB dipping and LS transferring processes to ensure the quality of lipid bilayers. The LB dipping process was achieved through a dipper connected with a motor and the LB layers were transferred to a glass substrate with a dipping speed of 24mm/min. LS transfer was accomplished by gently pushing the LB layer-coated glass substrate onto a depression slide that was previously positioned underneath air-water interface. Then the depression slide was removed from water interface and the bilayer was either placed into a petri dish for further protein reconstitution or

attached to the bottom of a 35mm petri dish with a 15 mm diameter hole in the middle for further fabrication of multiple bilayers and the study of cadherin linker dynamics.

To achieve the first three objectives described in the first chapter, three types of single bilayers were designed and fabricated (Fig. 3.1):

Type I   Type II   Type III
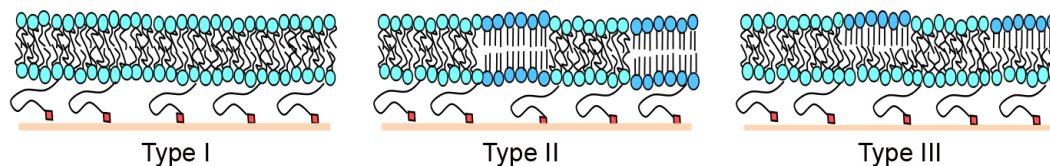
Fig. 3.1. Schematic of Type I (no observable lipid phase separation), Type II (bilayer spanning l_o-l_d phase separation, Type III (l_o-l_d phase separation only at top LS monolayer.

Type I: symmetric bilayer composition without any phase separation. There are two different bilayer systems in this class. The first one only contains phospholipids with 5mol% lipopolymer (diC$_{18}$M$_{50}$) in the bottom LB monolayer whereas the top LS monolayer is solely made of one type of phospholipids . The second bilayer system is comprised of binary lipid mixtures containing DOPC and CHOL at different ratio, where LB layers also contain 5mol% of diC$_{18}$M$_{50}$ to form the polymer tethering structure. More specifically, bilayers containing 0, 10, 20, 30 mol% CHOL were fabricated. To prepare the Type I bilayers, lipid suspensions were kept in the Langmuir trough at a surface pressure of 30mN/m for 30mins before LB dipping or LS transferring processes.

Type II: symmetric bilayer compositions with bilayer spanning l_o and l_d domains. In specific, the composition of bottom LB layer was 5mol% diC$_{18}$M$_{50}$, equimolar ratios of DOPC and DPPC, and varying CHOL concentrations. The LS monolayer contained the identical molar ratio of DOPC, DPPC and CHOL. The most commonly applied composition was DOPC: DPPC: CHOL at a 1:1:1 molar ratio, while bilayers 25, 28, 35, 37 mol% CHOL were also applied for the investigation of CHOL influence on membrane protein sequestration. In addition, 0.2mol% NBD-DHPE was applied as a reporter for large scale lipid phase separation. To prepare Type II Lipid suspensions were kept in Langmuir trough

at the surface pressure of 30mN/m for 50mins before LB dipping or LS transferring processes were conducted.

Type III: asymmetric bilayer composition with coexisting l_o and l_d phase separation in the top LS leaflet, but no phase separation in the bottom leaflet. The LS leaflet of the bilayer was a lipid mixture of DOPC: DPPC: CHOL at 1:1:1 molar ratio with added 0.2% NBD-PE as a reporter on lipid phase separation. The bottomn (LB) monolayer was similar to that of Type I bilayers that contain 5mol% $diC_{18}M_{50}$, 33mol% of CHOL, 0.2mol% of DiD with the remaining lipid composition DOPC lipids. To make this type of lipid bilayer, the bottom LB leaflet was kept in the trough at the surface pressure of 30mN/m for 30 minutes before dipping procedures while top LS leaflet was kept at the same pressure for 50 minutes before LS transfer.

3.2.2 Reconstitution of Membrane Proteins into Lipid Bilayers

Protein molecules were reconstituted into polymer-tethered lipid bilayers using modified Rigaud Method(Fig. 3.2) [54, 55]. Before membrane protein reconstitution, bilayer samples were extensively rinsed with PBS to replace MilliQ water, which as utilized in the initial model membrane assembly. Following buffer exchange step, 1.3×10^{-11} mol of membrane protein in 2ml of 250μM OG were added to the pre-assembled lipid bilayers and incubated for 2 hrs. In the case of investigating membrane protein complex formation and dynamics, two types of membrane protein were added at a 1:1 ratio, each protein was added at the total amount at 6.5×10^{-12} mol, while 0.6ml of 250M OG was applied to assist the reconstitution of membrane protein. After a 2hr incubation, OG surfactant was removed from the bilayer with a single layer of SM-2 Bio-Beads. In the research of investigating membrane protein complex formation and dynamics, two different membrane protein reconstitution procedures have been applied, simultaneous addition of all membrane proteins (in dual color labeling experiments on two different membrane proteins) and sequential addition of membrane proteins (in all single color experiments on reconstituted membrane proteins. Fluorescently labeled monoclonal antibodies (MAbs) were added at a 1.5:1 ratio

to the target protein and incubated for 2hrs. unbound antibodies were rinsed off with PBS. GM_3 in 0.2ml of 2.5μM OG as well as ligands, including FN and VN, were added at a 1:1 ratio to proteins and permitted for an overnight incubation (8-9 hrs). Unreconstituted ligands were removed by extensive rinsing with PBS.
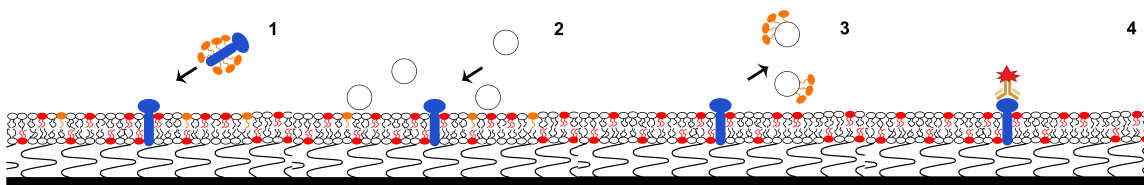
Fig. 3.2. Schematic of protein reconstitution into the pre-assembled polymer-tethered lipid bilayer. Membrane protein was reconstituted with the addition of surfactant (1) and incubated for 2 hrs, extra surfactant was removed by adding bio-beads(2 & 3), the reconstituted membrane protein was labeled with fluorescently tagged antibody (4).

3.2.3 Data acquisition using Confocor2 microscopic System

A Confocor2 microscope system (Carl Zeiss, Jena, Germany) equipped with an Axiovert 200M (Carl Zeiss, Oberkochen, Germany), a Zeiss C-Apochromat objective (water immersion, 40×NA=1.2), and a Zeiss AxioCam MRm monochrome digital camera was applied for Confocal spectroscopy XY scan (CS-XY), FCS, and PCH analyses(Fig. 3.3). The system was pre-warmed to thermal equilibrium to minimize drift.

For single color protein labeling assays, the data on protein distributions and diffusion was acquired using a 1.8mW HeNe laser (wavelength 543nm) at 70% intensity, with a combination of dichroic mirror and bandpass filter of 550-615nm. For dual color protein labeling assays, where Alexa 488 and Alexa 555 were both applied for the protein labeling, a specific beam path was set for best S/N while maintaining minimum signal bleed-through. In specific, 1.8mW HeNe laser (wavelength 543,70% laser power) as well as a 30mW argon laser (wavelength 488, 0.1% laser power) were applied to a major dichroic beam splitter of 488nm and 543nm (HFT488/543), additional laser shutter was also applied before reaching
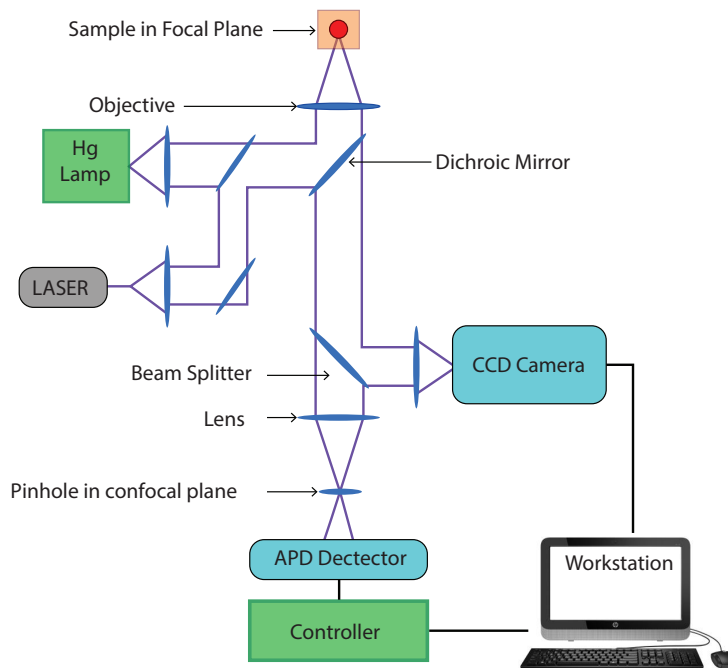
Fig. 3.3. Microscopic setup of FCS-EPI fluorescent combined system.

the sample. The excited light went through a secondary dichroic beam splitter (NT 50/50 IR) and separated into two channels. Alexa 488 could be detected through bandpass filter of (505-530nm) and Alexa 555 could be detected through a bandpass filter of (560-615nm). Since the Argon laser was controlled at relatively low power to minimize the laser bleed through, the pinhole diameter of the 488 channel was adjusted to be 10% larger than that of the other channel to collect enough signal while maintaining a quantitative signal-to-noise ratio. Prior to each analysis, samples were bleached for 3secs and measured at the same spot for 5 runs with 10secs/run.

3.2.4   Protein Distribution Analysis in Planar Bilayers Using The CS-XY Scans

Protein distribution was quantitatively analyzed using confocal based XY fluorescence intensity scans. Particularly, the dye-labeled lipid distribution was determined as an indicator of lipid phase separation. To analyze membrane proteins Type II and Type III lipid

bilayers, NBD-DHPE distribution was acquired using a 30mW Argon laser (wavelength 488) at 0.7% intensity combined with a dichroic mirror and bandpass filter of 505-530nm; while DiD-DHPE distribution in Type III lipid bilayers was detected using a 1.8mW HeNe laser (wavelength 633nm) with a dichroic mirror and a long pass filter of 654nm. The distribution of Alexa 555 labeled antibodies were monitored using the identical set up for FCS analysis in single color protein labeling assays described in the previous section .

Background fluorescence intensity was determined in separate control experiments. In specific, control samples were prepared using identical lipid bilayer compositions, however no membrane proteins were reconstituted. Following the same procedure as bilayer samples with membrane proteins reconstituted, monoclonal antibodies were added at an identical level. To exclude background signals, control experiments were conducted using comparable experimental conditions empolyed on bilayer samples without reconsituted membrane proteins. The average fluorescence intensity of the bilayer from the control experiment was subtracted from the experimental samples with membrane proteins, enabling quantitative analysis of membrane protein distribution using the normalized intensity parameter E_{raft}:

$$E_{raft} = \frac{I_{l_o} - I_{l_d}}{I_{l_o} + I_{l_d}} \tag{3.1}$$

3.2.5   Brightness and Oligomerization State Analyses Using Combined FCS and PCH

As mentioned in section 2.1.2.3, the average photon counts, $< k >$ is a product of the average number of particles N_{avg} and the brightness (Eq. 2.11). Here dimers are considered as particles with twice the brightness as monomers. Previous work in our group confirmed equal brightness of fluorescent markers on lipid bilayers and in solution. In addition, at low concentration, N_{avg} determined by PCH and FCS was determined to be equal. Therefore, standard R6G solution at the concentration of 0.15 nM was applied as a standard solution. This low concentration provided information at nearly single molecule level, and the brightness of R6G and particle numbers were determined by FCS analysis. Following that procedure, the labeling efficiency and the antibody concentration of Alexa

555 labeled antibody were determined by FCS analysis on antibody in solution. The Alexa 488-labeled antibodies were quantified using the same methodology with a different fluorescent standard (fluorescein).

After all the information on dye-labeled antibodies was obtained, the average brightness of single antibodies wasi applied as the monomer brightness. To solve for dimers, the dimer brightness was simply determined to be twice the brightness as a monomer. The total number of particles was determined to be close to the particle numbers determined by brightness. The data were run for multiple sets to find the best fit and to determine N_{avg} and ε.

A PCH curve is a combination of information including all the following factors: (1) obtained brightness of fluorophores, which is sensitive to laser fluctuation; (2) Case-specific background information, potentially determined by antibody non-specific binding and fluorescence bleed-through; (3) detected particle numbers of monomer and dimers. Therefore, all the control experiments mentioned above are critical to obtain a accurate PCH result. Fig. 3.4 illustrates the impact of dimerization ratio on model PCH curves. The solid curve in each situation is the best fitting curve obtained from a bilayer with 0.001mol% TRITC-DHPE in the bilayer with brightness and particle numbers being obtained from FCS analysis.

3.2.6 Determination of Protein Oligomerization States in Hetero-complexes Using Combined Dual-Color FCS and PCH

Since membrane proteins were reconstituted into the lipid bilayer at a low concentration (1.3×10^{-11} mol), single molecular events could be observed from an intensity-vs-time trace (FCS raw data). Protein oligomerization states in protein heterocomplexes were determined in two steps through a dual color assay. First, complexes were determined using intensity-vs-time trace. In this process, signals that were three-times higher than the average background intensity were determined as signal peaks. For each significant signal, t_{peak} was determined to be the time where highest intensity appeared. If the absolute differ-
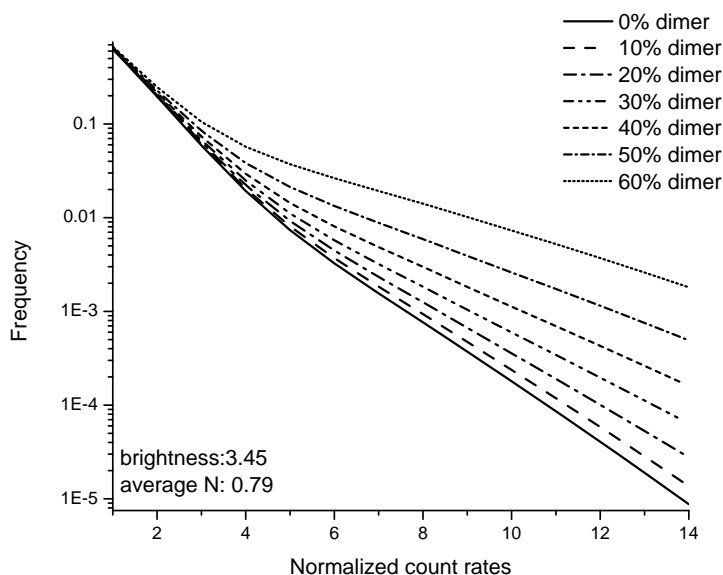
Fig. 3.4. PCH model curves illustrating the influence of dimerization ratio
on the shape of PCH curves [195].

ence of t_{peak} values from two fluorescent channels was smaller than 0.0256s (smallest time interval recorded), it would be considered that the event of single complex diffusion was observed (Fig. 3.5.A). Secondly, the peaks where complexes were observed were separated from the rest of the signals and were further combined to obtain a new intensity-vs-time trace(Fig. 3.5.B). According to this new trace, intensity readouts were binned for PCH analysis (Fig. 3.5.C). Signal bleed through between each channel was largely eliminated by adjusting the pinhole of each channel, as well as the excitation and detection set up which is optimized from a control experiment. In this control experiment, a solution containing 1×10^{-10} mol/l fluorescin and R6G at the same concentration as well as solutions with only 1×10^{-10} mol/l fluorescin and solution with only 1×10^{-10} mol/l R6G were applied for the determination of channel set up. The signal bleed through was determined by comparing signals at each channel obtained from solution containing both the fluorophores and solutions with single dye. After confirmation that signal bleed through from other channel did not exceed the intensity of background signals, single color PCH analysis was

conducted for each channel, thus revealing the oligomerization states of each component of the complex.

As the average brightness signal for each protein in complex was comparable to that in the membrane with individual membrane proteins, the brightness of signal from each channel was correlated to the brightness of dye labeled antibody in solution. Particle numbers were estimated from the frequency of the peaks in the intensity-vs-time trace by comparison to a standard DOPC bilayer with 0.001% TRITC-DHPE.
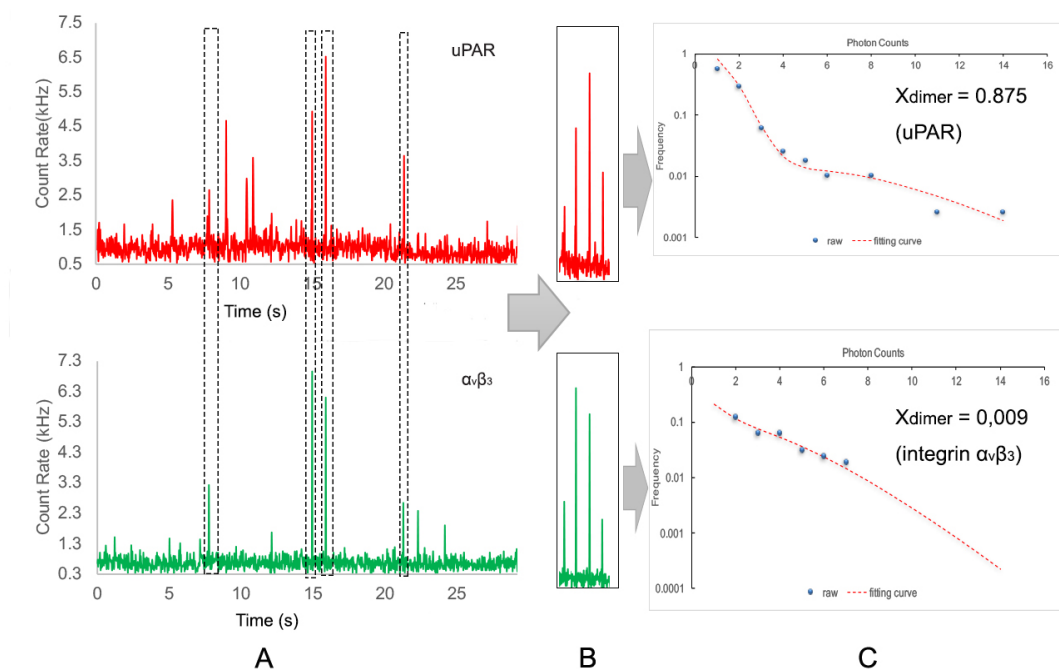
Fig. 3.5. A sample work flow for PCH analysis of protein complexes. In specific, signals from complexes were first identified from the FCS time-intensity-trace (A). Then the signals were isolated from the rest of the time-intensity-trace (B). The newly isolated signals were further binned and and analyzed using PCH analysis(C) to determine oligomerization states of protein in complex.

3.2.7 Fabrication of Polymer-Tethered Single Bilayer and Multi-Bilayer Stacks with Dynamic Linkers mimicking Cell-Cell Linkage

To fabricate polymer-tethered lipid bilayers for the purpose of mimicking the linker dynamics at cell-cell interface, single bilayers, as well as multi- bilayer stacks, were both applied. Single bilayers were made with LB/LS method in an identical way as making Type I lipid bilayers, albeit a different lipid composition was used. In this case, the LB layers of these lipid bilayers contained 5mol% of DSPE-PEG 2000, the remaining composition was POPC lipids, while the LS layer contained 0.005-0.5mol% of DGS-NTA Ni-chelating lipid for further binding of cadherin chimera with His-tag. The multi-bilayer stacks were fabricated as described in section 2.1.1. Specifically, the first bilayer in the multi-bilayer stack was fabricated using LB/LS method, where both LB and LS leaflets contained 5mol% PEG-2000-Mal and 95% POPC.

As mentioned in section 2.1.1.2, maleimide- thiol coupling chemistry between DPTE and PEG-2000- Mal were used to form stable linkages between adjacent bilayers and vesicle fusion process was applied for the layer-by-layer assembly. GUVs containing 5mol% DPTE and 95 mol% POPC were applied for the fabrication of second and fourth bilayer, whereas GUVs with 5% PEG-2000-Mal and 95mol% POPC were used to assemble the third bilayer. GUVs encapsulated a water based buffer with 0.1mM sucrose/1mM $CaCl_2$ to assist the GUV transportation to the substrate through gravitation. GUVs were allowed to bind to the previously formed bilayer by adding them into the earlier assembled bilayers surrounded with 0.1mM glucose/1mM $CaCl_2$ water solution. Following incubation for 2hrs, and then being rinsed with MilliQ water to remove excess GUVs. For GUVs in the top bilayer of the stack, 0.005-0.05mol% of DGS-NTA Ni-chelating lipids were substituted for the same amount of POPC and both the sucrose and glucose buffers were made to be Ca^{2+} free.

Followed by the fabrication of lipid bilayers and bilayer stacks, Alexa-555 labeled N-cadherin chimeras with 6 his-tags were added to the bilayer at a ratio of 5:1 ratio to DGS-NTA lipids in the bilayer. After a 1hr incubation, excess N-cadherin chimera were rinsed

off by extensive rinsing of PBS until no signal from Alexa-555 channel was observed in solution by FCS.

3.2.8 Cell Culture

C2C12 myoblast cells were kept at 37°C in a humidified 5% CO_2environment. DMEM based media described in the previous section was used for cell culturing. For cell passaging, 2ml of 2.5% trypsin were applied and incubated for 10min to fully detach cells from the 75ml culture flask. Cells were passaged at the ratio of 1:7 . C2C12 cells were cultured till confluent (3-4 days) before next passage and only cells beyond the 5th passage were applied to the substrate for quantitative analysis and no cells beyond 15th passage were applied for quantification.

Before adding cells to the lipid bilayer substrates, cell culture media with Ca^{2+} was added to the bilayer for the activation of cadherin chimeras. Following that, cells were plated at a density of 160cells/mm^2 and incubated for at least 2hrs to allow initial cell adhesion. Typically, cells were imaged after 24 and 48hrs after seeding.

3.2.9 Live Cell Imaging and Data Acquisition using Laser Scanning Confocal Microscopy

Live cell imaging was achieved through a combination of Laser Scanning Confocal Microscopy (FV1000, Olympus USA, Center Valley, PA) equipped with an active Z-drift compensation module (ZDC,Olympus USA, Center Valley, PA) and a stage incubator (Tokai Hit Co.Ltd, Japan). The stage incubator was adjusted to operate at the temperature of 37°C and humidified 5% CO_2 Bio-blend gas was applied during live cell imaging. A 60x objective was used for image acquisition (UPlanSAPo 60x/1.15).

To ensure the fluorescent signals acquired were indeed obtained from the cell-substrate interfaces, point spread function in the XY (Fig. 3.6.A) and Z (Fig. 3.6.B) dimensions were determined using 0.2μm fluorescent beads, thereby utilizing the Alexa 555 detection setup. While the thickness of spread C2C12 myoblast cells was evaluated by labeling with

a live/dead cell kit (Fig. 3.6.C). According to the Z-scale profile obtained from fluorescent beads and fluorescent labeled cell images, fluorecent images of Alexa555-labeled cadherin-chimeras were checked at the bilayer plane and 6μm above the plane. Only samples with no fluorescent signal obtained at the higher plane were considered for further image acquisition.
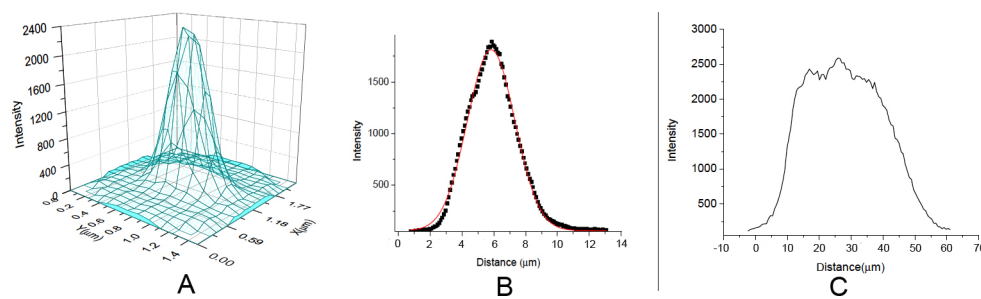
Fig. 3.6. Fluorescent intensity profile of fluorescent beads with a diameter of 0.2μm. (A) illustrates intensity profile at XY plane, while Z-scale intensity profile is shown in B. Point spread function will be determined by Gaussian fitting (shown as red curve) of the intensity profile. Moreover, the fluorescent intensity profile of a adhered cell is illustrated by C. B and C show distinct information on the intensity profile at Z-scale.

To quantify the cadherin chimera linker dynamics, time series image acquisition was applied. In specific, differential interference contrast (DIC) images and fluorescent images from Alexa 555 channel were acquired at the same time. Confocal images were taken every 20 seconds with ZDC being activated, at least 20 sets of images were acquired for a reliable quantitative analysis of linker clustering and dynamics. To determine the influence of cytoskeleton on cadherin linker dynamics, LaB, was added to the cell culture flask to the concentration of 10μM. Time series image acquisition was pursued at 0, 30, and 60mins after agent treatment, with the identical manner of image acquisition as before pharmacological agent treatment, thereby following identical imaging acquisition protocols as described on sample without LaB.

3.2.10   FRAP Experiment and Data Analysis

FRAP experiments were conducted using laser scanning confocal microscope (FV1000, Olympus USA, Center Valley, PA) combined with ZDC and stage incubator. Time series images were taken for the fluorescent intensity analysis. A specific tornado scan mode was applied for fast-intensive photon-bleaching of one specific ROI. Followed by the photon-bleaching procedure, images were taken until fluorescent intensity signal reached a plateau. Images were taken every 20secs for 20 minutes. Intensity values were corrected for pho-tobleaching caused during data acquisition. The FRAP data were analyzed as previously described (section2.1.2.4) [98].

3.2.11   Cluster Tracking

The cluster tracking analysis based on the LAP principles was achieved by the uTrack software. Cells were separated into the front area and the tail area according to the center of the nucleus and the migration orientation. All images were therefore cut into two different parts and analyzed. The tracking process was adjusted according to the nature of cadherin clustering.

First, to detect cadherin clusters, the comet detector mode in uTrack was applied. This detection algorithm was first introduced for the tracking analysis of micro-tubule dynamics, where the target was constantly assemble and disassemble during the tracking processes. The detecting algorithm includes two separate steps. The signals were rst processed using a difference-of-Gaussians approach [196] to eliminate high-frequency intensity fluctuations due to noise as well as potential larger scale variations in cell background and to create a relatively uniform background. Following that step, the coordinates of clusters were extracted using a watershed-based method which treated the cluster as a 3D intensity pro-file, allowing uniformed intensity in one particle as well as a variation on the size of the tracked clusters without any pre-assumption of the particle size and intensity. In this work, such intensity profiles are built based on PSF described in section 3.2.9(Fig. 3.6). In spe-cific, the minimum threshold was set as the standard deviation of the PSF determined by

0.2μm-diameter uorescent beads. The watershed threshold step size was set to be a standard deviation of the PSF. This setting, according to Applegate et al., allowed the detection of clusters larger than 0.2μm in diameter where the threshold step size ensured more than 99% successful detection of all clusters in one sample [196]. Additionally, to obtain optimized difference-of-Gaussian background filter, several parameters were tested for the most optimized condition. The final resulting filter was set with a low-pass Gaussian of 1 pixel and high-pass Gaussian of 4 pixels, where each pixel was 0.078μm. This filter setting prevents the detecting algorithm from treating background signals as cluster signals without losing the ability of detecting target clusters.

The tracking analysis was done under the Brownian and directed motion analysis to ensure successful tracking of both types of clusters that move randomly and oriented by cytoskeleton-driven forces. The Brownian search range was set from 2 to 10 pixels during a frame-to-frame linking. In the gap closing part, the gap was set to be 1 frame. This is according to our hypothesis that in our platform, dye-labeled cadherin chimera clusters only exist on bilayer substrates where no out-of-focus events are expected to happen. In the event of track merging, clusters were allowed to exhibit 30% intensity variation, and the merging radius was set to be identical to the Brownian searching range. Followed by the track analysis and merging analysis, the cluster moving speed and displacement were directly calculated from the resulting coordinates.

4. RESULTS AND DISCUSSION

4.1 Probing Oligomerization and Sequestration of Urokinase Plasminogen Activator Receptor (uPAR) Reconstituted in Model Membrane Mixtures

As mentioned in section 2.2.1, the raft-associated receptor function is considered one of the key features of lipid rafts in cellular functions [197]. It has been indicated that CHOL depletion interferes not only with raft affinity of GPI-AP but also with the oligomerization state of receptors [161]. Moreover, ligand-induced allosteric changes in membrane protein organization are recognized as one of the most important factors that may induce changes in membrane protein oligomerization and raft-association. For example, Caiolfa et al. reported the association between ligand-induced receptor dimerization state change and uPAR distribution in polarized cells, suggesting a mechanism of uPAR sorting through regulation of receptor oligomerization [31, 32]. This particular GPI-AP is one of the key members of the plasminogen system and plays important roles in processes including signal transduction, cellular adhesion, differentiation, proliferation, and migration, especially under pathological circumstances [27, 28] . Its function, partially achieved by functional dimer formation, is closely related to the development of certain diseases such as inflammation, infection and tumorigenesis [27, 28]. However, there is still uncertainty about the relationship between raft domains, ligand binding, and uPAR oligomerization. This uncertainty is not only due to the transient nature of lipid rafts in plasma membranes, but can also be attributed to the lack of knowledge about ligand-induced allosteric changes of uPAR conformation and their impact on uPAR raft-association [10, 116].

As illustrated by Fig. 4.1, we employed raft-mimicking lipid mixtures to investigate the interesting relationship between raft domains and uPAR oligomerization, and the role of native ligands. In this case, uPAR reconstitution, the resulting diffusion coefficient of uPAR as well as its oligomerization states were first determined in Type I lipid bilayers

with binary mixtures containing DOPC and CHOL without l_o-l_d phase separation. Subsequently,lipid bilayers containing DOPC-DPPC-CHOL with bilayer-spanning l_o-$l_d$phase separation (Type II) and lipid bilayers showing l_o-l_d phase separation only at LS leaflet (Type III) were both applied to explore the relationship between the receptor dimerization level and raft affinity. Native ligands, including uPA and vitronectin (VN), were added seperately to the membrane with reconstituted uPAR to reveal the influence of ligand binding on uPAR oligomerization states and raft affinity.
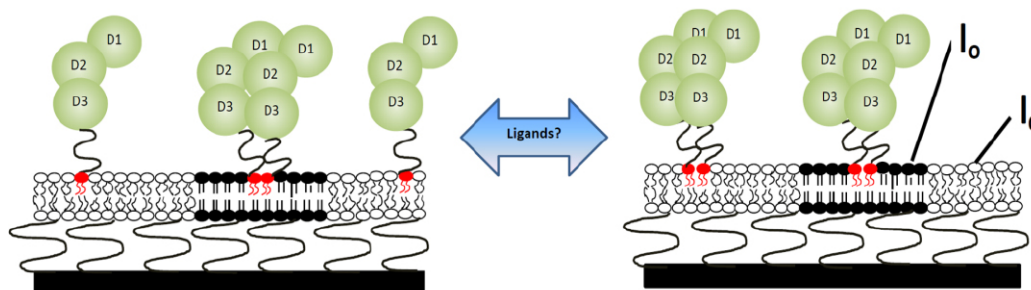
Fig. 4.1. Schematic of Type II polymer-tethered lipid bilayer with functionally reconstituted uPAR. The role of native ligands (uPA and VN) and lipid environment in uPAR dimerization and sequesteration is investigated [195].

4.1.1 Ligand Binding Alters Oligomerization in Type I Bilayers

An experimental assay was designed, in which, uPAR with a DDK-tag at the C-terminal was reconstituted into polymer-tethered lipid bilayers according to the protocol described in section 3.2.2. To enable fluorescence imaging experiments, uPAR was labeled with an Alexa-555-tagged anti-DDK monoclonal antibody, which binds to the DDK tag near the C-terminal region of uPAR, close to the GPI anchor. CS-XY analysis showed that, uPAR

was homogeneously distributed in Type I lipid bilayers (Fig. 4.2.A). The concentration of uPAR in Type I lipid bilayers was determined by comparing the fluorescence intensity of uPAR against TRITC-DHPE of known concentration serving as a standard. In this case, the molecular brightness of TRITC-DHPE and uPAR antibody are normalized. If all protein added were incorporated into the bilayer and 100% antibody-labeled, we would have the identical calibration curve as TRITC-DHPE (shown as solid black markers of uPAR intensities in Fig. 4.2.B). The slope of the TRITC-DHPE calibration curve is 1.069×10^5
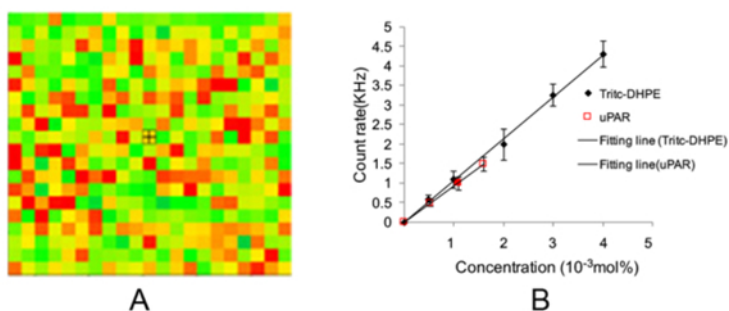
Fig. 4.2. Typical CS-XY scan data (A) of uPAR distribution (illustrated by Alexa 555-labeled MAb) in Type I bilayers containing DOPC only. No large-scale phase separations were observed. Box size 10 x 10 μm^2. Calibration of fluorescence intensity by comparing different concentrations of TRITC-DHPE (diamond) and antibody-labeled uPAR in the bilayer (square). The typical amount of uPAR (1.3×10^{-11} mol) is shown as a solid red square [195].

(kHz/mol%), whereas the slope for uPAR is 0.92×10^5, indicating that 86% of the uPAR are functionally labeled [195]. Moreover, the results from Fig. 4.2.B showed that there is no notable antibody-mediated uPAR crosslinking. Based on the 86% reconstitution rate, the highest possible crosslinking rate is 14%, assuming the highly unlikely situation that all uPAR molecules are reconstituted in the membrane. Even in that case, the crosslinking efficiency is extremely low. These results also confirmed that: (i) uPAR is sufficiently reconstituted with the functional orientation; and (ii) anti-DDK antibodies applied in this project have a high labeling efficiency to uPAR without interfering with the natural states of

uPAR clustering under our experimental setup. Therefore, Alexa 555- tagged anti-DDK antibodies work as excellent labeling agents for analyzing uPAR sequestration and oligomerization FCS analysis of a bilayer with reconstituted uPAR. Experiments on uPAR labeled with anti-DDK Mab was conducted in the absence of any ligands, as well as in the presence of uPA and VN, respectively. Such experiments were first conducted in Type I bilayers with DOPC. Fig. 4.3 illustrates the raw FCS intensity-time trace (Fig. 4.3.A) of uPAR in the presence of ligands in Type I CHOL free bilayers, together with the corresponding PCH raw data (Fig. 4.3.B) and X_{dimer} values obtained from PCH curve fitting (Fig. 4.3.C). As displayed in Fig. 4.3.C, in the absence of any ligands, the average X_{dimer} value was calculated to be 0.26, whereas uPA addition almost completely suppresses uPAR dimer formation, resulting in an average X_{dimer} value of 0.02. In contrast, the presence of VN triggers uPAR dimer formation (average X_{dimer}: 0.43) [195]. These results provide significant evidence that uPAR dimerization is highly dependent on the the presence of specific ligands.
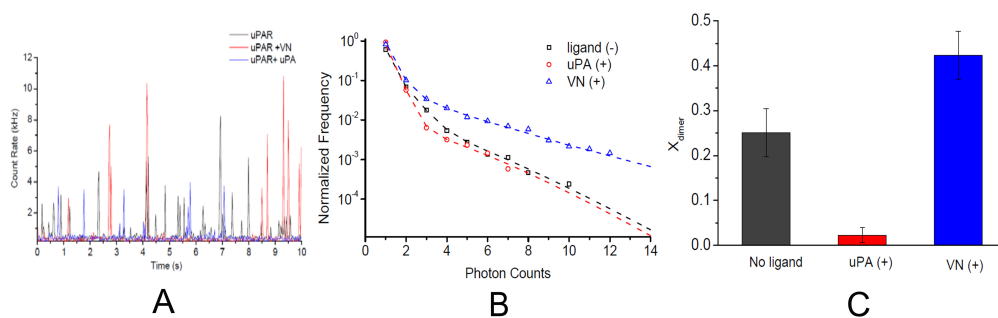
Fig. 4.3. FCS time-intensity-trace (A), experimental PCH data and fitting curves (B), and fraction of dimers, X_{dimer}, as obtained from PCH analysis (C), of uPAR (black), uPAR +uPA (red), and uPAR +VN (blue). The X_{dimer} data (ANOVA test: $p < 0.01$) indicate the distinctive influence of uPA and VN on uPAR dimerization levels. Each X_{dimer} histogram bar is based on 30 individual PCH readings from 6 bilayers. Error bars represent corresponding standard deviations. ANOVA test for each presented X_{dimer} value was conducted with 3 data sets of 10 PCH readings per data set [195].

The different uPAR dimerization levels obtained from PCH analyses are further confirmed by determining uPAR diffusion using FCS autocorrelation analysis (Fig. 4.4). Here the diffusion coefficient of uPAR (without ligand) in the bilayer was D = $1.37 \pm 0.26 \mu m^2$/s, whereas addition of uPA led to a faster diffusion of the receptor, D = $1.65 \pm 0.52 \mu m^2$/s [195]. Furthermore, relatively slow uPAR diffusion of D = $1.02 \pm 0.34 \mu m^2$/s was observed upon VN addition. In this assay, each diffusion coefficient was determined from 40 FCS readings obtained from ten different bilayer samples (error bar values represent corresponding standard deviations) [195]. The FCS data show that VN addition leads to the lowest lateral mobility of uPAR, which can be explained by the increased level of uPAR dimerization in the model membrane. In contrast, uPA addition increases uPAR lateral mobility, leading to a diffusion coefficient that is almost identical to the diffusion coefficient of TRITC-DHPE (D = $1.68 \pm 0.20 \mu m^2$/s) [195], while intermediate uPAR dimerization levels lead to an intermediate uPAR diffusion coefficient, in good agreement with the findings from the PCH analysis. Importantly, our results obtained from FCS and PCH analyses are in excellent qualitative agreement with previously reported uPAR dimerization behavior in epithelial cells [157]. In this cellular study, VN addition also promoted the formation of uPAR dimers, while uPA and uPA-PAI1 addition enhanced monomer formation in the monomer-dimer equilibrium. It has been revealed that for both soluble uPAR (suPAR) [198] and GPI-anchored uPAR [199], uPA and VN interact with D1 and D2 domains at different binding sites, thereby introducing structural changes to the receptor. Though the structural details of the uPAR dimer remain unclear, the effect of ligands on receptor oligomerization states has been reported in several occasions, including both GPI-anchored and transmembrane receptors [200–202]. In those cases, ligand-receptor interactions often trigger formation of connecting structures, such as dimerization loops [200] and disulfide bonds [202].

Recent reports indicate that uPA binding might induce uPAR to a closed conformation [203]. Moreover, it has been reported that uPA binding reduces uPAR-uPAR interactions by triggering uPAR cleavage [157]. Therefore, the observed uPA mediated suppression of uPAR dimerization in our model membrane assay suggests a similar mechanism
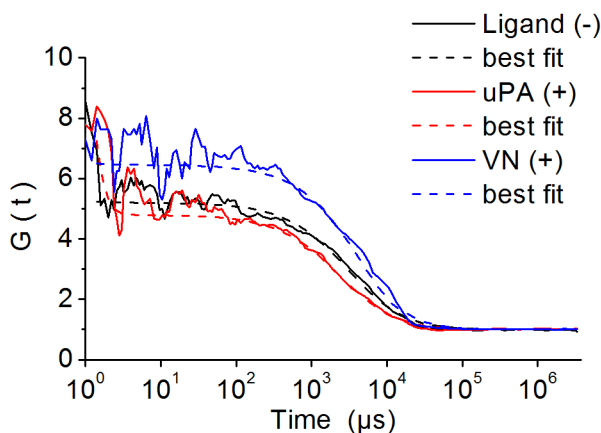
Fig. 4.4. Representative FCS auto-correlation data and fitting curves of uPAR, uPAR + uPA, and uPAR + VN on polymer-supported lipid bilayers. Detection of uPAR was accomplished using Alexa 555-tagged anti-uPAR MAbs [195].

of uPA-induced structural change of uPAR, as well as uPA-mediated cleavage of the D1 domain of uPAR. Previous cellular experiments indicated that uPA cleaves the D1 domain of uPAR under physiological conditions by interacting at two specific sites at the D1-D2 linking region [204]. Other experiments showed that uPA cleavage is dependent on the GPI-anchorage of uPAR, illustrating the fact that uPA cleavage of suPAR is relatively limited [205]. To probe the proteolytic activity of uPA, an Alexa-555 labeled N-terminal antibody was applied and the fluorescence intensity in solution above the uPAR containing bilayer was monitored through the Alexa-555 channel using a Confocor FCS system. This fluorescence-based assay has single molecule sensitivity. Its sensitivity is superior over traditional methods, such as western blotting. In this experiment, uPAR tagged with N-terminal specific anti-uPAR antibody was investigated under three different conditions (uPAR only, uPAR+ uPA, uPAR+VN). As illustrated by Fig. 4.5, a time-dependent increase of fluorescence intensity in solution can only be observed in the case of uPAR+uPA using Alexa-555 labeled N-terminal antibody. In contrast, a control experiment where a dye labeled anti-DDK MAb specifically binds to the C-terminal DDK-tag of uPAR, no variation

of fluorescence intensity was observed in solution. Together, these results indicate that uPA induces cleavage of the N-terminal of uPAR reconstituted into the polymer-tethered lipid bilayer, in good agreement with previous results of the same receptor during plasma membrane studies [204]. These findings are significant because they demonstrate that uPAR reconstituted into polymer-tethered lipid bilayers holds a similar activity relative to uPAR under physiological conditions. Moreover, our results support a relationship between uPA induced uPAR cleavage and drop of the dimerization level.
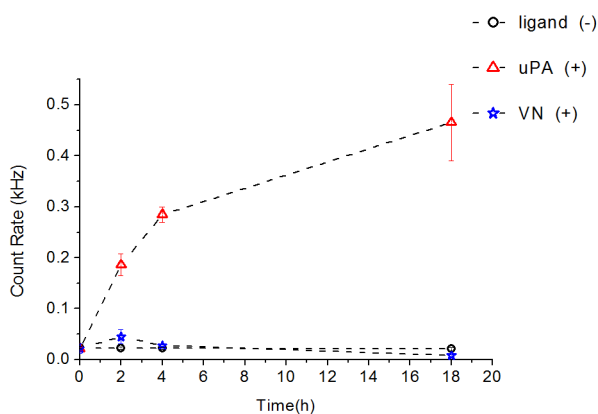
Fig. 4.5. Time evolution of confocal photon count rate in solution (200μm above the planar polymer-tethered lipid bilayer with incorporated uPAR). Experiments were conducted on uPAR (without ligands), uPAR +uPA, and uPAR +VN. Fluorescence intensity data were collected from 5 bilayers with 10 readings per bilayer for each time spot. Error bars indicate the standard deviation between each bilayer. The statistical significance was comfirmed through ANOVA with 5 data sets of 10 fluorescence readings per data set ($p < 0.005$) [195].

4.1.2 Analyzing Influence of CHOL Content on uPAR Oligomerization Using Type I Lipid Bilayers

The GPI anchor of GPI-AP has long been considered an apical sorting motif, possibly due to the association of such membrane to lipid rafts [13, 206]. However, this proposed

mechanism has been questioned by the finding that GPI-APs are sorted to both the apical and basolateral membrane of MDCK cells [31]. More interestingly, previous research indicated that CHOL content is a key requirement for GPI-AP oligomerization at the apical side of the cell [161]. However, the effect of CHOL on membrane protein oligomerization appears to be relatively complex. While some specific membrane proteins, such as Ras, show different oligomerization and clustering dependent upon on the CHOL contents at different parts of the cell membrane [118]; for other membrane proteins, such as GH-DAF, their clustering is largely affected by CHOL depletion [207]. To investigate the influence of CHOL content on uPAR oligomerization, the content of CHOL in TYPE I bilayers was systematically changed from 0 to 35 mol% CHOL and uPAR dimerization levels were determined using PCH analysis. Representative PCH data are shown in Fig. 4.6, while the resulting X_{dimer} values are presented in Fig. 4.7. As illustrated by Fig. 4.7, uPAR dimerization levels are slightly lower in the absence of CHOL, but did not change in response to different CHOL concentrations in the membrane. In contrast, addition of ligands, including uPA and VN, have a substantial influence on uPAR dimerization in Type I bilayers.
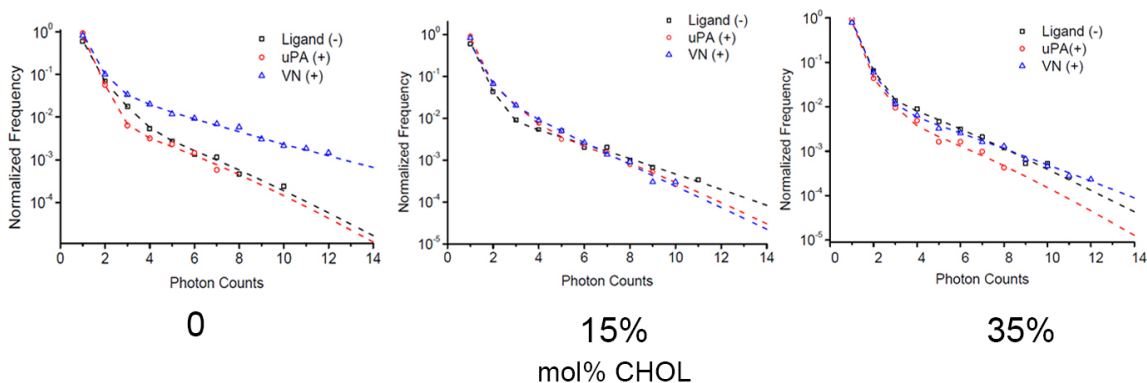
Fig. 4.6. Representative PCH data and fitting curves of uPAR embedded in a polymer-tethered lipid bilayer containing binary DOPC-CHOL lipid mixtures of 0 (left), 15 (center), and 35mol% (right). In each case, uPAR results are shown for three different situations: (1) uPAR without ligands, (2) uPAR + uPA, and uPAR + VN [195].
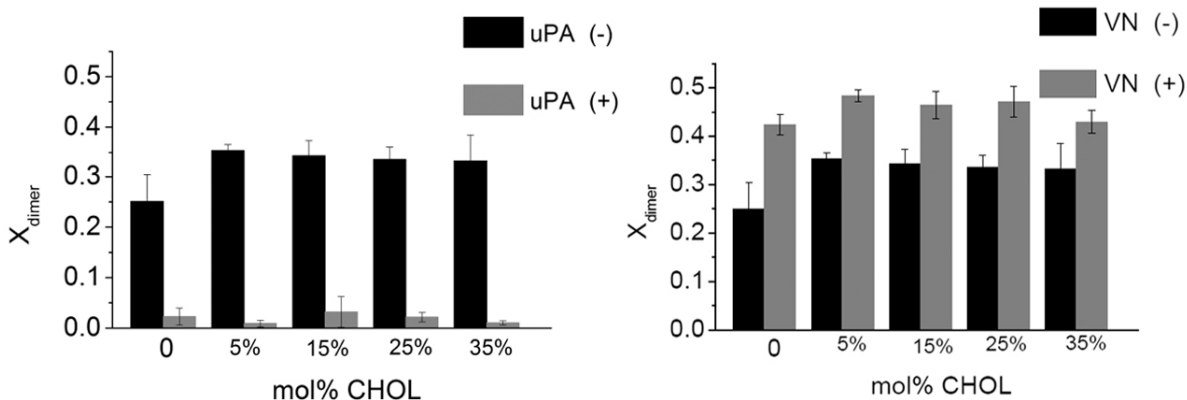
Fig. 4.7. Fraction of dimers, X_{dimer}, of uPAR, uPAR + uPA, and uPAR + VN in Type I lipid mixtures. The statistically significant X_{dimer} data (ANOVA test: $p < 0.005$) show that uPA suppresses uPAR dimerization (left), whereas VN has the opposite effect (right). Variation in CHOL contents has no notable impact on the dimerization levels of uPAR. Presented X_{dimer} values are obtained from six bilayers (ten spots each bilayer). Error bars illustrate standard deviations. ANOVA test was conducted with 3 data sets of 10 PCH readings per data set [195].

Together, our model membrane results indicate that uPAR dimerization is not directly linked to the membrane CHOL level. These results are in good agreement with corresponding results on uPAR in cell membranes, which showed that lower CHOL content in the plasma membrane does not alter dimerization of GPI-anchored uPAR and raftphobic transmembrane uPAR chimeras, indicating that uPAR dimerization is independent of both the GPI motif of the protein and CHOL content. [157]

4.1.3 Evaluating Influence of Native Ligands and CHOL content on uPAR Oligomerization and Sequestration in Type II lipid bilayers

To explore the mechanisms that drive GPI-AP association with lipid rafts, oligomerization and sequestration of uPAR were investigated using Type II lipid bilayers with co-existing l_o and l_d domains. Specifically, the oligomerization and sequestration of uPAR

were first investigated in DOPC/DPPC/CHOL lipid mixtures with 5mol% lipopolymer in the bottom leaflet. In each imaging experiment, $\sim 10^{-3}$mol% uPAR were incorporated into the bilayer system. As mentioned in the previous chapter, NBD-DHPE was applied
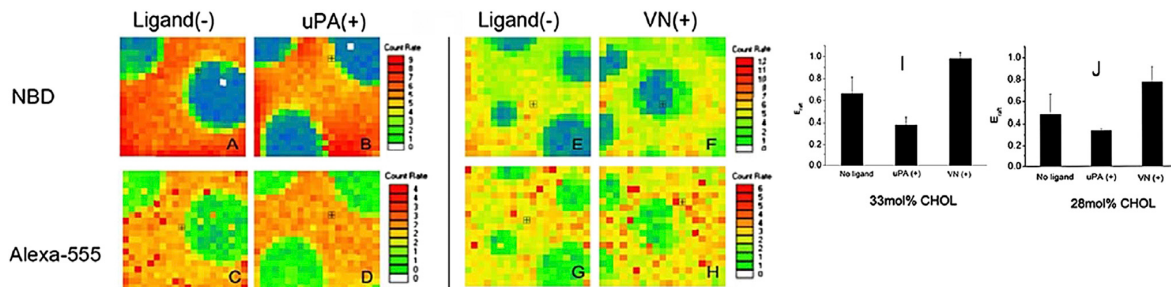
Fig. 4.8. Representative CS-XY scans (raw data) of uPAR distribution in a polymer-tethered lipid bilayers with coexisting l_o and l_d domains (33mol% CHOL, left) before (A, C, E, and G) and upon addition of the ligands uPA (B and D) and VN (F and H). The l_o and l_d lipid phase separation is illustrated through NBD-PE (top row: A, B, E, and F) and uPAR distribution is monitored using Alexa-555 (bottom row: C, D, G, and H). I and J, represent E_{raft} values (t-test: $p < 0.01$) of uPAR (without ligands), uPAR + uPA, and uPAR+ VN in Type II lipid mixtures with 33mol% CHOL (I) and 28mol% CHOL(J). Box size $10 \times 10m^2$. E_{raft} data for each ligand exposure state in I and J is based on four bilayers (five readings per bilayer). Error bars represent corresponding standard deviations. t-test was conducted with two data sets consisting of 10 E_{raft} readings per data set [195].

as an illustrator of the l_o-l_d lipid phase separation, while uPAR sequestration was revealed through Alexa-555 tagged anti-DDK antibody. Fig. 4.8 presents results of the uPAR sequestration in the 1:1:1 lipid mixtures acquired through the NBD (lipid distribution) and Alexa-555 (uPAR distribution) channels. In this case, E_{raft} values were determined for uPAR, uPAR+uPA, uPAR+VN. As illustrated by the CS-XY scans (A-H), the uPAR distribution is in good correlation to the NBD-DHPE distribution indicating l_o-l_d phase separation. Because NBD-DHPE shows a higher affinity for the raft-mimicking l_o phase, the colocalization of Alexa555 channel data demonstrates that uPAR, as GPI-AP, also exhibits a high l_o affinity. This raftophilic property of GPI-AP is not only well documented through

cellular membrane studies [17, 119] but also confirmed in the studies on model membrane studies with coexisting l_o-l_d domains [50]. As indicated through CS-XY scans of uPAR distribution shown in Fig. 4.8.C, D, G, H, which was quantified using E_{raft} values present in Fig. 4.8.I, addition of uPA decreases uPAR raft affinity, while VN-binding promotes uPAR recruitment toward the raft-mimicking l_o phase. These ligand-induced effects on uPAR raft-sequestration are intriguing in light of the observed impact of uPA and VN on uPAR dimerization in DOPC and CHOL mixtures, suggesting a link between ligand-mediated regulation of uPAR dimerization and sequestration in raft-mimicking lipid mixtures.
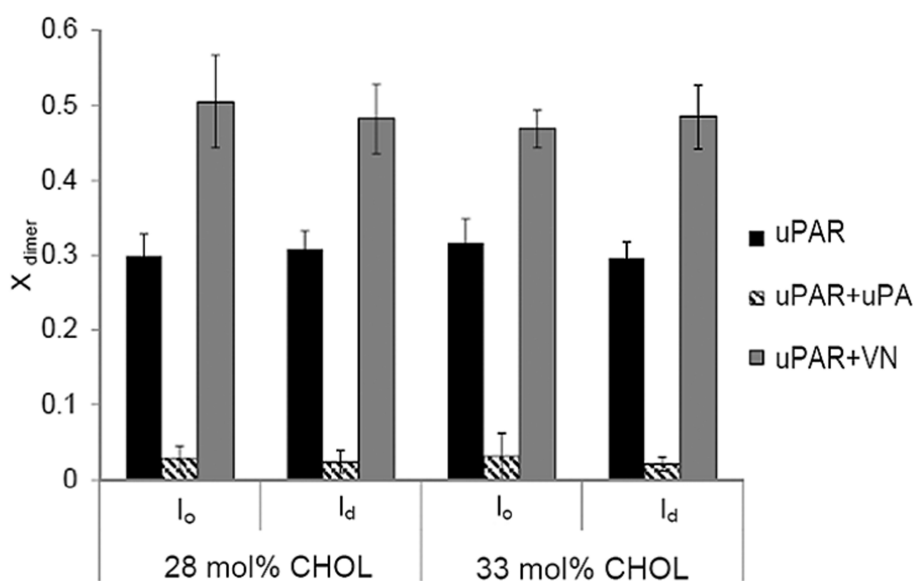
Fig. 4.9. Influence of uPA and VN on X_{dimer} in Type II lipid bilayers with 28 and 33mol% CHOL. In agreement with the X_{dimer} results in Type I lipid bilayers, both ligands alter X_{dimer} (ANOVA test p¡0.01) in a qualitatively different manner. No measurable difference in uPAR dimerization is observed in l_o and l_d phases. Furthermore, CHOL level in Type II lipid bilayers does not influence uPAR dimerization levels [195].

To further analyze the link between ligand binding, dimerization, and lipid environment, we next pursued the domain specific analysis of laterally mobile uPAR receptors in polymer-tethered lipid bilayers. In this case, Type II bilayers with 28mol% CHOL were investigated to determine uPAR sequestration (E_{raft} value presented in Fig 4.8J) and dimer-

ization (Fig. 4.9). Fig. 4.9 shows representative X_{dimer} data, which confirms that uPA and VN influence uPAR dimerization levels in a significant manner. As described before in Type I bilayers, uPA significantly depleted uPAR dimer formation, but greatly enhanced uPAR dimerization was seen upon the addition of VN. Notably, these ligand-induced effects are seen in both l_o and l_d phases regardless of CHOL level in the membrane.

The X_{dimer} results from Type II bilayers are in good agreement with those from Type I bilayers, where uPAR dimerization level is independent of CHOL content in the bilayer. Our results based on Type II bilayers do not support a mechanism, in which receptor sequestration is entirely regulated by the receptor dimerization level. Instead, the E_{raft} and X_{dimer} data in Figs. 4.8 and 4.9, respectively, suggest that other contributing factors may be involved in the regulation of uPAR sequestration in coexisting l_o-l_d domains. Indeed, as illustrated in Fig 4.10, uPAR exhibits moderate differences in raft affinity in Type II bilayers (Fig. 4.10.A) containing different CHOL levels (28, 33, 37mol%), while X_{dimer} values stay relatively constant (Fig. 4.10.B). This finding suggests a potential role of CHOL-induced lipid packing density variation in l_o and l_d domains in uPAR raft sequestration. However, such potential effects of CHOL-induced change in uPAR sequestration is not statistically significant based on our experimental assay. Further experiments with other lipid mixtures are required to verify this observation.

4.1.4   Investigating Impact of Bilayer Asymmetry on uPAR Sequestration and Oligomerization in Type III Lipid Bilayers

One important feature of the plasma membrane of eukaryotic cells is the asymmetric distribution of lipids and membrane proteins between each leaflet. One consequence of such an asymmetry is the higher possibility for lipid rafts to assemble in the exoplasmic leaflet of the membrane [13]. However, characterization of such asymmetric structures on membrane protein sequestration is quite limited, due to the complexity of the plasma membrane and the transient nature of raft structures therein. To investigate the influence of
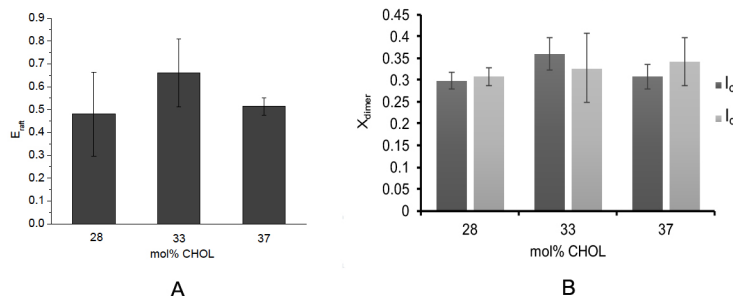
Fig. 4.10. uPAR dimerization and sequestration in Type II lipid bilayers with 28, 33, and 37 mol% CHOL. In agreement with the X_{dimer} results in Type I lipid bilayers, no measurable difference in uPAR dimerization is observed in l_o and l_d phases. Furthermore, adjustment of CHOL level in Type II lipid bilayers does not influence uPAR dimerization levels. However, uPAR raft affinity slightly changes in Type II bilayers of different membrane CHOL level.

bilayer asymmetry on uPAR sequestration and oligomerization, Type III lipid bilayers with l_o and l_d phase separation in the LS leaflet were used.

Type III bilayers were fabricated according to the description in section 3.2.1, followed by the identical reconstitution procedure of uPAR. As illustrated in Fig. 4.11, uPAR raft affinity is comparable in both Type II and Type III lipid bilayers (Fig. 4.11.A-E). Resulting E_{raft} values indicate a slightly lower raft affinity of uPAR in Type III bilayers, but the results are within the experimental error. Moreover, X_{dimer} values of uPAR were calculated in Type III lipid bilayers.Here we discovered that dimerization values of uPAR reconstituted in a Type III bilayer were slightly lower in both l_o and l_d phases of Type III lipid bilayers, relative to Type II bilayers. Although this effect was moderate compared to that of ligand binding (uPA and VN) shown in Fig. 4.11.

Our previous research has demonstrated that Type II and Type III bilayers show different characteristics in regards to lipid packing and hydrophobic thickness [55]. In particular, Type III bilayers exhibit lower lipid packing compared to Type II lipid bilayers. Moreover, the differences in the hydrophobic thickness between l_o and l_d domains in Type II bilayers are about 3.5 Å larger compared to the hydrophobic thickness of Type III bilayers [208].
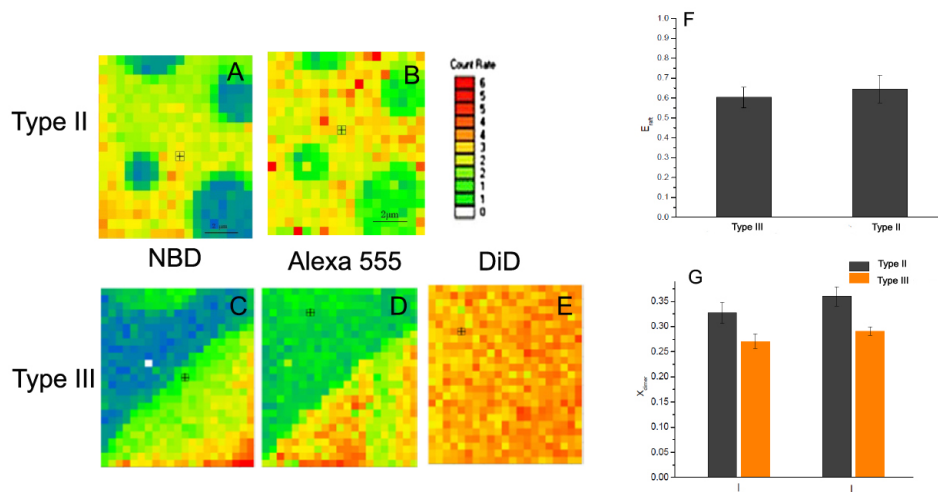
Fig. 4.11. Representative CS-XY scan of uPAR distribution in Type II (A, B) and Type III (C, D, E) lipid bilayers. In Type III lipid bilayers, l_o-l_d phase separation in LS monolayer was confirmed with NBD-DHPE (C), while homogeneous lipid distribution in the LB monolayer was verified by DiD-DHPE distribution (E). uPAR distribution in the Type III bilayer was determined through Alexa-555 channel (D) and quantified through E_{raft} analysis (F). The corresponding X_{dimer} values are illustrated in (G). Error bars show corresponding standard deviations from 4 bilayers. Each bilayer was read at 5 different positions for E_{raft} values, and 20 reads were conducted for PCH data sets to calculate X_{dimer}.

As a consequence, in our previous experiments, bilayer asymmetry was found to have a profound influence on the sequestration of transmembrane integrin [55]. In contrast, GPI-anchored uPAR exhibits almost identical sequestration and oligomerization properties in the two types of raft-mimicking bilayers, indicating that bilayer asymmetry may play a less significant role in the sequestration of GPI-AP, such as uPAR, similarly, bilayer asymmetry as a limited impact on the l_o-l_d sequestration of dye-labeled lipids like TRITC-DHPE [55].

In summary, our data showed GPI-anchored uPAR is preferentially located at raft-mimicking l_o domains in both Type II and Type III lipid bilayers. While lipid environment changes introduced by alternating CHOL content and bilayer asymmetry do not have a significant impact on uPAR dimerization and sequestration, exposure to natural ligands has a profound influence on uPAR oligomerization regardless of the lipid environment. More-

over, this ligand-induced change in uPAR oligomerization potentially influences uPAR raft sequestration properties. Our results, which are in good agreement with previous findings from cellular experiments [32, 157], demonstrate that polymer-tethered lipid bilayers work as a good mimetic system for the investigation of GPI-AP sequestration and oligomerization. Additionally, our results revealed that binding native ligands, rather than CHOL content variation, significantly influences the dimerization and sequestration of uPAR, indicating their important role in the sequestration of GPI-AP.

4.2 Analyzing Influence of CHOL on Integrin Sequestration

Integrins are a family of transmembrane proteins that are usually organized as non-covalently associated heterodimers containing α and β subunits [209]. They are not only important cell adhesion receptors that mediate cell-cell adhesion and cell-ECM interaction, but also act as crucial signaling proteins that are involved in both inside-out and outside-in signaling [210, 211]. Moreover, the function of integrin is considered an essential regulatory factor during cancer progress and stem cell behavior [212]. Recent advances in electron microscopy and crystallography have provided crucial insight into integrin-mediated signaling [209]. In specific, it is generally believed that integrin undergoes a conformational transition from a bent structure to an upright conformation upon ligand-induced activation [213], which alters the secondary structure of integrin both at the ectodomain interface and transmembrane domain.

In the previous section, we established a ligand-dominated mechanism in regulating GPI-AP oligomerization and sequestration. According to lipid raft hypothesis, lipid heterogeneities may have distinct impact on the processes of transmembrane protein sorting and the sorting of lipid-anchored membrane protein [7, 14, 214]. In fact, previous work in our group demonstrated differences of integrin sequestration in Type II bilayers with bilayer spanning l_o-l_d phase separation [54] ,and Type III bilayers which only show l_o-l_d phase separation in the LS leaflet [55]. These results suggest the importance of lipid environment on the sequestration of transmembrane integrins. Importantly, cellular ex-

periments indicated that integrin function is closely associated with lipid rafts [121, 215]. Moreover, CHOL depletion assays have indicated that CHOL is an essential regulatory factor in functionally important integrin clustering [19, 33], and cellular experiments has shown that integrin clusters at cellular FAs are dependent on the structure of lipid rafts and that FAs are enriched in CHOL [19, 34]. Regardless of these interesting observations, the role of membrane CHOL level in the regulation of integrin sequestration and recruitment processes during raft-mediated integrin adhesion and signaling is still elusive. For example, arguments still exist on whether integrin sorting and clustering are majorly due to biophysical regulation of membrane structure or biochemical processes including ligands and adapter proteins [216, 217].

To investigate the influence of CHOL on integrin oligomerization and sequestration, we applied Type II raft-mimicking bilayers with well-defined lipid composition. Specifically, we systematically changed the CHOL level in the model membrane and studied the sequestration and oligomerization of reconstituted integrin $\alpha_v\beta_3$ in lipid bilayers exhibiting coexisting l_o l_d domains. In addition, the native ligand, vitronectin (VN), was added to reveal integrin sequestration in its activated state.

4.2.1 Investigating Influence of CHOL Concentration on Lipid Packing in Raft-Mimicking Lipid Mixtures

As mentioned in chapter 2, one of the fascinating features of applying saturated lipid/ unsaturated lipid/CHOL mixtures as a raft-mimicking model system is attributed to the well defined lipid mixing behavior in such model systems. For instance, the miscibility transition temperatures can be measured as a function of lipid composition [46, 218]. Therefore, reconstituted membrane protein distribution and dynamics can be correlated to the physical properties of the bilayer, including line tension, lipid packing and hydrophobic thickness [51, 218].

To enable experiments on protein behavior in raft-mimicking model lipid mixtures of varying CHOL concentration, we used Type II lipid bilayers with equimolar amounts of

DOPC/DPPC and variable CHOL content. Previously, Veatch and Keller established a phase diagram of the DOPC/DPPC/CHOL in GUV systems and the influence of different temperatures therein (Fig. 4.12). Based on this information, we identified the phase boundary of l_o-l_d coexistence phase region at 25°C (illustrated as black dash curve in Fig. 4.12), representative Type III bilayer, and fabricated Type II bilayers with five different compositions exhibiting l_o-l_d phase separation (A-E). In addition, bilayers containing 40mol% CHOL (F) were applied to verify the phase boundary between l_d phase and l_o-l_d two phase coexistence region.
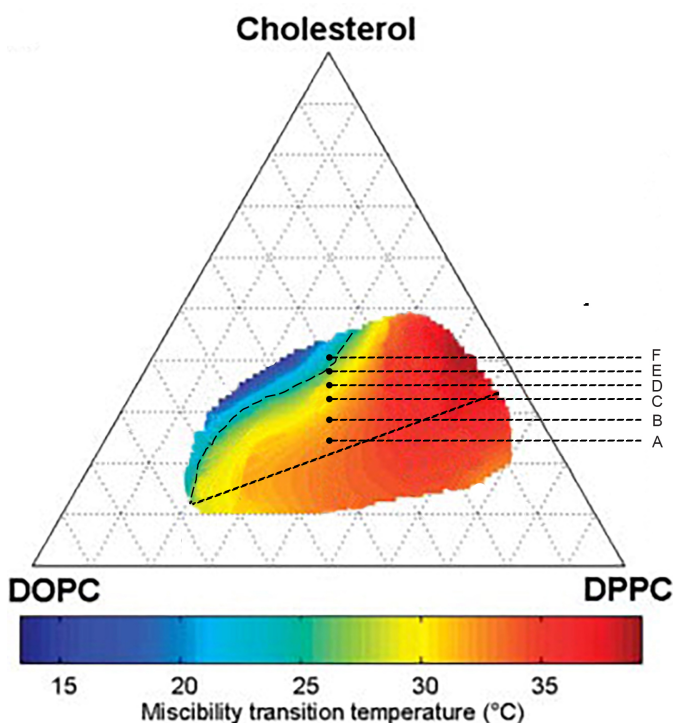
Fig. 4.12. Phase diagram of DOPC/DPPC/CHOL lipid mixtures adapted from Veatch et.al. [46]. Colored area indicates l_o-l_d coexistence phase at different lipid concentrations. Black dashed curve indicates phase boundary at 25C while points A-E indicate composition used in this research with the CHOL content of 25, 28, 33, 35, 37 mol% with DOPC and DPPC at the same ratio. 40mol% of CHOL was also applied to verify the phase boundary.

Upon fabrication of lipid bilayers, lipid phase separation was first examined using an EPI fluorescent microscope. In specific, NBD-PE was applied as a probe to visualize l_o-l_d phase separations. As illustrated in Fig. 4.13, the heterogeneous distribution of NBD-DHPE observed in bilayers containing 25, 28, 33, 35, 37 mol% CHOL indicates l_o-l_d phase separation at these compositions, where enrichment of NBD-DHPE (bright phases in EPI image) shows the raft-mimicking l_o phase. As predicted by the ternary phase diagram of DOPC/DPPC/CHOL (Fig. 4.12), bilayers containing 40 mol% CHOL exhibit a homogenous distribution of NBD-PE, suggesting the presence of a single l_d phase. This result indicates the similarity of the lipid mixing behavior in a GUV system compared to polymer-tethered lipid bilayers. Fig. 4.13 illustrates an increase in the total area of l_o domains and distinctive domain sizes in DOPC/DPPC/CHOL mixture of different CHOL content. This result is plausible because different lipid compositions (Fig. 4.12, A-F) are located at different tie-lines. Therefore, the line tensions between l_o and l_d phases at different compositions are distinguishable [218, 219]. Moreover, lipid bilayers containing 25 mol% and 37 mol% CHOL exhibit smaller domain sizes compared to other compositions, possibly due to the line tension between l_o and l_d phases decreasing as the composition approaches the phase boundary, which is in good agreement with previous reports [46, 219].

| 25 | 28 | 33 | 35 | 37 | 40 |

mol% CHOL
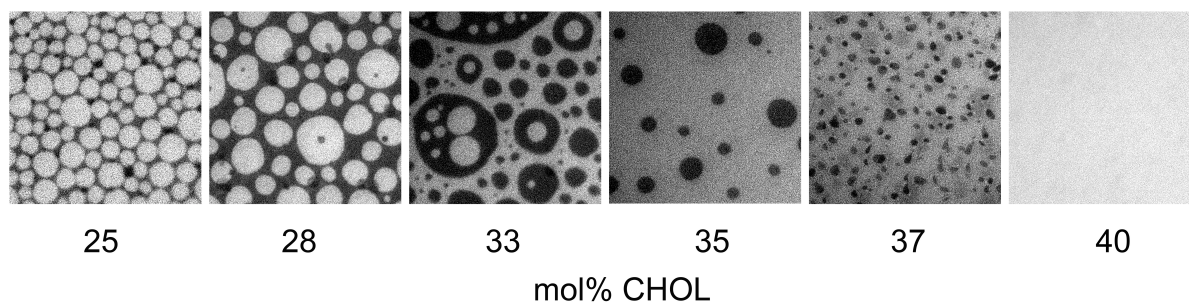
Fig. 4.13. EPI fluorescent micrographs of lipid phase separation in Type II bilayers of different CHOL content. Box size 50μm × 50μm.

Next, lipid diffusion in the various lipid mixtures was investigated using FCS autocorrelation analysis. In this case, Type II bilayers comprised of DOPC/DPPC/CHOL mixtures of varying CHOL content, with 0.001 mol% TRITC-DHPE were fabricated. FCS analyses and sequential diffusion coefficient calculation were pursued according to the description in Chapter 3. As illustrated in Fig. 4.14, lipid diffusion slows down with an increasing amount of CHOL, indicating membrane packing density increases with increasing CHOL content . Moreover, bilayers with 25 and 37 mol% CHOL showed similar lipid diffusion in l_o and l_d phases, indicating similar lipid packing in l_o and l_d phases at these compositions. This analysis also showed that the difference of l_o and l_d lipid diffusion is the largest at 33 mol% of CHOL. These findings suggest that lipid packing characteristics in Type II bilayers differs with CHOL levels in agreement with previously reported data [51]. Moreover, this difference is in agreement with line tension differences revealed by the phase diagram and domain morphology.
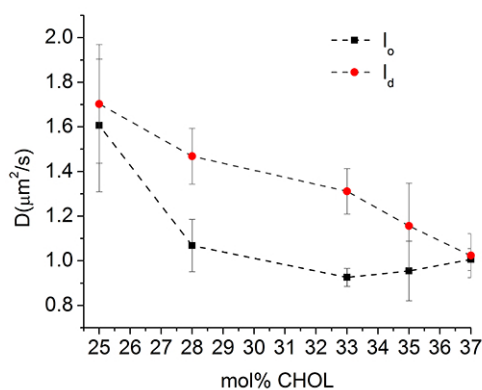
Fig. 4.14. Domain-specific diffusion coefficients of TRITC-DHPE in Type II lipid bilayers with varying CHOL content. Error bars indicate standard deviation from diffusion coefficient, data obtained from 6 different bilayers.

4.2.2 Examining Integrin Sequestration and Oligomerization in Raft - Mimicking Lipid Mixtures with Different CHOL levels

To evaluate the influence of CHOL on integrin sequestration, we reconstituted integrin $\alpha_v\beta_3$ into Type II bilayers containing 25, 28, 33, 35, and 37 mol% of CHOL. Integrin distribution was observed using Alexa-555 labeled anti-β_3 MAb, while lipid distribution was visualized using NBD-DHPE. Integrin distribution was analyzed with and without native ligand, vitronectin (VN). As illustrated in Fig. 4.15 integrin in its inactive state has a preference to reside in the l_d phase, especially in bilayers containing 33mol% of CHOL, in good agreement with our previous findings [54, 55]. However, this raftophobic behavior becomes less pronounced in bilayers with 25mol% and 37mol% CHOL. In fact, quantitative E_{raft} values indicate that integrin $\alpha_v\beta_3$ has almost no preference to the l_d phase under these two conditions. On the other hand, VN binding assists the redistribution of integrins to the raft-mimicking l_o phases. This ligand-induced integrin translocation could be seen as a consequence of a structural change in the transmembrane region upon integrin activation [54]. Again, integrins did not show a significant difference in preference to the l_o phase in bilayers containing 25mol% and 37mol% CHOL.
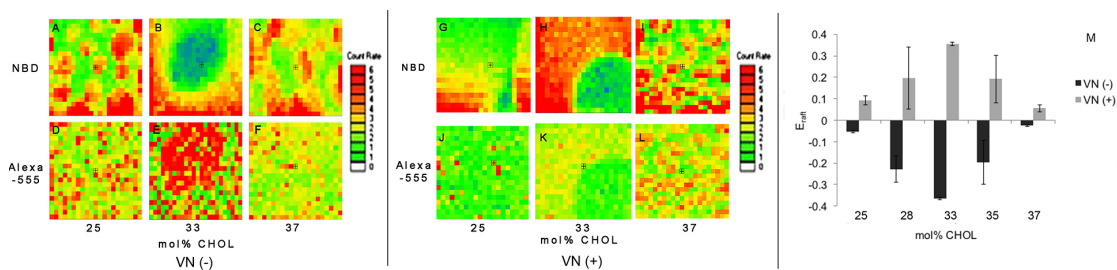
Fig. 4.15. Representative CS-XY scans of integrin and lipid sequestration before (left) and after (middle) VN addition in Type II bilayers with 25 (D,J) ,33 (E,K), and 37 (F,L) mol% of CHOL. Lipid phase separations are visualized by NBD-PE, presented in the top row, while integrin sequestration were observed through Alexa-555, presented in the bottom row. (Box sizes: $10 \times 10 \mu m^2$). Corresponding E_{raft} values are presented in M. Error bars represent standard deviation from 6 bilayers at each concentration.

Next, we analyzed integrin oligomerization states in bilayers with different CHOL content. As illustrated by Fig. 4.16, X_{dimer} values obtained from PCH analysis indicated that integrins remain mostly monomeric. Furthermore, neither changes in CHOL content nor exposure to VN have a significant influence on integrin dimerization. Together, E_{raft}
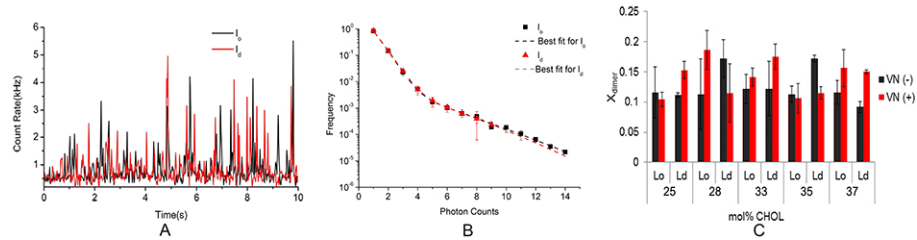
Fig. 4.16. X_{dimer} values of integrin $\alpha_v\beta_3$ in Type II bilayers containing different level of CHOL. X_{dimer} values of integrin samples with and without VN addition are calculated from FCS raw data (A) and PCH curves (B). Error bars indicate standard deviation of X_{dimer} values obtained from 4 different bilayers under each condition.

and X_{dimer} data in Fig 4.15 and Fig. 4.16 demonstrate that there is no significant correlation between CHOL level and oligomerization states of integrin. Additionally, integrin oligomerization and sequestration are not related to the CHOL level in our model membranes.

Results in section 4.1 indicate that sequestration of GPI- anchored uPAR is not significantly influenced by cholesterol content in the membrane. To quantify the different impacts of CHOL content on the sequestration of GPI-anchored uPAR (presented in section 4.1) and transmembrane integrin, we compared the E_{raft} values of uPAR and integrin $\alpha_v\beta_3$ in Type II bilayers with 37mol% and 33mol% CHOL and determined the net translocation of both uPAR and integrin $\alpha_v\beta_3$ using the following expression:

$$X_{migrate} = \left| \frac{E_{raft(33mol\%CHOL)} - E_{raft(37mol\%CHOL)}}{2} \right| \tag{4.1}$$

As illustrated by Fig. 4.17, the impact of CHOL level on the sequestration of transmembrane integrin $\alpha_v\beta_3$ and GPI-anchored uPAR in Type II lipid bilayers is distinguishable.
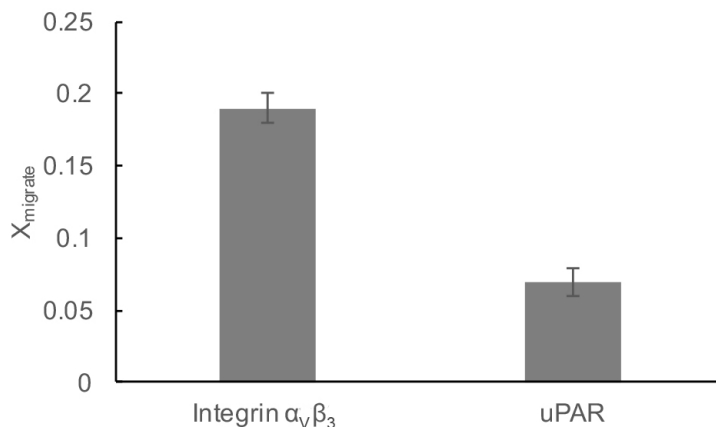
Fig. 4.17. X_{migrate} values of integrin $\alpha_v\beta_3$ and uPAR.

While 19% of integrins altered their phase preference upon CHOL concentration change, less than 7% of uPAR translocated to the other phase in the same lipid mixtures. These findings indicate that transmembrane proteins are more sensitive to a change of CHOL level in the lipid bilayer than GPI-APs. This result indicates an important role of CHOL-induced hydrophobic mismatch in the sorting of transmembrane proteins, whereas the relocation of GPI-AP between l_o and l_d phases can only be induced by changes in lipid packing.

In this section, we revealed the important role of CHOL in regulating integrin sequestration without perturbing its oligomerization states. In contrast to results on GPI-anchored uPAR, these results indicated a distinctive role for CHOL in integrin sequestration. Together, these findings highlight the critical role of CHOL in transmembrane protein sorting through purely biophysical proccesses. These findings also illustrate the potentially important role of CHOL in integrin-mediated signaling. Abnormal CHOL levels in the plasma membrane are related to several diseases, such as Alzheimers disease and cancer, and several raft-associated membrane proteins have been identified as important therapeutic targets [12]. Our platform is not limited to uPAR and integrin but also could be applied to other membrane proteins and protein complexes. Furthermore, gaining a better understanding of the biophysical role of CHOL in membrane protein dynamics, distribution and sequestration would be beneficial for the development of new therapeutic strategies.

4.3 Examining Complex Formation Between Integrin $\alpha_5\beta_1$ and GM$_3$ in Model Membrane Mixtures

Gangliosides, subspecies of glycolsphingolipids (GSLs), are known to reside in the outer leaflet of the plasma membrane [5] and are considered as important marks of lipid rafts [7, 10, 12, 23]. Additionally, ganliosides may act as important regulatory factors of several membrane proteins. Prominent examples of such as a ganglioside function include human epidermal growth factor receptor (EGFR) [220], G protein coupled receptor (GPCR) [221], prion protein [222], and integrin [137]. Previously, direct interaction between gangliosides and membrane proteins has been demonstrated through a CHOL depletion assay [39] and single molecule tracking [26], suggesting its importance in regulation of membrane protein distribution and function in the plasma membrane.

Exemplary, complex formation between integrin and GSLs might potentially play an important role in physiological and pathological pathways. For example, GSL clusters at the cell surface interact with integrins during formation of glycosynaptic domains [223], causing the GSL-dependent regulation of cell adhesion, growth, and motility. Similarly, GM$_3$/ tetrasoanins/ CD9 complexes interact with integrins, thereby controlling tumor cell phenotype and its reversion to normal cell phenotype [137]. Intriguingly, a previously applied CHOL depletion assay confirmed the CHOL-dependent direct interaction between GM$_3$ and integrin $\alpha_5\beta_1$, which potentially leads to a lower affinity of integrin $\alpha_5\beta_1$ to its ECM ligand, fibronectin [39]. This result provides important insights on the potential GM$_3$-integrin complex in regulating integrin functionality. However, due to the limitations of CHOL and sphingolipid depletion assays in cellular experiments, the potential role of gangliosides in integrin sequestration and clustering remains poorly understood. To overcome these challenges, here we apply a polymer-tethered lipid bilayer as model membrane platform to investigate the complexation between GM$_3$ and integrin. In specific, the potential role of GM$_3$ in integrin oligomerization and raft-sequestration in a model membrane environment will be discussed.

4.3.1 Examining Influence of GM_3 on Integrin Oligomerization in Type I bilayers

First, the influence of GM_3 on integrin oligomerization was investigated in Type I lipid bilayers. Here, integrin $\alpha_5\beta_1$ was reconstituted in Type I lipid bilayers and tagged with Alexa555 labelled anti-β_1 MAb. Following the initial FCS data acquisition of fluorescent-tagged integrins in the bilayer, GM_3 was reconstituted at a 1:1 ratio relative to $\alpha_5\beta_1$ into the membrane using a formulation with the same amount of OG, as employed during integrin reconstitution. Next, the extra OG was removed by extensive rinsing and confocal fluorescence readings of labeled integrins were taken again.
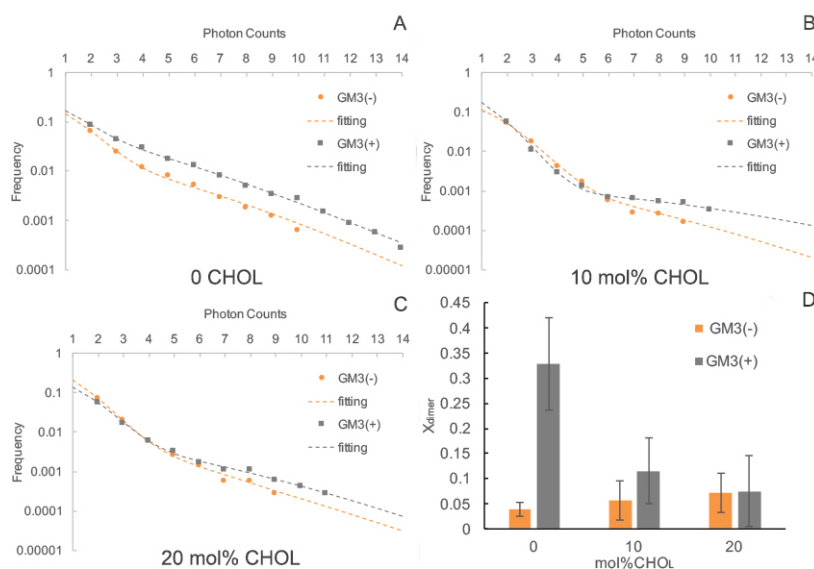
Fig. 4.18. Representative PCH curves of integrin $\alpha_5\beta_1$ labelled with Alexa 555-tagged MAb in type I bilayers without CHOL (A), 10mol% CHOL (B), and 20mol% CHOL (C), before (orange) and after (grey) GM_3 addition to the bilayer. The PCH curve for $\alpha_5\beta_1$ showed distinctive differences before and after GM_3 addition in bilayers without CHOL (A). Resulting X_{dimer} values showed elevated dimerization upon GM_3 addition in CHOL free bilayer, while this effect is less significant in CHOL-containing bilayers.

As illustrated in Fig. 4.18.A, the PCH curve of integrin $\alpha_5\beta_1$ in CHOL free bilayers exhibits distinctive differences upon GM_3 reconstitution. However, in bilayers containing 10mol% and 20mol% CHOL, this GM_3-induced change in PCH curves is less obvious.

Resulting X_{dimer} values support this observation of the PCH curves. Particularly, X_{dimer} values of reconstituted integrin $\alpha_5\beta_1$ in the CHOL-free bilayer increased upon GM_3 addition. While in CHOL containing bilayers, X_{dimer} values of integrin $\alpha_5\beta_1$ do not exhibit obvious difference upon GM_3 addition. Note that, in this experiment, which is based on FCS time-intensity-trace analysis, only relatively small clusters could be tracked and quantified. Therefore, we can not exclude the possible formation of larger scale integrin clusters using PCH analysis.

It is well known that during cell migration, integrin clustering is one of the major features during focal adhesion formation [163, 168]. This clustering process, is partially regulated by CHOL and sphingolipid content as these molecules regulate the lipid environment in the plasmamembrane [224, 225]. However, such a regulation mechanism based on a changing lipid environment is not applicable in our experimental assay where GM_3 was added at 1:1 ratio to integrin $\alpha_5\beta_1$, resulting in a concerntration of GM_3in the lipid bilayer of 0.001mol% of the total lipid population. As a consequence, the influence of GM_3 on the physical properties of lipid bilayers is negligible. Therefore, elevated integrin dimerization levels upon GM_3 reconstitution observed in the DOPC only bilayer suggests potential complex formation between GM_3 and integrin $\alpha_5\beta_1$.

There have been arguments on whether GM_3 is able to form complexes with integrin $\alpha_5\beta_1$ under physiological conditions. For example, Wang et.al [226] investigated complex formation between gangliosides and integrin $\alpha_5\beta_1$ and claimed no complexes were found between GM_3 and integrin $\alpha_5\beta_1$ using coimmunoprecipitate from lysed cells. On the other hand, Gopalakrishna et al. reported the fomation of complexes between GM_3 and integrin $\alpha_5\beta_1$ using a live cell fluorescent assay and confirmed the important role of membrane CHOL level in such a complex formation [39]. Our model membrane study supports the results by Gopalakrishna et al. Nevertheless, the distinct role of ECM ligands and GM_3 in integrin oligomeriztion suggested a different ligand-binding mechanism. Such a GM_3-specific mechanism is indeed supported by findings, which indicate that gangliosides form complexes with integrin through carbohydrate-carbohydrate interaction [226].

Similar GM_3-induced membrane protein clustering effects are also seen during glycosynapse formation where N-glycosylated integrins are able to associate with carbonhydrate chains of GSLs [37]. Interestingly, the formed glycosynapse was found to be CHOL free [37]. This is in good agreement with our findings that GSLs induces integrin oligomerization only in the CHOL-free bilayers. Previous experiments showed that the GM_3 and $\alpha_5\beta_1$ are not strongly associated, while changing in CHOL content leads to the redistribution of GM_3-associated and GM_3-free $\alpha_5\beta_1$ [39]. In addition, it has been indicated that GM_3 binding site of integrins transfer from the α subunit to the β subunit upon CHOL addition [39]. Moreover, recent findings on GM_1 suggest that membrane CHOL triggers conformational change of the ganglioside head group of the glycolipid, causing a switch from an upright structure of ganglioside to an "umbrella" structure [227]. Such CHOL-mediated structural change could provide a potential explanation to understand the observed influence of CHOL in the GM_3 induced oligomerizationof integrin. Interestingly, this GM_3-induced oligomerization effect is not limited in to GM_3-integrin complex, but has also been observed in the processes of complexation between GM_3 and other membrane proteins such as GPI-AP [26]. Additionally, recent research indicated that GM_3 is able to regulate EGFR function by promoting active dimer formation in through complex formation [220]. All these reports suggest a mechanism in which GM_3 influences membrane protein fucntion by regulating receptor oligomerization in the membrane.

4.3.2 Probing Influence of GM_3 on Integrin Sequestration in Type II Lipid Bilayers

As observed in the previous section, GM_3 addition increases integrin dimerization level under conditions where no CHOL is present in the membrane, this effect is not obvious in CHOL-containing bilayers. Moreover, gangliosides, such as GM_3, are known to prefer lipid rafts, and were treated as important biological markers for lipid rafts in cellular membrane, whereas integrins in their inactivate state, are raftophobic. In the current work, we hypothesized that GM_3-$\alpha_5\beta_1$ complexation is associated with a net translocation of complexed integrins to the raft-mimicking $l_o$phases. to confirm that integrin $\alpha_5\beta_1$ forms

complex in the membrane with CHOL and to confirm the influence of GM_3 in integrin sequestration, Type II bilayers with DOPC/DPPC/CHOL at 1:1:1 molar ratio were applied. In specific, integrin $\alpha_5\beta_1$ reconstituted into raft-mimicking type II bilayers was labelled using Alexa 555 tagged anti-β_1 MAb and the istribution of integrin $\alpha_5\beta_1$ was recorded before (Fig. 4.19.A.B) and after (Fig. 4.19.C.D) GM_3 reconstitution. As illustrated in Fig.4.19 integrin $\alpha_5\beta_1$ showed a substantial translocation to raft-mimicking l_o phases upon GM_3 addition. This net translocation could be quantified using E_{raft} analyses (Fig. 4.19.E). Again, in this experiment, integrin and GM_3 were reconstituted at a molar ratio of 1:1. Therefore, GM_3 will not induce any modification in lipid mixing and the raft-recruitment effect of GM_3 on integrin can be attributed to the direct intaction between integrin and GM_3.
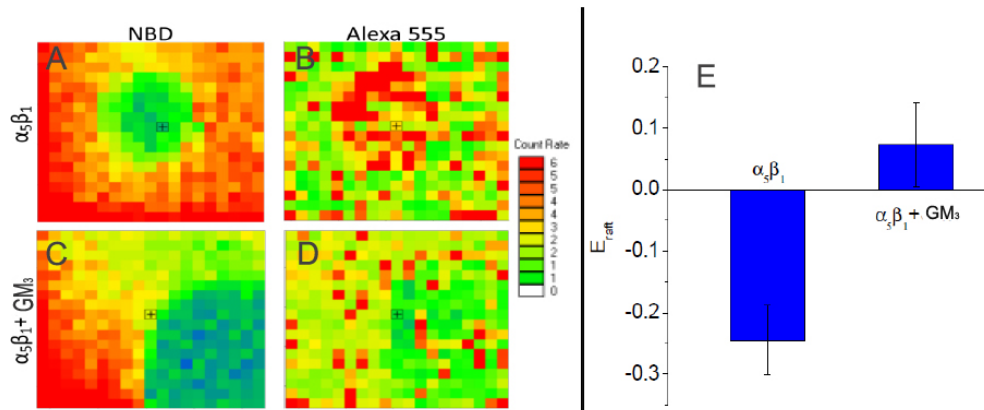
Fig. 4.19. Representative CS-XY scans of integrin $\alpha_5\beta_1$ before (A, B) and after reconstitution of GM_3 in the membrane (C, D). Specifically, the lipid distribution is indicated through NBD-PE, while the integrin $\alpha_5\beta_1$ illustrated through the Alexa-555 channel. Upon GM_3 addition, integrin $\alpha_5\beta_1$ were translocated from l_d phase (B) to l_o phase (D) as quantitively confirmed through E_{raft} analysis (E). Box size $10 \times 10 \mu m^2$.

Both ganglioside and CHOL are important membrane lipid components that may play crucial roles in the regulation membrane protein function. This functional relationship is illustrated by the observation that decrease in ganglioside levels is not only associated with certain pathological conditions during disease development including cystic fibrosis [228] and Parkinsons disease [229], but also induces abnormal protein function [230, 231]. Sim-

ilarly, it has been shown that reduced levels of GM_1 result in the decrease of β_1 integrin signaling during cystic fibrosis [228]. These observations illustrate the importance of gangliosides as membrane-associated ligands that modulate membrane protein functionality.

In this section, through a model membrane approach, we have shown that GM_3 functions as a membrane-associated ligand to integrin at low concentrations. This complexation further influences integrin oligomerization, which is affected by CHOL levels in the membrane. Moreover, our experiment demonstrated that the process of complex formation assists the translocation of integrin from l_d phase to l_o phase. Our experiments are significant because they provide important insights into the role of gangliosides in regulating membrane protein function. Additionally, this work has shown that the polymer-tethered membrane comprised of raft-mimicking lipid mixtures is well suited as a powerful experimental platform for the analysis of membrane protein- ganglioside complexes in well-defined lipid environments.

4.4   Probing uPAR-Integrin Complex Formation in Model Membrane Mixtures

As a GPI-AP, uPAR does not have an cytosolic domain. Yet, it controls several important signal pathways and transfers signals from the external environment to the interior region of cells [27, 28]. It is widely accepted that uPAR laterally interact with other membrane receptors to fulfill the processes of uPAR mediated signal transduction. In fact, an increasing number of receptors has been identified, which are members of the uPAR interactome. This uPAR interactome includes 42 proteins that directly interact with uPAR, with members from G protein-coupled receptors, receptor tyrosine kinases, and integrins [171]. Among which, uPAR can form complexes with VN receptors, like $\alpha_v\beta_6$ and $\alpha_v\beta_3$ [232], and is able to trigger the activation processes of other signal pathways such as FAK and ERK/MAPK pathway [233], and Rac pathway [234]. Direct interaction between uPAR and integrin has also been observed for both GPI-anchored uPAR and soluble uPAR [35]. The process of uPAR-integrin complexation is also considered to mediate cancer cell mi-

gration, highlighting the significance of cell-cell interaction as important promoting factor of tumor progression and metastasis [232].
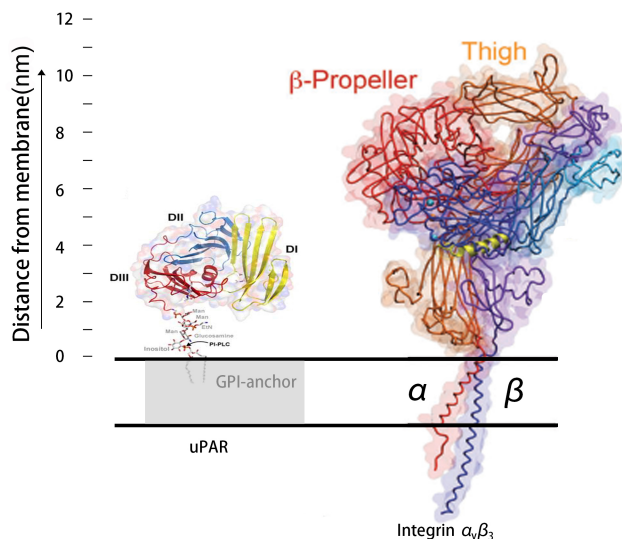
Fig. 4.20. Schematic of uPAR and integrin$\alpha_v\beta_3$ in the membrane, where uPAR is located in raft-mimicking l_o phase illustrated as grey blocks, while integrin in is inactive state prefers l_d phase. The protein crystal structures are adapted from [235](integrin$\alpha_v\beta_3$) and (uPAR) [156], The scale bar were set according to previous description by Tang et.al [236].

Though the complex formation between uPAR-integrin has been extensively studied [35,232,237,238], little is known about the molecular details of this complexation. Recent development in proteomics helped to identify the possible binding sites between uPAR and different integrins, suggesting direct binding between uPAR and integrin is possible [237]. This was also supported by immunoprecipitation results [36], fluorescent colocalization [239], and FRET experiments [238]. Yet, it remain unclear whether uPAR-integrin complex formation can occur without adaptor proteins [240]. Intriguingly, it has been suggested that uPAR-integrin complexation is raft-associated [171]. In addition, the uPAR-dependent redistribution of integrin $\alpha_5\beta_1$ was shown to be an essential process of the VEGF-induced endothelial cell migration [172]. Moreover, experimental results from treated cells revealed membrane tension is functionally involved in the complexation between uPAR and integrin

[240], indicating a potentially important role of the plasma membrane environment in such a process.

To overcome the experimental challenge associated with the characteristic of uPAR-integrin complex formation in plasma membranes, we address this hetero-complex formation between a GPI-AP and a transmembrane protein in a model membrane environment. In this case, experiments on uPAR-integrin complex formation are investigated using polymer-tethered lipid biayers containing lipid mixtures exhibit homogeneous l_d phase (Type I) and l_o-l_d phase coexistance (Type II). The interaction between uPAR and integrin was investigated from the following three perspectives: (i) changes in raft sequestration and oligomerization of integrin $\alpha_v\beta_3$ upon GPI-anchored uPAR addition; (ii) changes in uPAR oligomerization upon integrin $\alpha_v\beta_3$ reconstitution; (iii) composition of uPAR- integrin complex and influence of CHOL contents and ligand binding therein.

4.4.1 uPAR-integrin Complex Formation Relocates Integrin $\alpha_v\beta_3$ into Raft-mimicking l_o Domains in Type II Lipid Bilayers

As mentioned in the previous sections, uPAR, as a GPI-AP, prefers the raft-like l_o phase. In contrast, integrin $\alpha_v\beta_3$ in its inactive form is a raftophobic transmembrane protein when inactivated, but favors the raft-mimicking l_o phase upon ligand activation. To investigate the intriguing question of how these two membrane proteins with different preference to lipid environment might interact with each other, we first reconstituted integrin $\alpha_v\beta_3$ into type II lipid bilayers containing a 1:1:1 DOPC/DPPC/CHOL lipid mixture. The distribution of integrin $\alpha_v\beta_3$ was first observed using Alexa 555-labeled anti-integrin β_3 MAb, (Fig. 4.21.B) while the lipid distribution was illustrated using NBD-PE (Fig. 4.21.A). Following this procedure, uPAR was reconstituted overnight at a 1:1 ratio to integrin $\alpha_v\beta_3$. While a control experiment of integrin with overnight incubation at the same level of OG, without an additional protein, showed no obvious differences in integrin distribution, uPAR addition, however, significantly influenced the distribution of integrin. As Fig. 4.21.D illustrates, uPAR addition causes the translocation of integrins from the l_d to raft-mimicking

l_o phases. This translocation effect was quantitatively confirmed by the accompanying E_{raft} analysis (Fig. 4.21.E), Interestingly the effect of uPAR mediated integrin translocation to raft-like domains was also observed between uPAR and integrin $\alpha_5\beta_1$ in cellular systems [172].
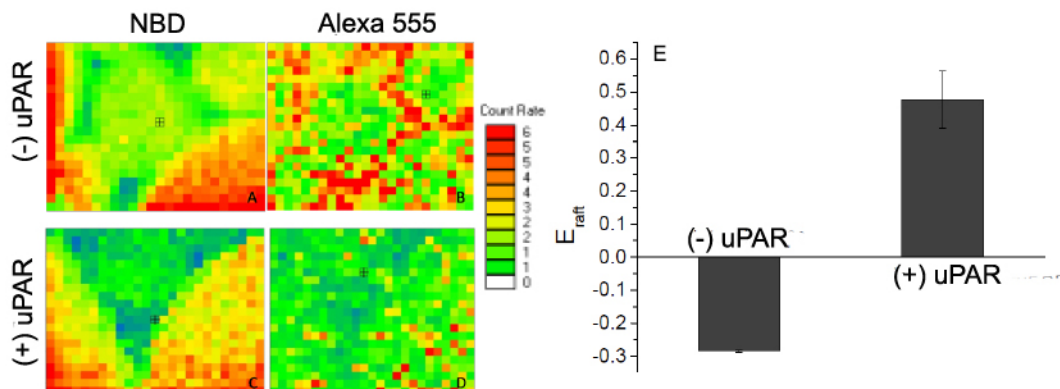
Fig. 4.21. Representative CS-XY scans (A-E) of integrin distribution in Type II lipid bilayers. Lipid phase separation is indicated with NBD-DHPE (A,C) while integrin distribution is illustrated using Alexa 555 labeled anti-β_3 MAbs (B,D). The CS-XY scans show distinguishable sequestration of integrin $\alpha_v\beta_3$ before and after uPAR addition (B,D). Resulting E_{raft} values confirmed integrin relocation from l_d phases to raft-mimicking l_o phases. Error bars represent standard deviation obtained from three different bilayers, five random spots were considered at each bilayer.

Previous research has indicated that soluble uPAR interacts with integrin β_1 and β_3 in a similar way as the interaction between integrin and its soluble ligands such as vascular cellular adhesion molecule-1 (VCAM-1) [35] that results in a raftphilic activated form of integrin [241]. A similar complex was also confirmed to form between GPI-anchored uPAR and integrin in two adjacent cells and form hetero-junctions [35]. Moreover, the GPI-anchored uPAR and integrin were proposed through direct interaction between both membrane proteins [35]. Additionally, the uPAR induced integrin recruitment of lipid rafts has also been confirmed from a CHOL depletion assay in the presence of uPAR and integrin $\alpha_5\beta_1$ [38]. Structural analysis of integrins using crystallography and electron microscopy has identified the head groups at the N-terminal domain as the major ligand-binding region

of the integrin receptor. It is well established that the N-terminal domain of the α subunit of integrin forms a seven-bladed β propeller, which includes a loop that can interact with uPAR [216]. Moreover, it has been suggested that the head groups at the α and β subunit of the respective integrin have to dissociate to open up the interacting loop for uPAR association [216, 239]. Notably, this structural change has profound influence on the structure of the transmembrane region of integrins. In that case, the structure of the transmembrane region is altered to a high-affinity conformation, where the length of the transmembrane region is increased [217]. These findings provide, at least in part, a good explanation for the translocation of integrin to the l_o phase by applying hydrophobic matching arguments.

We further analyzed the oligomerization of integrin reconstituted in Type II bilayers through PCH analysis. As indicated by Fig. 4.22, integrin reconstituted into such a bilayer system was mostly monomeric with an initial $X_{dimer} \sim 0.13$ in both l_o and l_d phases. The
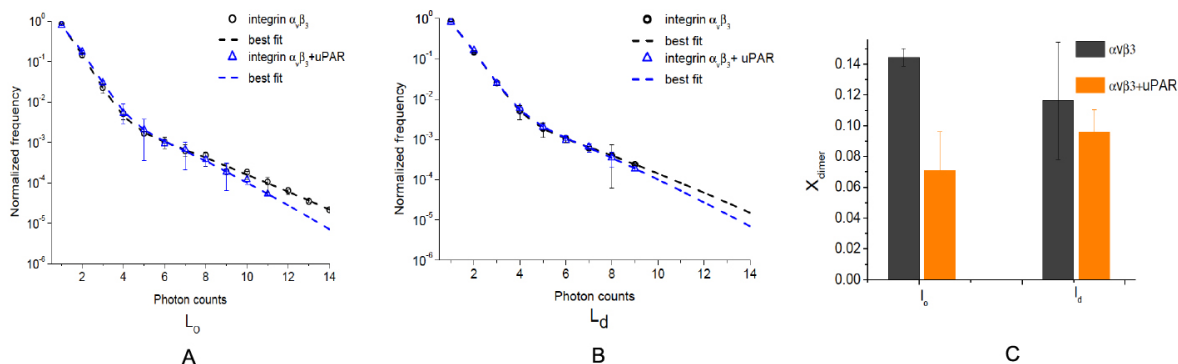
Fig. 4.22. Representative PCH curves of integrin $\alpha_v\beta_3$ before and after uPAR reconstitution in Type II lipid bilayer (A,B) and the resulting X_{dimer} of integrin in l_o and l_d phases (C). The addition of uPAR decreases the dimerization level of integrin in l_o phase, whereas the dimerization level in the l_d phase remains largely unchanged. These results illustrate the potential role of membrane composition in uPAR-induced change in integrin oligomerization.

subsequential reconstitution of uPAR lowered the level of dimerization of integrins especially in the l_o phases (ANOVA test $p < 0.005$) whereas the dimerization level in l_d phases

remained largely unchanged. These results indicate a potential role of membrane organization including CHOL content in the uPAR-induced change in integrin oligomerization, highlighting the potential significance of bilayer composition in uPAR-integrin complex formation.

4.4.2 Investigating uPAR oligomerization upon uPAR-Integrin $\alpha_v\beta_3$ Complexation and Its Dependence on CHOL

To investigate the influence of uPAR-integrin complex formation on uPAR oligomerization, we first reconstituted uPAR into Type I lipid bilayers. Here uPAR was labeled with Alexa-555 tagged anti-DDK MAb at the C-terminal. Following sample analysis and data collection, integrin was reconstituted at the equimolar ratio (relative to uPAR) into the same bilayer sample. As illustrated by Fig. 4.23, before integrin reconstitution, uPAR diffusion was D = $1.47 \pm 0.32(\mu m^2/s)$ which is in good agreement with previously reported values [195]. The addition of integrin lowers the overall uPAR diffusion coefficient to D = $0.78 \pm 0.13(\mu m^2/s)$, which is close to the previously reported value of integrin diffusion in a similar system (D = $0.71 \pm 0.07 \mu m^2/s$ in DOPC only bilayers) [54]. This
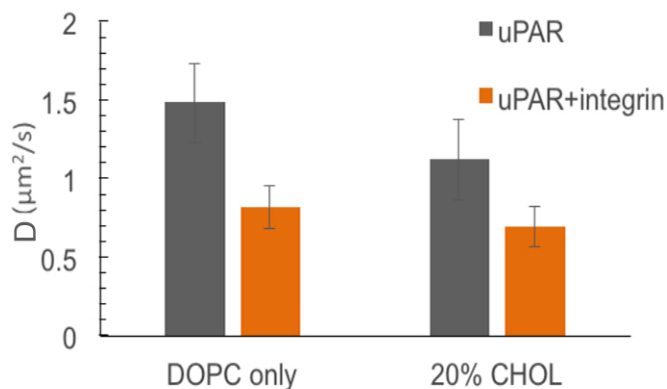
Fig. 4.23. uPAR diffusion coefficient obtained from FCS analysis. uPAR diffusion slows down upon integrin reconstitution to match the diffusion of integrin in the bilayer, suggesting a lateral association between uPAR and integrin $\alpha_v\beta_3$ in the model membrane environment.

finding indicates the formation of a laterally organized complex between uPAR and integrin being observed in the bilayer sample. Interestingly, with CHOL addition, both uPAR diffusion and complex diffusion decrease, presumably due to the CHOL-induced change in membrane packing density as discussed in section 4.2.2.

It is well known that uPAR achieves its function through the formation of homo-oligomers [27, 28]. However, little is known about changes in uPAR oligomerization state upon complex formation with other membrane proteins. In fact, this potentially important issue has
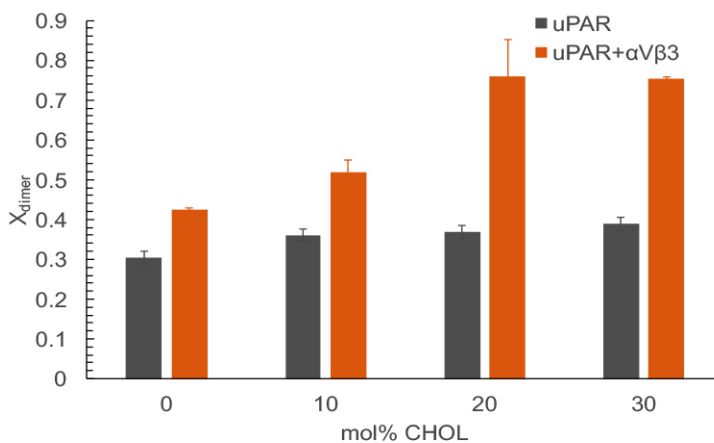
Fig. 4.24. uPAR dimerization states in Type I lipid bilayers. uPAR dimerization in the membrane is not influenced by CHOL in the membrane, the addition of integrin triggers the dimer formation of uPAR in a CHOL dependent way (differences in uPAR dimerization between conditions with and without existing integrin were verified by ANOVA test $p < 0.005$, CHOL dependence was confirmed through t-test until 20mol% of CHOL $p < 0.005$) Error bars represent the corresponding standard deviation obtained from 3 different bilayers.

been neglected in hetero-membrane protein complexes containing lipid-anchored membrane proteins, most of which are known to form oligomers during activation. To investigate uPAR oligomerization upon complex formation, we further analyzed uPAR dimerization upon integrin reconstitution and correlated this property with varying membrane CHOL content. As illustrated by Fig. 4.24, X_{dimer} increases upon integrin reconstitution,

indicating that the uPAR monomer-dimer equilibrium has shifted toward increased dimer levels.

The influence of uPAR-integrin complexation on uPAR dimerization was also tested in Type II lipid bilayers. As illustrated in Fig. 4.25, the uPAR dimerization level increases upon integrin addition, which supports the data shown in Fig. 4.24. Moreover, uPAR dimerization levels in the l_d phase is not substantially changed after integrin addition, while the dimerization level in the l_o phase are significantly increased by about 30% (ANOVA test $p < 0.005$). The finding illustrated in Fig. 4.25 is consistent with the data shown in Fig. 4.22.C where integrin dimerization remained at a similar level in the l_d phase with and without uPAR. Together, this result illustrates that the lipid environment may have a significant influence on the composition of uPAR-integrin complexes in a model membrane.
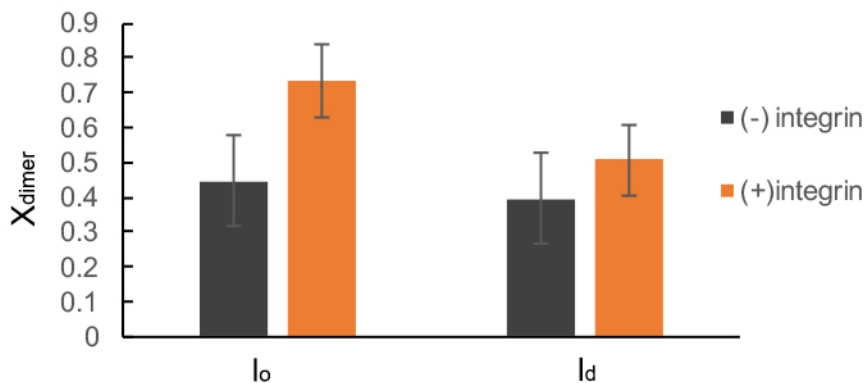
Fig. 4.25. uPAR dimerization states in Type II lipid bilayers with (shown in orange) and without (black) integrin reconstituted. Similar to dimerization levels of integrin in the same system, uPAR dimerization levels are not significantly changed upon addition of integrin in the l_d phase. However, in l_o phase, the dimer level of uPAR increases significantly when integrin is also present in the membrane.

4.4.3 Investigating uPAR-Integrin Complexes Through Dual-color Fluorescent Assay in Type I Bilayers

The single color fluorescent assays described in the previous section are limited in their ability to unambiguously confirm the formation of uPAR-integrin complexes and to determine the composition of such membrane protein hetero-complexes. Therefore, the uPAR-integrin complex is further analyzed using a dual-color fluorescent assay . In this case, equal moles of uPAR and integrin were simultaneously reconstituted into a Type I lipid bilayer. Next, uPAR was labeled with Alexa-555-tagged anti-DDK MAb, while integrin $\alpha_v\beta_3$ was labeled with anti-integrin β_3 MAb tagged with Alexa-488. This antibody binds integrin at the N-terminal of the β_3 subunit without binding the proposed ligand binding or uPAR binding amino acid sequences nor inducing structure change of the integrin. Following membrane protein reconstitution and labeling, FCS intensity-time-traces were recorded through both Alexa-555 and Alexa-488 channels.

According to the description in chapter 3, the uPAR-integrin complex is clearly identified through parallel analysis of the intensity-time trace in the two fluorescent channels. Here protein complexes can be observed when peak signals from both channels are read out within the same time interval. As illustrated in Fig. 4.26, both uPAR and integrin can be observed as components of the complex or as individual membrane proteins. Importantly, peaks associated with complexes can be merged into a new set of time-intensity-traces, thus enabling PCH analysis from complexes according to the description in chapter 3. Fig. 4.26 shows two sets of typical signals obtained from the dual color labeling assay of uPAR and integrin $\alpha_v\beta_3$ in Type I lipid bilayers. In this case, bilayers without CHOL (left) or with 20mol% CHOL (right) were applied. As indicated from the raw time-trace, uPAR-integrin complexes are more frequently seen in a CHOL-containing bilayer sample than its CHOL-free counterpart. The level of complexation can be roughly estimated from raw data. Overall data based on four different bilayers at each composition indicated that $\sim$28.5% of the total peaks from Alexa-488 channel (integrin) are identified to be associated with uPAR-integrin complexes in CHOL-free bilayers, whereas $\sim$68% of the integrin sig-
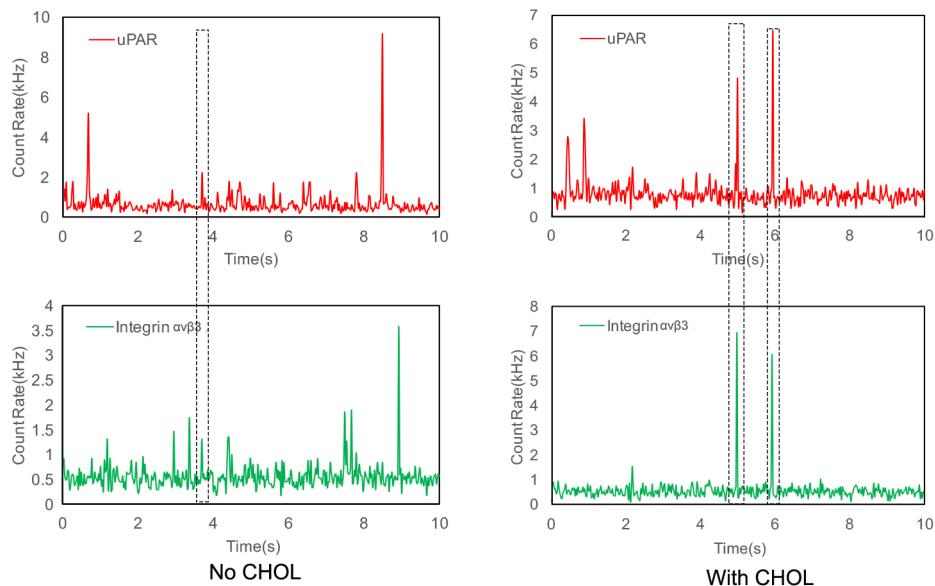
Fig. 4.26. Intensity-vs-time trace of uPAR (labeled by Alexa-555 tagged MAbs) and integrin $\alpha_v\beta_3$ (labeled by Alexa-488 tagged MAbs) reconstituted in Type I lipid bilayers with (20mol%, right) and without (left) CHOL. Peaks indicating potential complexes are marked in dashed rectangles.

nals are identified to be complex signals in CHOL-containing bilayer samples. Based on qualitative observation, these findings show that uPAR-integrin complex formation is indeed CHOL dependent and more likely to occur in the membrane region of elevated CHOL level, such as lipid rafts.

Currently existing methods are limited in their ability to determine the composition of hetero-protein-complexes. One of the most powerful tools is electron microscopy, especially cyro-EM [242]. However, this methodology has limitations to detect dynamic complexation processes in a fluid membrane environment [159]. Other methods, such as NMR and X-ray crystallography, often encounters problems in terms of resolution [159]. Fluorescent-based methods have the advantage that they provide real-time dynamic information on potential complexes with single molecule sensitivity. Fluorescence cross-correlation spectroscopy, which defines complex formation through a fluorescent cross-correlation function of two different species, allows a precise analysis of kinetics during

dynamic protein assembly, but fails to give information about the composition of the resulting protein complexes. Previously, dual-color-2D PCH has been applied to determine the oligomerization states of two fluorescent species in one system [243]. Although being quite powerful, this method does not provide complex-specific information. Furthermore, dual-color 2D PCH usually requires a complicated algorithm to acquire final results. In light of the described limitations of existing experimental methods, there is currently very limited information about membrane protein homo-oligomerization within hetero-complexes and the underlying mechanisms that regulate the composition of such complexes.

To address these shortcomings, here we applied a simplified dual-color fluorescence detection method, which is based on the single-color PCH algorithm to identify the oligomerization states of each component in the uPAR-integrin complex. In contrast to dual-color PCH, we created new PCH data from signals exclusively from complexes and conducted PCH analysis through the same deconvolution function as employed in single color PCH. This approach does not require a complicated algorithm. However, as the single color algorithm does not consider any fluorescence bleeding through from another channel, here we adjust the intensity of the bleed through to the same level to the other channels background and ignore the background photon counts during PCH analysis. Another potential effect is FRET induced enhancement of fluorophore signal, which might influence the resulting dimerization level data. Here, we chose Alexa-555 and Alexa-488 as fluorescent pairs based on the sensitivity of the detectors of our optical system. In this case, FRET artifacts cannot be excluded. To minimize such a potential artifact we used an integrin antibody that binds at the N-terminal of the receptor, that lies relatively far away from the bilayer surface upon integrin activation, while the uPAR antibody is linked to the DDK tag next to the GPI anchor of uPAR. Indeed, unlike a previously reported FRET assay applied for uPAR-integrin complexes, where both antibodies were near the N-terminal of membrane proteins [238], in our experimental design the distance between two fluorophores showed a limited FRET effect (Fig. 4.27). Therefore, the single color PCH analysis approach is still reasonably precise once the brightness in both fluorescent channels is adjusted according to the count rates shown in Fig. 4.27.
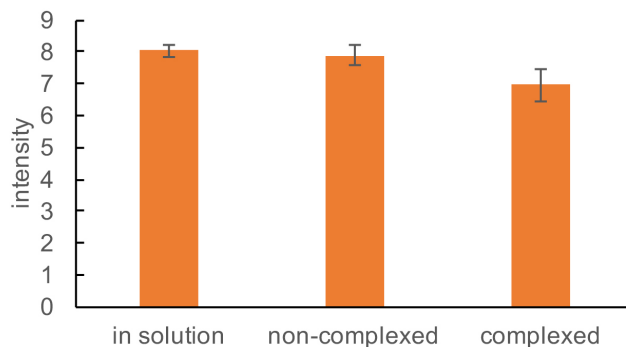
Fig. 4.27. Maximum fluorescence intensity of Alexa-488 channel in each bilayer. Bars from left to right indicate the intensity obtained from Alexa-488 labelled integrin β_3 MAb in solution (left), integrin reconstituted in bilayer (middle), reconstituted integrin in the uPAR-integrin complex (right). The drop in maximum intensity of complexed integrin indicates potential FRET happening during complexation.

The described dual-color fluorescence detection method was applied to determine the oligomerization states of uPAR and integrin in the complex using single color PCH analysis of complex-specific fluorescence signals (Fig. 4.28). The resulting PCH curves indicate distinct dimerization levels for uPAR and integrin $\alpha_v\beta_3$ in the complex. In particular, X_{dimer} data show that uPAR exhibits higher levels of dimerization in the complex than outside of the complex as shown in Fig. 4.24. In the case of integrin, though mostly monomeric proteins are observed in the complex and outside of the complex, albeit X_{dimer} values suggest slightly lower dimerization values in the complex (relative to integrin dimerization outside the complex). Notably, the presence of CHOL enhances the dimerization level of uPAR in the complex, whereas, according to results described in section 4.1, uPAR dimerization levels without integrin is largely independent of CHOL content in the membrane. Importantly, the dual-color results support the CHOL-dependence of uPAR oligomerization upon uPAR-integrin complex formation observed in the single color labeling assay, where both complexed and uncomplexed uPAR are considered at the same time. Based on the dimerization level results, we propose a model for this uPAR-integrin complex in which two uPAR molecules form a complex with one integrin receptor. Intriguingly, this model is
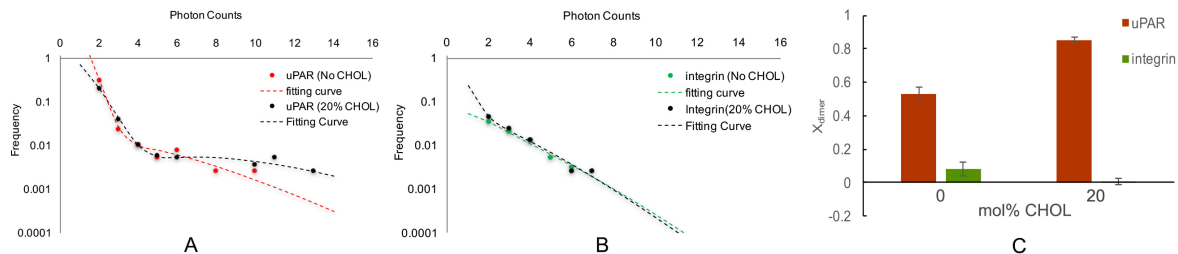
Fig. 4.28. Typical PCH curves and corresponding fitting for uPAR (A) and integrin (B) in Type I bilayers with and without CHOL. As indicated by PCH curves and resulting X_{dimer} the existence of CHOL promotes dimerization of uPAR in the complex, whereas integrin is mostly monomeric under each condition. Error bars represent corresponding standard deviation from five bilayers; each bilayer was scanned at ten different positions.

supported by previous proteomic studies which indicate that uPAR binds to integrin possibly through D2 and D1, whereas, both integrin α_v subunit and β_3 subunit have possible binding sites for uPAR D2 [237]. The observed effect of CHOL on the uPAR-integrin complex can presumably be attributed to the bilayer-thickening effect of CHOL, which may induce allosteric changes on the intergin receptor, thereby promoting uPAR-integrin association.

uPAR and its related signal pathways are considered to be limited in normal cell functions, however, in cancer cells, uPAR is expressed at an abnormally high level. Furthermore, uPAR-integrin signaling is considered one of the key mechanisms for tumor invasion and migration. Moreover, it was confirmed that certain cancer cells contain elevated levels of CHOL in the plasma membrane [148]. Our data on uPAR-integrin complex formation and composition, and the corresponding regulatory role of CHOL, may provide significant mechanistic insights into this pathologically important protein hetero-complex.

Our experiments were not limited to the role of CHOL in uPAR-integrin complex formation, we explored the influence of, VN, a common ligand of uPAR and integrin. In particular, the influence of VN on uPAR-integrin complexation was determined by analyzing uPAR-dimerization in the complex (Fig. 4.29). Interestingly, the uPAR dimerization

level increases in CHOL free bilayer upon VN addition, but not in bilayers containing 20mol% CHOL. This suggests that the presence of VN, either through transferring integrin to its activated state or through promoting uPAR dimer formation, supports the formation of complexation consisting of an uPAR dimer and an integrin monomer.
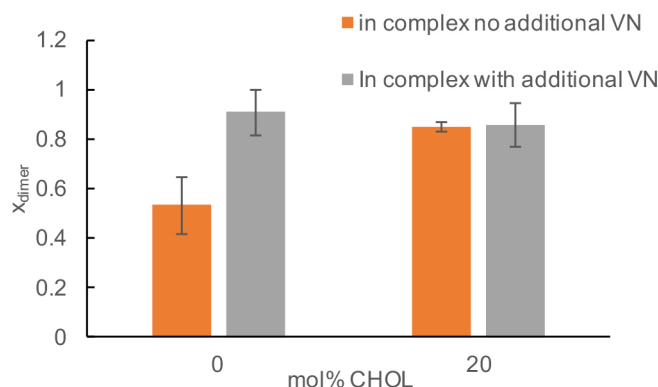
Fig. 4.29. X_{dimer} of uPAR in the uPAR-integrin complex before (orange) and after (gray) VN addition. The addition of VN promotes dimerization of uPAR within uPAR-Integrin complexes in CHOL free bilayers. Error bars of samples with no additional VN represent corresponding standard deviation from three different bilayers, ten scans were conducted for each bilayer. Error bars from samples with VN indicate the probability distribution obtained from two bilayers, fifteen scans were conducted for each bilayer.

By combining single-color FCS, PCH analysis, and CS-XY scans together with dual color fluorescent signal analysis, we are able to provide valuable insights into the complex formation between uPAR and integrin in a model membrane environment. By empolying this methodology, we confirmed that uPAR and integrin are able to form laterally mobile complexes without the a need for additional adaptor proteins. Our dual-color data suggest that uPAR-integrin complexation is enhanced in membrane regions with elevated CHOL content. This uPAR-integrin complexation promotes integrin translocation to the raft-mimicking l_o phase, and increases uPAR dimerization level in a CHOL dependent manner. Our experimental data suggested that uPAR-integrin complexes in CHOL-containing membranes are comprised of a uPAR-dimer and an integrin monomer. Addition

of native ligands, such as VN, appears to stabilize the formation of such membrane protein hetero-complexes. Our work demonstrates that polymer-tethered lipid bilayers can be applied as a powerful tool to investigate functional protein hetero-complexes in a well defined lipid environment. Together, our experimental findings highlight the potential significance of the local lipid environment in the formation and composition of uPAR-integrin complexes plasma membranes. The dual color fluorescent assay, which was developed as part of this Ph.D thesis, has the potential to become a useful tool to analyze the molecular compositions of protein hetero-complexes in both model membranes and cellular membranes. This work, for the first time, looked into the potentially important topic of protein homo-oligomerizaton in heterocomplexes of membrane proteins, thereby providing important molecular insights about the role of lipid composition in complex formation. As demonstrated for uPAR-integrin complexation, these experiments may provide critical information about the underlying mechanisms of pathological significant hetero-complexes in different disease models.

4.5 Investigating Cadherin Chimera Dynamics and Spatial Distribution During Cell Migration on Polymer-Tethered Lipid Bilayers

In previous sections, the role of local lipid environment and native ligands on the distribution and oligomerization states of membrane proteins and hetero-complexes of membrane proteins have been explored using single molecule-sensitive confocal fluorescent detection methodology. In particular, this methodology was applied to GPI-anchored uPAR, integrins and uPAR-integrin complexes. In the current section, a comparable confocal method is utilized to analyze the assembly and dynamics of cadherin linkages between cells and a cell surface-mimicking substrate of adjustable stiffness. Specifically, the details of cadherin linkage assembly and mobility will be explored using a polymer-tethered lipid bilayer system, which is functionalized with cadherin chimera (Fig. 4.30). In particular, we will emphasize investigation of the clustering and dynamics of such cadherin chimera clusters underneath migrating cells. In this experimental system, substrate stiffness can

be altered by changing the number of bilayers in a polymer-tethered multi-bilayer stack, thus providing valuable insights into the poorly understood relationship between external mechanical cues and cadherin linkage dynamics at the cell-cell interface.
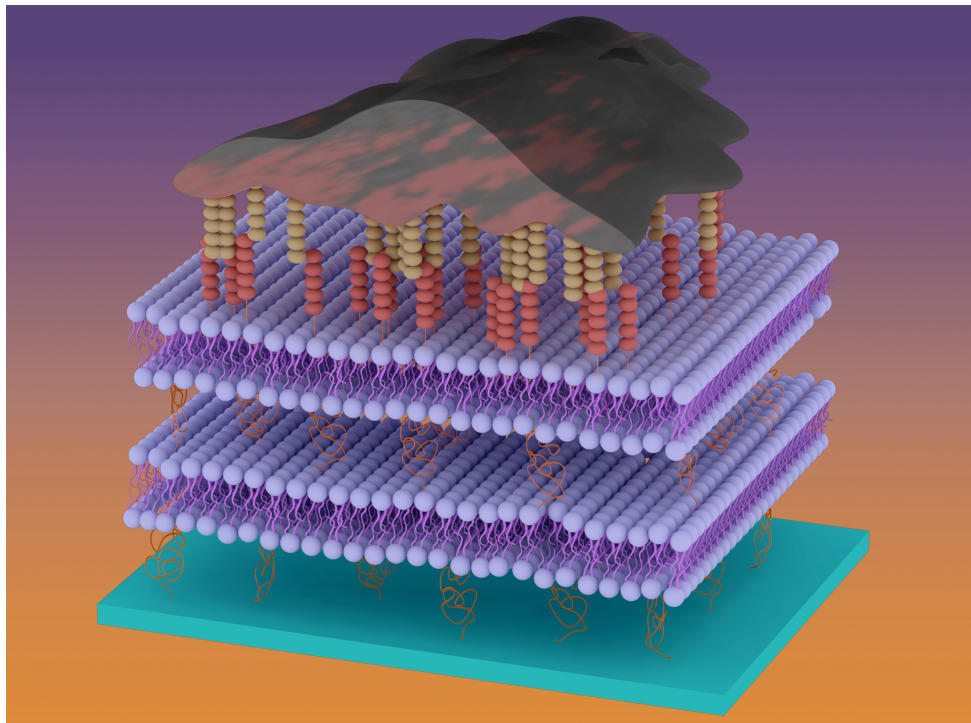
Fig. 4.30. A schematic of the experimental concept of a cadherin functionalized polymer- tethered lipid bilayer system as a cellular substrate. In this case, cadherin chimera (red) are freely diffusing on the polymer-tethered bilayer surface (purple), but assemble into clusters to form linkages with cellular cadherins. The clustered cadherin-chimera which are labeled using Alexa-555 dyes can be observed using fluorescent microscopy techniques.

4.5.1 Characterization of Cadherin Chimera Fluidity, Oligomerziation State, and Distribution on Polymer-Tethered Lipid Bilayers

Upon fabrication of polymer-tethered lipid bilayers, N-cadherin chimera, which consist of the ectodomain of N-cadherin, Fc domain from IgG with 6 His-tags was applied to functionalize the bilayer substrate. N-cadherin chimera were bound to DGS-NTA Ni-chelating

lipids on the top leaflet of the bilayer system. To enable fluorescence analysis, N-cadherin chimera were fluorescently labeled with Alexa-555. Fluorescence analysis revealed a homogenous distribution of lipids and N-cadherin chimera on the bilayer surface in Ca^{2+} free PBS buffer prior to cell plating (Fig. 4.31).
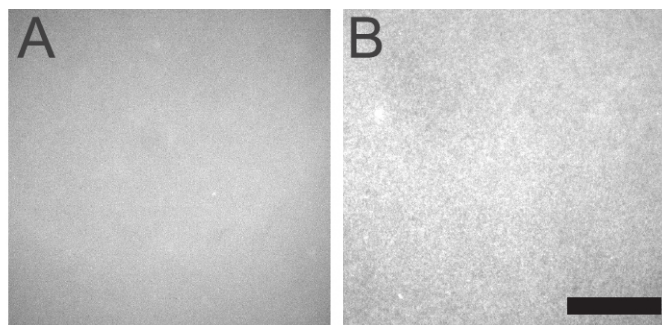
Fig. 4.31. EPI micrographs of TRITC-DHPE (A) and N-cadherin chimera (labeled with Alexa 555-tagged anti-N-cadherin antibody, (B) on the surface of a polymer-tethered lipid bilayer. The featureless EPI micrographs indicate a homogenous distribution of both dye labeled lipids and N-cadherin chimera. Scale bar: 50μm [244].

To gain a better understanding of the properties of N-cadherin chimera on top of the polymer-tethered lipid bilayers, FCS and PCH analyses of Alexa-555 labeled N-cadherin chimera were conducted at fixed positions on the bilayer in Ca^{2+}-free PBS, the resulting peaks in the fluorescence intensity-vs-time track (Fig. 4.32.A) demonstrate the lateral mobility of bilayer-bound cadherin chimera. FCS autocorrelation analysis (Fig. 4.32.B) of these time-intensity tracks provides a diffusion coefficient of N-cadherin chimera of D = 0.34 ± 0.05μm^2/s [244], which is in good agreement with previously reported results [245]. In comparison, TRITC-DHPE, use as a standard, exhibits the diffusion coefficient of D = 1.66 ± 0.39m^2/s which is in good agreement with previously reported values [54]. PCH analysis (Fig. 4.32.C) indicates that N-cadherin chimeras are predominately monomeric on the bilayer surface. Altogether, the data in Fig. 4.32 suggests that individual lipid-bound N-cadherin chimera are freely diffusive without forming observable clusters.
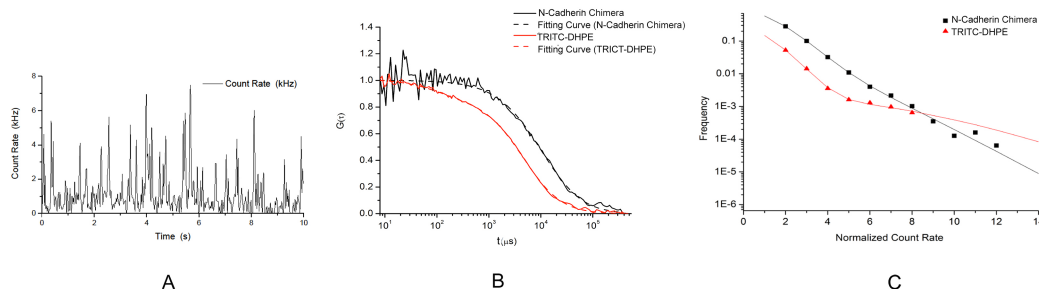
Fig. 4.32. Intensity-time-trace (B) of the Alexa-555 labeled cadherin chimera linked to the polymer-tethered lipid bilayer in Ca^{2+} free PBS buffer (A). Typical autocorrelation curves of TRITC-DHPE and N-cadherin chimera (B). PCH curves, displayed in (C) lead to X_{dimer} values of 0.16 ± 0.01 (N-cadherin chimera) and 0.018 ± 0.012 (TRITC-DHPE), illustrating the monomeric nature of lipids and bilayer-bound N-cadherin chimera [244].

Next, the lateral mobility of N-cadherin chimera clusters in polymer-tethered lipid bilayers is examined using an N-cadherin chimera functionalized fluorescent bead assay. In this case, N-cadherin functionalized red fluorescent beads (500nm) were allowed to bind on an N-cadherin functionalized (0.1mol%) polymer-tethered lipid bilayer. As confocal imaging analysis shows (Fig. 4.33.B), N-cadherin chimera-functionalized beads were able to bind on the polymer-tethered lipid bilayer either in the absence functionalized with N-cadherin chimera in Ca^{2+}-containing medium. In contrast, comparable beads are unable to bind to the cadherin functionalized lipid bilayer either in the absence of Ca^{2+} (Fig. 4.33.C) or without bilayer-bound N-cadherin-chimera. Unlike individual N-cadherin chimera, beads functionalized with N-cadherin chimera are completely immobilized if bound to the N-cadherin-functionalized polymer-tethered lipid bilayer. This finding illustrates the remarkable material properties of polymer-tethered single and multiple lipid bilayer systems, which can be attributed to the presence of lipopolymers in such membrane architectures, resulting in a strong inter-leaflet coupling of lipopolymer-induced obstructed diffusion [65, 66, 86]. Here, membrane components with a larger size than the average tethering distance are largely immobilized, whereas smaller probes maintain their lateral mobility [86].
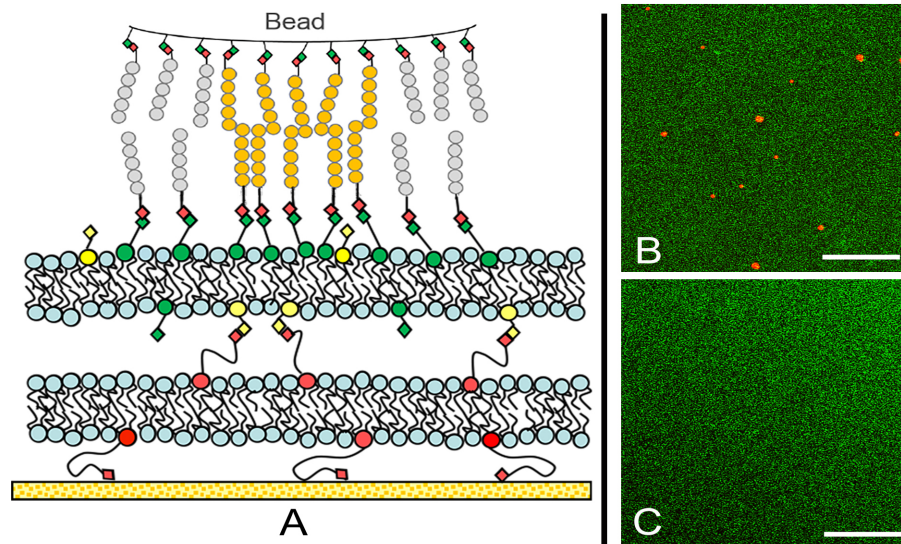
Fig. 4.33. Schematic of N-cadherin chimera functionalized fluorescent bead linked to N-cadherin-functionalized multi-bilayer stack (A). Dual color fluorescent micrograph shows that N-cadherin functionalized beads (red) are bound to N-cadherin-chimera-containing polymer-tethered bilayer stacks (labeled with NBD-DHPE) in the presence of Ca^{2+}(B), whereas, without Ca^{2+} addition, no bound fluorescent beads are observed on top of the bilayer after rinsing. Scale bar: 5μm [244].

4.5.2 Studies of N-Cadherin Cluster Dynamics and Distribution During C2C12 Myoblast Migration

The distribution and lateral mobility of fluorescently labeled N-cadherin chimera were first investigated on a single polymer-tethered lipid bilayer containing 0.1mol% DGS-NTA in the top leaflet. As illustrated in Fig. 4.34, the lipid distribution (indicated by TR-DHPE, Fig. 4.34.A) was not altered by the presence of adherent cells (24hrs after plating), indicating good membrane integrity and suitability as artificial cell substrate. Moreover, FRAP analysis was conducted according to the description in Chapter 3. In this case TR-DHPE underneath spreading cells exhibits nearly fully recovery (Fig. 4.34.B, IF=9%) exhibiting a diffusion coefficient of D = 1.67 ± 0.05μm/s^2 [244]. This finding indicates that cell migration does not alter the lateral mobility of lipids in the model membrane system. In contrast, N-cadherin chimera are no longer homogeneously distributed in the presence of

plated cells. Unlike TR-DHPE, they exhibit an enrichment at the periphery and extensions of migrating cells. This heterogeneity suggests that N-cadherin chimera distribution can be seen as a mirror image of actual cellular adhesions of migrating cells. As illustrated by Fig. 4.34.C, there is little cadherin enrichment underneath the nucleus area of the migrating cell, in good agreement with recent results of cadherins in cell-cell junctions [246]. FRAP analysis shows that cadherin chimera have a substantial immobile fraction of IF=59.5% and the mobile fraction displays a diffusion coefficient of D = $0.047 \pm 0.004 \mu m/s^2$ (Fig. 4.34.D) [244].
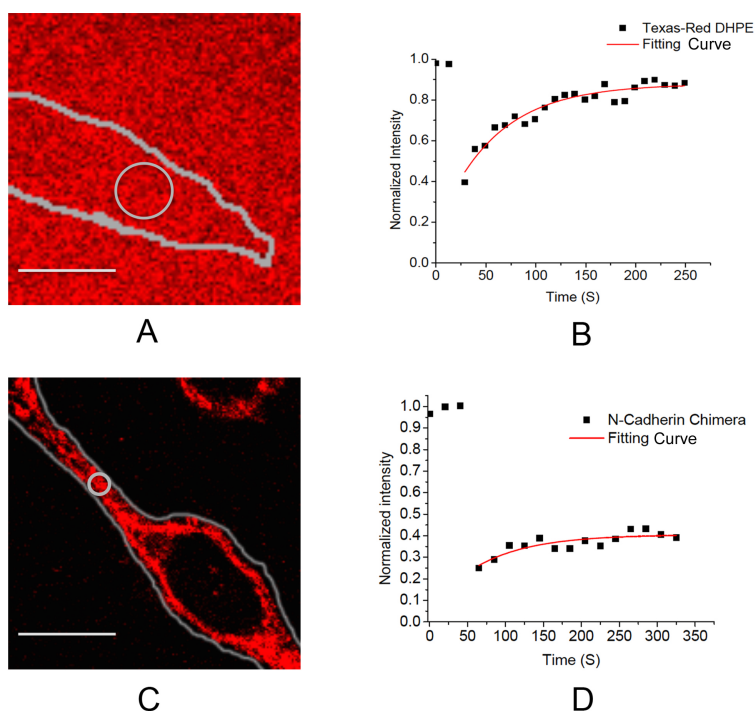
Fig. 4.34. Cellular adhesion and migration processes do not alter the homogeneous lipid distribution in the polymer-tethered lipid bilayer (A). Accompanying FRAP analysis reveals nearly full fluorescent recovery of TR-DHPE lipids underneath plated cells (B). In contrast, enrichment of Alexa-555 labeled cadherin chimera can be observed underneath cells in comparable substrates (C). FRAP analysis of the N-cadherin chimera indicates a substantial immobile fraction of cadherin chimera clusters underneath plated cells (D). The contours of plated cells obtained from the DIC micrographs are indicated as a gray line, bleached areas are depicted as circles. Scale bar: 5μm [244].

The spreading of cells and the accompanying accumulation of N-cadherin chimera illustrates the fascinating properties of polymer-tethered lipid-bilayers as a biomembrane-mimicking cell substrate. Observed cadherin chimera accumulation into clusters underneath cells, can be attributed to the dynamic properties of such linkers in the polymer-tethered membrane. Notably, this accumulation property cannot be observed on polymer substrates with chemically conjugated linkers. As a result, cell spreading on the polymer-tethered lipid bilayer substrate is largely independent from linker density. In fact, the average linker distance ranges between 48nm to 160nm is employed in this study, has no significant impact on cell spreading area and migration of C2C12 myoblasts. In contrast, cell spreading was substantially suppressed on polymer substrates with chemically conjugated linkers if a linker distance of $\sim$70 nm or greater was used [247]. Interestingly, a similar heterogeneous distribution of E-cadherin chimera underneath epithelial cells was reported by Biswas et.al using the platform of SLBs with high membrane viscosity. In their research, a nucleation of E-cadherin chimera clustering was observed, suggesting an important role of the cytoskeleton during E-cadherin enrichment [70].

4.5.3 Examining Influences of Cytoskeletal Organization on N-Cadherin Cluster Assembly and Dynamics

The role of the cytoskeleton of plated cells in N-cadherin chimera cluster assembly was next examined using confocal microscopy. In this case, the concentration of DGS-NTA on the surface of the polymer-tethered lipid bilayer was kept at 0.1mol%. The distribution of fluorescently tagged N-cadherin chimera in this cell surface-mimicking substrate was monitored at the front and tail region of plated cells over time. Fig. 4.35. B-C show the time evolution of N-cadherin chimera distribution at the cells front, whereas (Fig. 4.35.D-E) provide corresponding data from the tail region. These micrographs demonstrate that N-cadherin chimera clusters are not static; both areas are characterized by substantial long-range movements of N-cadherin chimera patches.
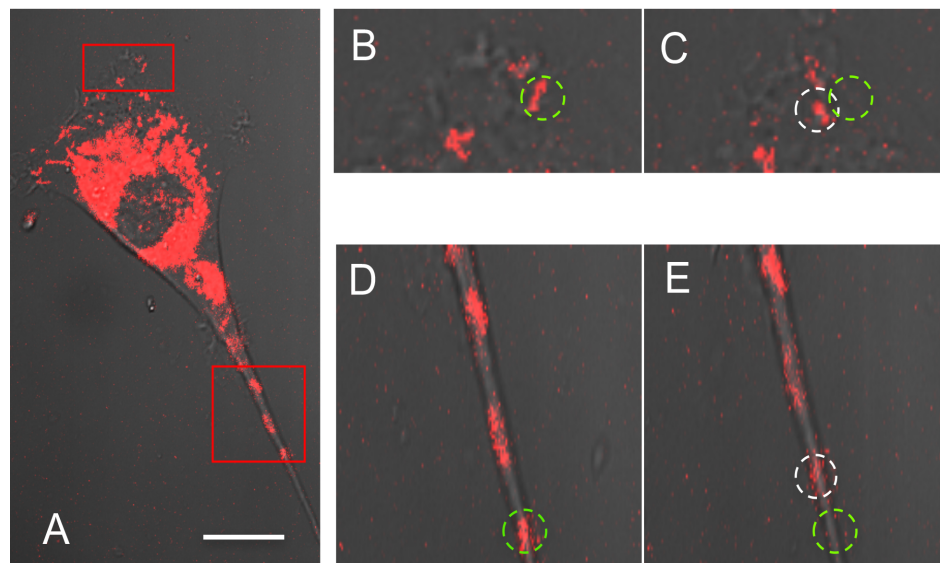
Fig. 4.35. Spatiotemporal analysis of Alexa 555-labeled N-cadherin chimera underneath a C2C12 myoblast (A) shows long-range mobility of chimera clusters at the front (B, C), and tail regions (D, E) of the cell. Enlarged areas are indicated by red rectangles (A). Green and white circles illustrate N-cadherin cluster positions at times t=0s (green) and t= 40s (white), respectively. Scale bar: 20μm [244].

As confirmed from section 4.5.1, linker clusters larger than 200nm in diameter are unable to freely diffuse in polymer-tethered lipid bilayers. Therefore, the long-range movements of N-cadherin chimera clusters observed on the polymer-tethered bilayers underneath plated cells can likely be attributed to cytoskeleton forces of plated cells. In order to better quantify the dynamics of linker clusters, The concentration of DGS-NTA was adjusted to 0.005mol% and the N-cadherin chimera cluster movement was tracked using uTrack following procedures decribed in section 3.2.11. Fig. 4.36.A illustrates a typical uTrack image with resulting tracks (represented as red lines) obtained from a twenty-minute movie. This tracking analysis demonstrated that the long-range movement of N-cadherin chimera clusters is approximately three times faster than the previously reported cell migration speed [65]. Moreover, the N-cadherin chimera cluster movement is slightly asymmetric within one cell, it is more orientated at the tail of spreading cells while more random movements of such clusters can be seen at the front region of cells.
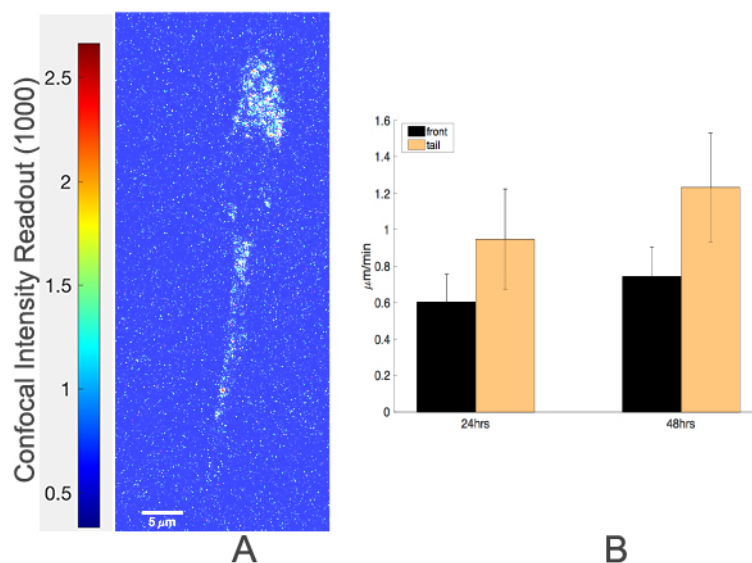
Fig. 4.36. Representative tracking result of N-cadherin chimera clusters underneath spreading C2C12 myoblast cells using uTrack analysis (A). Average cluster-moving speed was determined through analysis of 10 different cells (B). For each cell, 50 tracks were considered at front and tail area of the cell. Cells analyzed 24 hrs and 48hrs after plating showed comparable cluster moving speed. Error bars show the standard deviation of the results from 10 cells. Scale bar: 5μm.

In addition to cluster tracking analysis, the influence of Latrunculin B (LaB), an inhibitor of actin polymerization, on the assembly and dynamics of N-cadherin chimera was examined. These experiments were considered to clarify the role of cytoskeleton in N-cadherin chimera assembly and dynamics underneath adhered cells. In this experimental assay, addition of 10μM LaB substantially impaired cell spreading/migration on linker-functionalized polymer-tethered lipid bilayers (Fig. 4.37). Furthermore, cadherin chimera clusters became largely immobilized after ten minutes of incubation with LaB (Fig. 4.37.C). After thirty minutes, most of the N-cadherin chimera clusters were dissolved (D). These findings confirmed the important role of the cytoskeleton in the formation and mobility of N-cadherin chimera clusters. In previous reports, AJs were reported to exhibit a remarkable long-range mobility including apical-to-basal [178] flow and treadmilling of AJs [62]. In light of these findings, our observation of long-range movement of N-cadherin
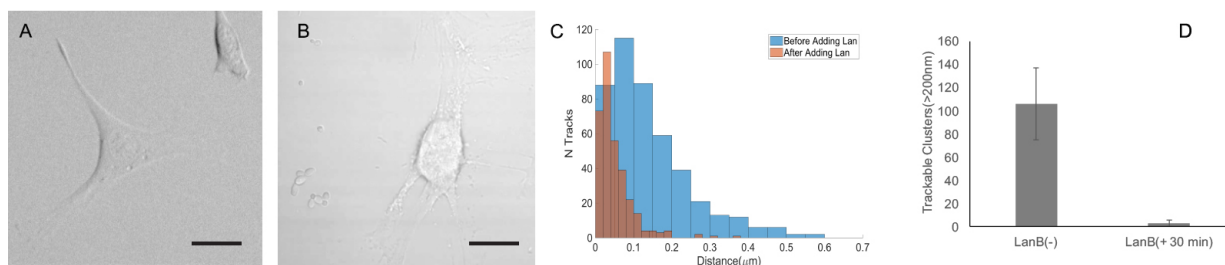
Fig. 4.37. Effects of LaB on cell spreading and linker dynamics. Representative DIC image of cells on polymer-tethered lipid bilayers before (A) and immediately after (B) addition of 10μM LaB reveal substantial changes of cell morphology upon LaB treatment. (C) illustrates the histogram of N-cadherin cluster movement distance before (blue) and 5mins after LaB addition (red) as obtained using uTrack. (D) shows that LaB addition leads to substantial drop of trackable cluster. In this case, cluster size threshold was set at 200nm in diameter. Error bars indicate standard deviation from tracking analysis obtained from 5 different cells (ANOVA test, P<0.005). Scale bar: 10μm.

chimera linkers at the cell-substrate interface is intriguing, as it suggests that our substrate functions as a compelling cell surface-mimicking platform for the analysis of adhesion linker dynamics at cell-cell interfaces.

4.5.4 Evaluating Influence of Multi-Bilayer Stacking on N-Cadherin Clustering Underneath C2C12 Myoblasts

Due to the limitations of existing cellular substrates for the investigation of cell-cell linkages, the impact of external mechanical signals on the dynamics of cadherin-based adherens junctions, which act as sensitive mechanosensors at the cell-cell interface, remains largely unknown. Previously, our group established polymer-tethered multi-bilayer stacks with a laminin-functionalized surface as cellular substrates for the analysis of cellular mechanosensitivity of 3T3 fibroblasts [64, 65]. Using this biomembrane-mimicking cell substrate, we demonstrated that substrate stiffness decreases with increasing numbers of bilayers in the stack. To investigate the correlation between linker cluster dynamics and

substrate stiffness, simila multi-bilayer stacks functionalized with Alexa-555 labeled N-cadherin chimera (instead of laminin) were employed. N-cadherin chimera cluster tracking analysis was conducted underneath cells (24 hours after cell plating) on single (Fig. 4.38.A), double (Fig. 4.38.B) and quadruple (Fig. 4.38.C) bilayer stacks.
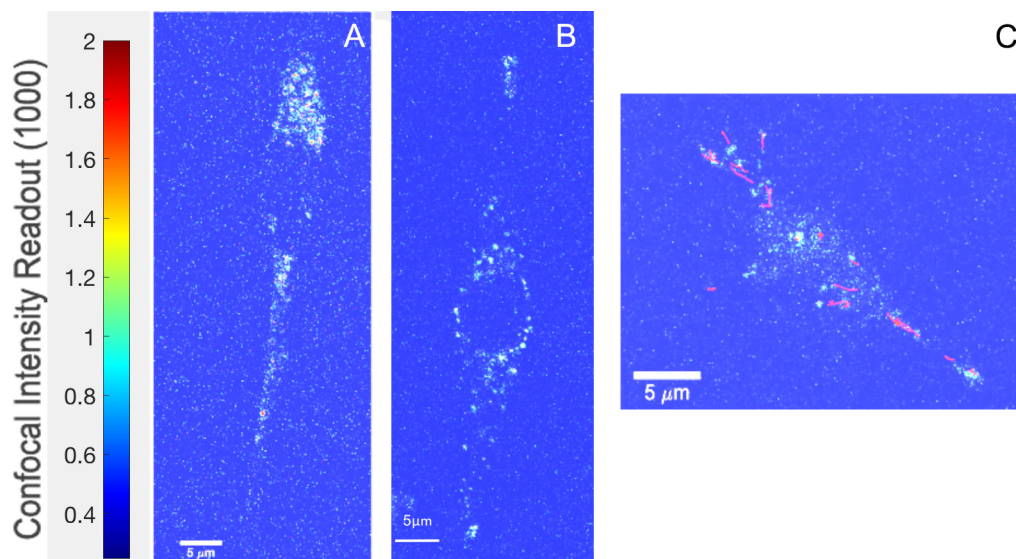
Fig. 4.38. Representative uTrack cluster tracking result of N-cadherin chimera clusters underneath spreading C2C12 myoblasts on single (A), double (B), quadruple (C) bilayers. Tracks over 20 mins are indicated as red lines. Color bar indicates confocal readout intensity. Scale bar: 5μm.

As indicated by Fig. 4.38, the number of trackable linker clusters decreases with increasing bilayer stacking. Further quantitative analysis shows that the number of trackable linker clusters for each cell dropped from approximately 100 clusters per cell on a single bilayer to about 30 clusters per cell on a quadruple bilayer (Fig. 4.39.A). Moreover, uTrack cluster tracking analysis identified that clusters of N-cadherin chimera move faster as the bilayer stack increases (Fig. 4.39.B). These results illustrate a correlation between linker cluster dynamics and previously established properties of cellular mechanosensitivity, such as cellular traction force, cell migration speed, and cytoskeletal organization in response to a change in bilayer stacking. This finding supports the concept that linker cluster dynamics is closely associated with cellular mechanosensitivity.
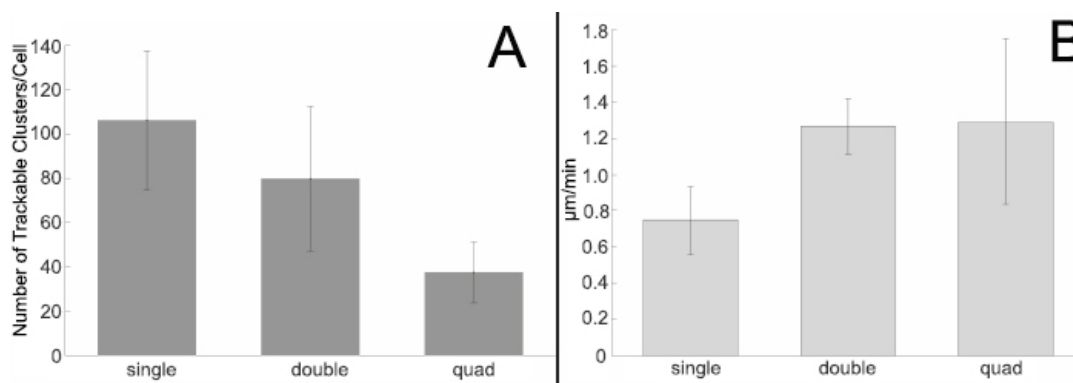
Fig. 4.39. Cluster properties of cells plated on single, double, and quadruple bilayers. In specific, number of trackable clusters decrease as stacking level increases (A), while linker mobility increases (B) with an increase in the degree of bilayer stacking.

In addition to cell property changes in response to bilayer stacking, we have also observed that cells on multiple-bilayer substrates functionalized with N-cadherin chimera are more tolerant to LaB treatment than cells on a corresponding single bilayer. As illustrated by Fig. 4.40, the addition of 10μM LaB did not significantly impair cell spreading and N-cadherin chimera cluster mobility on double bilayers (Fig. 4.40.C-D). Whereas the most substantial change in cell spreading and linker cluster mobility can be observed on a corresponding single bilayer system (Fig. 4.40.A-B). These observations suggest an intriguing relationship between substrate stiffness and the impact of LaB treatment on properties of plated cells.

Our experiment demonstrates that N-cadherin-chimera-functionalized polymer-tethered lipid bilayers and bilayer stacks work as a powerful cell surface-mimicking substrate system for the analysis of cellular mechanosensitivity. Taking advantage of the unique properties of this platform, the dynamic assembly of cadherin chimera linker clusters was investigated during cell mechanosensing. Cadherin linker dynamics was evaluated, for the first time, at a surface that mimics cell-cell adhesions. In combination with confocal-based fluorescence imaging techniques including FRAP and particle tracking, we were able to detect the enrichment of N-cadherin chimera linkers during cell migration and to characterize the
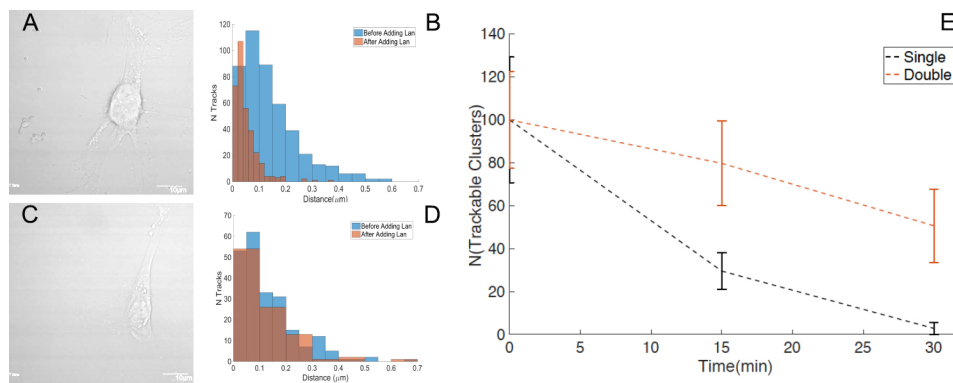
Fig. 4.40. Representative DIC images of cells plated on single polymer tethered lipid bilayer (A) and double bilayer stack (C) indicate a better cell integrity for cells plated on double bilayers after the same dose of LaB treatment. As illustrated by (B) and (D), long range movement of cadherin linker clusters underneath cells plated on double bilayer stacks are less significantly hindered by the addition of LaB. Moreover, amount of trackable clusters only moderatedly decreases compared to single bilayer systems (E, cluster size threshold was set as 200nm in diameter). Error bars indicate standard deviation from tracking analysis obtained from 5 different cells (ANOVA test, P < 0.01).

differences in linker movement at different areas underneath plated cell. Moreover, our results showed that cadherin linker assembly and dynamics is closely related to cytoskeletal organization. This work provides an initial example of quantitatively characterizing physiologically and pathologically important cell-cell linker dynamics based on cell-surface mimicking polymer-tethered single and multi-lipid bilayer substrates that better replicate the rich dynamics found at cell-cell interfaces than traditional polymeric substrates with chemically immobilized linkers [244]. The introduced experimental platform and quantification methodology can be adapted in future adhesion linker dynamic analyses in cell systems.

5. CONCLUSIONS AND OUTLOOK

5.1 Conclusions

It is widely accepted that the distribution and dynamic rearrangement of membrane proteins and membrane protein complexes play essential roles in cellular function. The significance of such membrane protein properties is illustrated by the fact that there is an emerging trend in developing novel therapeutic strategies targeted at membrane protein assembly processes in diseases, such as cancer and neurodegenerative diseases [248–250]. However, due to the complexity of the biological membrane and the limitations of existing experimental methods, the underlying mechanisms of membrane protein assembly and dynamics often remain obscure. To solve this shortcoming, the central goal of this thesis was to develop a methodology to explore the distribution and dynamic assembly of proteins and protein complexes in planar model lipid mixtures of well-defined composition with single molecule sensitivity. Using this experimental strategy, selected membrane proteins were analyzed using a combination of complementary confocal-based fluorescent imaging techniques, which provide insight into the distribution, lateral mobility and oligomerization states. Using these models and techniques, this work explored membrane protein distribution and dynamic rearrangement that are related in two different areas, membrane biophysics and cell mechanics. The membrane proteins analyzed included integrins, GPI-anchored uPAR, and cadherin, all of which are implicated in several key physiological and pathological processes.

In the first section of this dissertation, the distribution and oligomerization states of reconstituted membrane proteins were examined in raft-mimicking lipid mixtures. Using combined FCS, PCH, and CS-XY scans, we revealed that GPI-anchored uPAR is specifically enriched in raft-mimicking l_o phases. Thereby displaying a moderate ratio of dimers. Importantly the addition of natural ligands, including uPA and VN, has a significant impact

on uPAR dimerization level and uPAR distribution in model membranes. Moreover, by applying three types of raft-mimicking lipid mixtures, we discovered that uPAR oligomerization and sequestration are not significantly influenced by CHOL level in the membrane.

In contrast, changes in CHOL concentration were found to have a profound effect on the distribution of integrin $\alpha_v\beta_3$ and $\alpha_v\beta_3$+VN in raft-mimicking lipid mixtures with coexisting l_o and l_d domains. Here the observed relocation of integrins in response to CHOL concentration can be attributed to the effect of this sterol on physical properties of the bilayer, such as hydrophobic thickness and lipid packing [251]. By looking into the details of sequestration and oligomerization, influences of ligand binding and lipid environment on the distribution and oligomerization of GPI-anchored uPAR and transmembrane integrin were determined in raft-mimicking environments. Remarkably, findings from these two proteins revealed distinctive sorting mechanisms for GPI-AP and transmembrane protein, suggesting different roles of ligand binding and lipid environment in regulating membrane protein distribution and function.

The described methodology was not limited to the analysis of a single type of membrane protein in the model membrane, but also included the characterization of lipid-membrane protein and membrane protein-membrane protein complexes in corresponding model lipid compositions. The influence of CHOL and ligand binding on the formation and sequestration of such complexes was examined together with the oligomerization states of membrane protein in complexes. The first complex under investigation was a complex of integrin $\alpha_5\beta_1$ and GM_3. Using combined CS-XY scans and PCH analysis, we found that the complexation between the GM_3 and $\alpha_5\beta_1$ possibly formed through specific chemical interactions. Intriguingly, GM_3 caused the translocation of integrin $\alpha_5\beta_1$ from the l_d to l_o phase in raft-mimicking lipid mixtures. Moreover, in CHOL free lipid bilayers, the complexation between GM_3 and $\alpha_5\beta_1$ was accompanied by a substantial increase in the dimerization state of $\alpha_5\beta_1$, whereas no comparable effect was observed in the CHOL-containing lipid mixtures. These results are interesting as they provide important insight into some physiologically relevant structure developments, such as glycosynapse formation [37].

In another set of experiments, the complex formation between uPAR and integrin $\alpha_v\beta_3$ complex was investigated. This work is significant as this is the first biological complex between a transmembrane protein and a GPI-AP established in an artificial model membrane. In addition, in this project, we developed a dual color quantification method to explore the formation and composition of uPAR-$\alpha_v\beta_3$ complexes. A particular strength of the methodology represents the ability to identify the homo-oligomerization state of each membrane protein in the hetero-complex. Identification of oligomerization within membrane protein complexes is technically challenging. Nevertheless, by introducing a novel dual-color confocal fluorescence quantification method and by combining this methodology with our previously established single color FCS, PCH, and CS-XY scan methods, we were able to investigate the influence of membrane-protein-complex formation on sequestration, oligomerization, and dynamics of uPAR and integrin. In particular, we observed that $\alpha_v\beta_3$ relocated from the l_d to l_o phase in raft-mimicking lipid mixtures upon uPAR reconstitution, which could be attributed to complex formation and/or the allosteric change of integrins upon complex formation. Remarkably, we found that uPAR dimerization increased as the uPAR-integrin complex formed, suggesting a critical role of CHOL in complex formation. From the dual color assay, we found that uPAR dimerization level in the complex is extremely high while $\alpha_v\beta_3$ stays mostly monomeric. Based on that information, we proposed a dimer-monomer model for uPAR-integrin $\alpha_v\beta_3$ complexes. Also, we observed that the addition of the common ligand, VN, helped to promote complex formation between uPAR and $\alpha_v\beta_3$ in CHOL-free lipid bilayers. These findings are potentially significant in light of the physiological and pathological importance of this complex. Our experimental results show that this novel dual color assay provides a powerful experimental platform to decipher properties of a wide-range of hetero-complexes in model membranes and cellular systems with unprecedented accuracy.

In the second section of this thesis, processes of membrane protein distribution and assembly were considered during cell adhesion and migration. In specific, we studied the clustering and dynamics of N-cadherin chimera at the cell-substrate interface during cell migration. Here we investigated the influence of substrate stiffness and cytoskeletal organi-

zation on such dynamic clustering processes. We fabricated polymer-tethered single lipid bilayers and corresponding multi-bilayer stacks as a cell-surface-mimicking substrate of adjustable stiffness. Using laser-scanning confocal microscopy in combination with FCS, PCH, FRAP, and cluster tracking analysis (uTrack), we were able to quantitatively characterize the accumulation , distribution, and dynamics of N-cadherin chimera underneath plated cells. Our results indicated that cadherin chimera linker cluster formation and mobility are primarily driven by the cytoskeleton, with both random and orientated movements being observed. Furthermore, linker cluster dynamics were observed to change in response to mechanical property changes of the substrate due to alternation of the number of bilayers in the multi-bilayer stack. In softer multi-bilayer stacks, linker cluster size decreases and clusters move at a faster speed compared to clusters found on a stiffer substrate. Additionally, induced breakdown of the cytoskeleton stops cadherin chimera cluster movements and disassembles such clusters over time. In this project, we applied cluster tracking to the analysis of cell-cell cadherin-based linkages for the first time. These experiments revealed interesting insights into linker cluster movement between cell and cell-surface-mimicking substrate. In that sense, this project demonstrated the suitability of cell-surface-mimicking substrates for the quantitative analysis of linker clusters at the cell-cell interface, which links to processes such as tissue recovery, stem-cell differentiation, and cancer development.

Together, the experiments described in both sections of the thesis demonstrated the power and versatility of singe molecule-sensitive confocal methodology for the analysis of protein distribution and assembly in membrane systems. Our data also show that polymer-tethered lipid bilayers function as an excellent model membrane platform for the investigation of membrane protein dynamics, distribution and oligomerization.

5.2   Outlook

The work described in this thesis is mainly focused on analyzing membrane protein dynamics, distribution, and oligomerization using polymer-tethered lipid bilayers in com-

bination with confocal-based fluorescent imaging techniques. In this work, we furthered understanding of membrane protein dynamics in an environment that mimics the natural environment of biomembranes. More significantly, we introduced two innovative quantification tools that can be applied broadly to study dynamic membrane protein assemblies. With these tools and the results in this thesis, future research could be expanded to the following type of problems:

1. In uPAR-integrin complexes, other ligands, such as uPA and plasminogen activator inhibitor-1, might play interesting roles in complex formation. It would be worth examining complex formation under the condition that more ligands are associated with the complex. Moreover, other membrane protein-membrane protein complexes, such as integrin cross-talk and EGFR association with uPAR-integrin complexation, are also potential targets for future analysis.

2. In this work, the potential complex between integrin and GM_3 was investigated using a single color strategy. This complex can be further analyzed by dual color assay to reveal the mechanism of GM_3 induced integrin clustering and the effect of CHOL in this process. Such experiments could provide clues into some of the molecular processes in the development of neurodegenerative diseases.

3. In the current thesis work, we explored the assembly and dynamics of N-cadherin linkages between plated cells (C2C12 myoblasts) and a cell-surface-mimicking substrate of adjustable stiffness. The described experimental strategy is equally applicable to other cadherins, such as E-cadherin and VE-cadherin. The analysis of such processes could be potentially significant to better understand the role of mechanical signals during epithelial cell polarization and metastasis. Such experiments may be useful in the development of new therapeutic tools for diseases, such as cancer and inflammation.

LIST OF REFERENCES

LIST OF REFERENCES

[1] G. van Meer, "Cellular lipidomics," *EMBO J*, vol. 24, no. 18, pp. 3159–65, 2005.

[2] G. van Meer, D. R. Voelker, and G. W. Feigenson, "Membrane lipids: where they are and how they behave," *Nat Rev Mol Cell Biol*, vol. 9, no. 2, pp. 112–24, 2008.

[3] C. Klose, M. A. Surma, and K. Simons, "Organellar lipidomics–background and perspectives," *Curr Opin Cell Biol*, vol. 25, no. 4, pp. 406–13, 2013.

[4] J. C. Holthuis and A. K. Menon, "Lipid landscapes and pipelines in membrane homeostasis," *Nature*, vol. 510, no. 7503, pp. 48–57, 2014.

[5] J. L. Sampaio, M. J. Gerl, C. Klose, C. S. Ejsing, H. Beug, K. Simons, and A. Shevchenko, "Membrane lipidome of an epithelial cell line," *Proc Natl Acad Sci U S A*, vol. 108, no. 5, pp. 1903–7, 2011.

[6] D. M. Engelman, "Membranes are more mosaic than fluid," *Nature*, vol. 438, no. 7068, pp. 578–80, 2005.

[7] D. Lingwood and K. Simons, "Lipid rafts as a membrane-organizing principle," *Science*, vol. 327, no. 5961, pp. 46–50, 2010.

[8] H. I. Ingolfsson, M. N. Melo, F. J. van Eerden, C. Arnarez, C. A. Lopez, T. A. Wassenaar, X. Periole, A. H. de Vries, D. P. Tieleman, and S. J. Marrink, "Lipid organization of the plasma membrane," *J Am Chem Soc*, vol. 136, no. 41, pp. 14554–9, 2014.

[9] S. Tan, H. T. Tan, and M. C. Chung, "Membrane proteins and membrane proteomics," *Proteomics*, vol. 8, no. 19, pp. 3924–32, 2008.

[10] K. Simons, "Cell membranes: A subjective perspective," *Biochim Biophys Acta*, 2016.

[11] A. L. Hopkins and C. R. Groom, "The druggable genome," *Nat Rev Drug Discov*, vol. 1, no. 9, pp. 727–30, 2002.

[12] K. Simons and R. Ehehalt, "Cholesterol, lipid rafts, and disease," *J Clin Invest*, vol. 110, no. 5, pp. 597–603, 2002.

[13] K. Simons and E. Ikonen, "Functional rafts in cell membranes," *Nature*, vol. 387, no. 6633, pp. 569–72, 1997.

[14] D. A. Brown and E. London, "Functions of lipid rafts in biological membranes," *Annu Rev Cell Dev Biol*, vol. 14, pp. 111–36, 1998.

[15] J. Lippincott-Schwartz, E. Snapp, and A. Kenworthy, "Studying protein dynamics in living cells," *Nat Rev Mol Cell Biol*, vol. 2, no. 6, pp. 444–56, 2001.

[16] K. Simons and D. Toomre, "Lipid rafts and signal transduction," *Nat Rev Mol Cell Biol*, vol. 1, no. 1, pp. 31–9, 2000.

[17] K. G. Suzuki, "Lipid rafts generate digital-like signal transduction in cell plasma membranes," *Biotechnol J*, vol. 7, no. 6, pp. 753–61, 2012.

[18] S. Manes, E. Mira, C. Gomez-Mouton, R. A. Lacalle, P. Keller, J. P. Labrador, and A. C. Martinez, "Membrane raft microdomains mediate front-rear polarity in migrating cells," *EMBO J*, vol. 18, no. 22, pp. 6211–20, 1999.

[19] K. Gaus, S. Le Lay, N. Balasubramanian, and M. A. Schwartz, "Integrin-mediated adhesion regulates membrane order," *J Cell Biol*, vol. 174, no. 5, pp. 725–34, 2006.

[20] A. Gorgens, J. Beckmann, A. K. Ludwig, M. Mollmann, J. Durig, P. A. Horn, L. Rajendran, and B. Giebel, "Lipid raft redistribution and morphological cell polarization are separable processes providing a basis for hematopoietic stem and progenitor cell migration," *Int J Biochem Cell Biol*, vol. 44, no. 7, pp. 1121–32, 2012.

[21] S. T. Yang, V. Kiessling, and L. K. Tamm, "Line tension at lipid phase boundaries as driving force for hiv fusion peptide-mediated fusion," *Nat Commun*, vol. 7, p. 11401, 2016.

[22] M. Kaparakis-Liaskos and R. L. Ferrero, "Immune modulation by bacterial outer membrane vesicles," *Nat Rev Immunol*, vol. 15, no. 6, pp. 375–87, 2015.

[23] K. Simons and J. L. Sampaio, "Membrane organization and lipid rafts," *Cold Spring Harbor Perspectives in Biology*, vol. 3, no. 10, 2011.

[24] S. Munro, "Lipid rafts," *Cell*, vol. 115, no. 4, pp. 377–388, 2003.

[25] S. Mayor and H. Riezman, "Sorting gpi-anchored proteins," *Nat Rev Mol Cell Biol*, vol. 5, no. 2, pp. 110–20, 2004.

[26] N. Komura, K. G. Suzuki, H. Ando, M. Konishi, M. Koikeda, A. Imamura, R. Chadda, T. K. Fujiwara, H. Tsuboi, R. Sheng, W. Cho, K. Furukawa, K. Furukawa, Y. Yamauchi, H. Ishida, A. Kusumi, and M. Kiso, "Raft-based interactions of gangliosides with a gpi-anchored receptor," *Nat Chem Biol*, vol. 12, no. 6, pp. 402–10, 2016.

[27] F. Blasi and N. Sidenius, "The urokinase receptor: focused cell surface proteolysis, cell adhesion and signaling," *FEBS Lett*, vol. 584, no. 9, pp. 1923–30, 2010.

[28] F. Blasi and P. Carmeliet, "upar: a versatile signalling orchestrator," *Nature reviews Molecular cell biology*, vol. 3, no. 12, pp. 932–943, 2002.

[29] A. Kusumi, K. G. Suzuki, R. S. Kasai, K. Ritchie, and T. K. Fujiwara, "Hierarchical mesoscale domain organization of the plasma membrane," *Trends Biochem Sci*, vol. 36, no. 11, pp. 604–15, 2011.

[30] P. W. Janes, S. C. Ley, A. I. Magee, and P. S. Kabouridis, "The role of lipid rafts in t cell antigen receptor (tcr) signalling," *Semin Immunol*, vol. 12, no. 1, pp. 23–34, 2000.

[31] S. Paladino, S. Lebreton, S. Tivodar, V. Campana, R. Tempre, and C. Zurzolo, "Different gpi-attachment signals affect the oligomerisation of gpi-anchored proteins and their apical sorting," *J Cell Sci*, vol. 121, no. Pt 24, pp. 4001–7, 2008.

[32] V. R. Caiolfa, M. Zamai, G. Malengo, A. Andolfo, C. D. Madsen, J. Sutin, M. A. Digman, E. Gratton, F. Blasi, and N. Sidenius, "Monomer dimer dynamics and distribution of gpi-anchored upar are determined by cell surface protein assemblies," *J Cell Biol*, vol. 179, no. 5, pp. 1067–82, 2007.

[33] D. Dibya, N. Arora, and E. A. Smith, "Noninvasive measurements of integrin microclustering under altered membrane cholesterol levels," *Biophys J*, vol. 99, no. 3, pp. 853–61, 2010.

[34] A. Norambuena and M. A. Schwartz, "Effects of integrin-mediated cell adhesion on plasma membrane lipid raft components and signaling," *Mol Biol Cell*, vol. 22, no. 18, pp. 3456–64, 2011.

[35] T. Tarui, A. P. Mazar, D. B. Cines, and Y. Takada, "Urokinase-type plasminogen activator receptor (cd87) is a ligand for integrins and mediates cell-cell interaction," *J Biol Chem*, vol. 276, no. 6, pp. 3983–90, 2001.

[36] H. W. Smith and C. J. Marshall, "Regulation of cell signalling by upar," *Nat Rev Mol Cell Biol*, vol. 11, no. 1, pp. 23–36, 2010.

[37] S. I. Hakomori Si, "The glycosynapse," *Proc Natl Acad Sci U S A*, vol. 99, no. 1, pp. 225–32, 2002.

[38] L. M. Grove, B. D. Southern, T. H. Jin, K. E. White, S. Paruchuri, E. Harel, Y. Wei, S. O. Rahaman, C. L. Gladson, Q. Ding, C. S. Craik, H. A. Chapman, and M. A. Olman, "Urokinase-type plasminogen activator receptor (upar) ligation induces a raft-localized integrin signaling switch that mediates the hypermotile phenotype of fibrotic fibroblasts," *J Biol Chem*, vol. 289, no. 18, pp. 12791–804, 2014.

[39] P. Gopalakrishna, N. Rangaraj, and G. Pande, "Cholesterol alters the interaction of glycosphingolipid gm3 with alpha5beta1 integrin and increases integrin-mediated cell adhesion to fibronectin," *Exp Cell Res*, vol. 300, no. 1, pp. 43–53, 2004.

[40] V. Kiessling, S. T. Yang, and L. K. Tamm, "Supported lipid bilayers as models for studying membrane domains," *Curr Top Membr*, vol. 75, pp. 1–23, 2015.

[41] M. J. Richards, C. Y. Hsia, R. R. Singh, H. Haider, J. Kumpf, T. Kawate, and S. Daniel, "Membrane protein mobility and orientation preserved in supported bilayers created directly from cell plasma membrane blebs," *Langmuir*, vol. 32, no. 12, pp. 2963–74, 2016.

[42] T. Baumgart, S. T. Hess, and W. W. Webb, "Imaging coexisting fluid domains in biomembrane models coupling curvature and line tension," *Nature*, vol. 425, no. 6960, pp. 821–4, 2003.

[43] I. L. Jorgensen, G. C. Kemmer, and T. G. Pomorski, "Membrane protein reconstitution into giant unilamellar vesicles: a review on current techniques," *Eur Biophys J*, 2016.

[44] T. Baumgart, A. T. Hammond, P. Sengupta, S. T. Hess, D. A. Holowka, B. A. Baird, and W. W. Webb, "Large-scale fluid/fluid phase separation of proteins and lipids in giant plasma membrane vesicles," *Proc Natl Acad Sci U S A*, vol. 104, no. 9, pp. 3165–70, 2007.

[45] E. Sezgin, H. J. Kaiser, T. Baumgart, P. Schwille, K. Simons, and I. Levental, "Elucidating membrane structure and protein behavior using giant plasma membrane vesicles," *Nat Protoc*, vol. 7, no. 6, pp. 1042–51, 2012.

[46] S. L. Veatch and S. L. Keller, "Separation of liquid phases in giant vesicles of ternary mixtures of phospholipids and cholesterol," *Biophysical Journal*, vol. 85, no. 5, pp. 3074–3083, 2003.

[47] W. C. Lin, L. Iversen, H. L. Tu, C. Rhodes, S. M. Christensen, J. S. Iwig, S. D. Hansen, W. Y. Huang, and J. T. Groves, "H-ras forms dimers on membrane surfaces via a protein-protein interface," *Proc Natl Acad Sci U S A*, vol. 111, no. 8, pp. 2996–3001, 2014.

[48] Q. Xu, W. C. Lin, R. S. Petit, and J. T. Groves, "Epha2 receptor activation by monomeric ephrin-a1 on supported membranes," *Biophys J*, vol. 101, no. 11, pp. 2731–9, 2011.

[49] I. H. Lee, S. Saha, A. Polley, H. Huang, S. Mayor, M. Rao, and J. T. Groves, "Live cell plasma membranes do not exhibit a miscibility phase transition over a wide range of temperatures," *J Phys Chem B*, vol. 119, no. 12, pp. 4450–9, 2015.

[50] D. Lingwood, J. Ries, P. Schwille, and K. Simons, "Plasma membranes are poised for activation of raft phase coalescence at physiological temperature," *Proc Natl Acad Sci U S A*, vol. 105, no. 29, pp. 10005–10, 2008.

[51] D. Scherfeld, N. Kahya, and P. Schwille, "Lipid dynamics and domain formation in model membranes composed of ternary mixtures of unsaturated and saturated phosphatidylcholines and cholesterol," *Biophysical Journal*, vol. 85, no. 6, pp. 3758–3768, 2003.

[52] S. L. Veatch and S. L. Keller, "Miscibility phase diagrams of giant vesicles containing sphingomyelin," *Phys Rev Lett*, vol. 94, no. 14, p. 148101, 2005.

[53] J. V. Bleecker, P. A. Cox, R. N. Foster, J. P. Litz, M. C. Blosser, D. G. Castner, and S. L. Keller, "Thickness mismatch of coexisting liquid phases in noncanonical lipid bilayers," *J Phys Chem B*, vol. 120, no. 10, pp. 2761–70, 2016.

[54] A. P. Siegel, A. Kimble-Hill, S. Garg, R. Jordan, and C. A. Naumann, "Native ligands change integrin sequestering but not oligomerization in raft-mimicking lipid mixtures," *Biophys J*, vol. 101, no. 7, pp. 1642–50, 2011.

[55] N. F. Hussain, A. P. Siegel, Y. Ge, R. Jordan, and C. A. Naumann, "Bilayer asymmetry influences integrin sequestering in raft-mimicking lipid mixtures," *Biophys J*, vol. 104, no. 10, pp. 2212–21, 2013.

[56] B. Geiger, J. P. Spatz, and A. D. Bershadsky, "Environmental sensing through focal adhesions," *Nat Rev Mol Cell Biol*, vol. 10, no. 1, pp. 21–33, 2009.

[57] W. M. Brieher and A. S. Yap, "Cadherin junctions and their cytoskeleton(s)," *Curr Opin Cell Biol*, vol. 25, no. 1, pp. 39–46, 2013.

[58] A. D. Bershadsky, N. Q. Balaban, and B. Geiger, "Adhesion-dependent cell mechanosensitivity," *Annu Rev Cell Dev Biol*, vol. 19, pp. 677–95, 2003.

[59] G. A. Gomez, R. W. McLachlan, and A. S. Yap, "Productive tension: force-sensing and homeostasis of cell-cell junctions," *Trends Cell Biol*, vol. 21, no. 9, pp. 499–505, 2011.

[60] D. E. Discher, P. Janmey, and Y. L. Wang, "Tissue cells feel and respond to the stiffness of their substrate," *Science*, vol. 310, no. 5751, pp. 1139–43, 2005.

[61] I. L. Ivanovska, J. W. Shin, J. Swift, and D. E. Discher, "Stem cell mechanobiology: diverse lessons from bone marrow," *Trends Cell Biol*, vol. 25, no. 9, pp. 523–32, 2015.

[62] F. Peglion, F. Llense, and S. Etienne-Manneville, "Adherens junction treadmilling during collective migration," *Nat Cell Biol*, vol. 16, no. 7, pp. 639–51, 2014.

[63] M. Takeichi, "Dynamic contacts: rearranging adherens junctions to drive epithelial remodelling," *Nat Rev Mol Cell Biol*, vol. 15, no. 6, pp. 397–410, 2014.

[64] D. E. Minner, P. Rauch, J. Kas, and C. A. Naumann, "Polymer-tethered lipid multi-bilayers: a biomembrane-mimicking cell substrate to probe cellular mechano-sensing," *Soft Matter*, vol. 10, no. 8, pp. 1189–98, 2014.

[65] L. A. Lautscham, C. Y. Lin, V. Auernheimer, C. A. Naumann, W. H. Goldmann, and B. Fabry, "Biomembrane-mimicking lipid bilayer system as a mechanically tunable cell substrate," *Biomaterials*, vol. 35, no. 10, pp. 3198–207, 2014.

[66] M. A. Deverall, S. Garg, K. Lüdtke, R. Jordan, J. Rühe, and C. A. Naumann, "Trans-bilayer coupling of obstructed lipid diffusion in polymer-tethered phospholipid bilayers," *Soft Matter*, vol. 4, no. 9, pp. 1899–1908, 2008.

[67] M. Loose and P. Schwille, "Biomimetic membrane systems to study cellular organization," *J Struct Biol*, vol. 168, no. 1, pp. 143–51, 2009.

[68] M. Tanaka and E. Sackmann, "Polymer-supported membranes as models of the cell surface," *Nature*, vol. 437, no. 7059, pp. 656–63, 2005.

[69] B. A. Cornell, V. L. B. BraachMaksvytis, L. G. King, P. D. J. Osman, B. Raguse, L. Wieczorek, and R. J. Pace, "A biosensor that uses ion-channel switches," *Nature*, vol. 387, no. 6633, pp. 580–583, 1997.

[70] K. H. Biswas, K. L. Hartman, C. H. Yu, O. J. Harrison, H. Song, A. W. Smith, W. Y. Huang, W. C. Lin, Z. Guo, A. Padmanabhan, S. M. Troyanovsky, M. L. Dustin, L. Shapiro, B. Honig, R. Zaidel-Bar, and J. T. Groves, "E-cadherin junction formation involves an active kinetic nucleation process," *Proc Natl Acad Sci U S A*, vol. 112, no. 35, pp. 10932–7, 2015.

[71] P. S. Cremer and S. G. Boxer, "Formation and spreading of lipid bilayers on planar glass supports," *The Journal of Physical Chemistry B*, vol. 103, no. 13, pp. 2554–2559, 1999.

[72] E. T. Castellana and P. S. Cremer, "Solid supported lipid bilayers: From biophysical studies to sensor design," *Surface Science Reports*, vol. 61, no. 10, pp. 429–444, 2006.

[73] W. Li, J. K. Chung, Y. K. Lee, and J. T. Groves, "Graphene-templated supported lipid bilayer nanochannels," *Nano Lett*, vol. 16, no. 8, pp. 5022–6, 2016.

[74] I. Langmuir, "The constitution and fundamental properties of solids and liquids. ii. liquids.1," *Journal of the American Chemical Society*, vol. 39, no. 9, pp. 1848–1906, 1917.

[75] K. B. Blodgett, "Monomolecular films of fatty acids on glass," *Journal of the American Chemical Society*, vol. 56, no. 2, pp. 495–495, 1934.

[76] I. Langmuir and V. J. Schaefer, "Activities of urease and pepsin monolayers," *Journal of the American Chemical Society*, vol. 60, no. 6, pp. 1351–1360, 1938.

[77] M. Antonietti and S. Frster, "Vesicles and liposomes: A self-assembly principle beyond lipids," *Advanced Materials*, vol. 15, no. 16, pp. 1323–1333, 2003.

[78] J. Voskuhl and B. J. Ravoo, "Molecular recognition of bilayer vesicles," *Chem Soc Rev*, vol. 38, no. 2, pp. 495–505, 2009.

[79] Y. H. Chan and S. G. Boxer, "Model membrane systems and their applications," *Curr Opin Chem Biol*, vol. 11, no. 6, pp. 581–7, 2007.

[80] S. Sankhagowit, S. H. Wu, R. Biswas, C. T. Riche, M. L. Povinelli, and N. Malmstadt, "The dynamics of giant unilamellar vesicle oxidation probed by morphological transitions," *Biochim Biophys Acta*, vol. 1838, no. 10, pp. 2615–24, 2014.

[81] R. P. Richter, R. Berat, and A. R. Brisson, "Formation of solid-supported lipid bilayers: an integrated view," *Langmuir*, vol. 22, no. 8, pp. 3497–505, 2006.

[82] J. Raedler, H. Strey, and E. Sackmann, "Phenomenology and kinetics of lipid bilayer spreading on hydrophilic surfaces," *Langmuir*, vol. 11, no. 11, pp. 4539–4548, 1995.

[83] P. Lenz, C. M. Ajo-Franklin, and S. G. Boxer, "Patterned supported lipid bilayers and monolayers on poly(dimethylsiloxane)," *Langmuir*, vol. 20, no. 25, pp. 11092–9, 2004.

[84] P. Nollert, H. Kiefer, and F. Jhnig, "Lipid vesicle adsorption versus formation of planar bilayers on solid surfaces," *Biophysical Journal*, vol. 69, no. 4, pp. 1447–1455, 1995.

[85] R. Richter, A. Mukhopadhyay, and A. Brisson, "Pathways of lipid vesicle deposition on solid surfaces: A combined qcm-d and afm study," *Biophysical Journal*, vol. 85, no. 5, pp. 3035–3047, 2003.

[86] D. E. Minner, V. L. Herring, A. P. Siegel, A. Kimble-Hill, M. A. Johnson, and C. A. Naumann, "Iterative layer-by-layer assembly of polymer-tethered multi-bilayers using maleimidethiol coupling chemistry," *Soft Matter*, vol. 9, no. 40, p. 9643, 2013.

[87] A. Vaziri, J. Tang, H. Shroff, and C. V. Shank, "Multilayer three-dimensional super resolution imaging of thick biological samples," *Proc Natl Acad Sci U S A*, vol. 105, no. 51, pp. 20221–6, 2008.

[88] Y. Min, K. Kristiansen, J. M. Boggs, C. Husted, J. A. Zasadzinski, and J. Israelachvili, "Interaction forces and adhesion of supported myelin lipid bilayers modulated by myelin basic protein," *Proc Natl Acad Sci U S A*, vol. 106, no. 9, pp. 3154–9, 2009.

[89] Y. Zhu, A. Negmi, and J. Moran-Mirabal, "Multi-stacked supported lipid bilayer micropatterning through polymer stencil lift-off," *Membranes (Basel)*, vol. 5, no. 3, pp. 385–98, 2015.

[90] M. Chung, R. D. Lowe, Y. H. Chan, P. V. Ganesan, and S. G. Boxer, "Dna-tethered membranes formed by giant vesicle rupture," *J Struct Biol*, vol. 168, no. 1, pp. 190–9, 2009.

[91] D. B. Murphy, *Fundamentals of light microscopy and electronic imaging*. John Wiley & Sons, 2002.

[92] D. Magde, E. Elson, and W. W. Webb, "Thermodynamic fluctuations in a reacting systemmeasurement by fluorescence correlation spectroscopy," *Physical Review Letters*, vol. 29, no. 11, p. 705, 1972.

[93] J. Mütze, T. Ohrt, and P. Schwille, "Fluorescence correlation spectroscopy in vivo," *Laser & photonics reviews*, vol. 5, no. 1, pp. 52–67, 2011.

[94] R. Rigler and E. S. Elson, *Fluorescence correlation spectroscopy: theory and applications*, vol. 65. Springer Science & Business Media, 2012.

[95] E. Haustein and P. Schwille, "Fluorescence correlation spectroscopy: novel variations of an established technique," *Annu Rev Biophys Biomol Struct*, vol. 36, pp. 151–69, 2007.

[96] W. Becker, B. Su, O. Holub, *et al.*, "Flim and fcs detection in laser-scanning microscopes: Increased efficiency by gaasp hybrid detectors," *Microscopy research and technique*, vol. 74, no. 9, pp. 804–811, 2011.

[97] Y. Chen, J. D. Mller, P. T. C. So, and E. Gratton, "The photon counting histogram in fluorescence fluctuation spectroscopy," *Biophysical Journal*, vol. 77, no. 1, pp. 553–567, 1999.

[98] M. Kang, C. A. Day, A. K. Kenworthy, and E. DiBenedetto, "Simplified equation to extract diffusion coefficients from confocal frap data," *Traffic*, vol. 13, no. 12, pp. 1589–600, 2012.

[99] M. J. Saxton and K. Jacobson, "Single-particle tracking: applications to membrane dynamics," *Annu Rev Biophys Biomol Struct*, vol. 26, pp. 373–99, 1997.

[100] N. Chenouard, I. Smal, F. de Chaumont, M. Maska, I. F. Sbalzarini, Y. Gong, J. Cardinale, C. Carthel, S. Coraluppi, M. Winter, A. R. Cohen, W. J. Godinez, K. Rohr, Y. Kalaidzidis, L. Liang, J. Duncan, H. Shen, Y. Xu, K. E. Magnusson, J. Jalden, H. M. Blau, P. Paul-Gilloteaux, P. Roudot, C. Kervrann, F. Waharte, J. Y. Tinevez, S. L. Shorte, J. Willemse, K. Celler, G. P. van Wezel, H. W. Dan, Y. S. Tsai, C. Ortiz de Solorzano, J. C. Olivo-Marin, and E. Meijering, "Objective comparison of particle tracking methods," *Nat Methods*, vol. 11, no. 3, pp. 281–9, 2014.

[101] K. Jaqaman, D. Loerke, M. Mettlen, H. Kuwata, S. Grinstein, S. L. Schmid, and G. Danuser, "Robust single-particle tracking in live-cell time-lapse sequences," *Nat Methods*, vol. 5, no. 8, pp. 695–702, 2008.

[102] A. Matov, K. Applegate, P. Kumar, C. Thoma, W. Krek, G. Danuser, and T. Wittmann, "Analysis of microtubule dynamic instability using a plus-end growth marker," *Nat Methods*, vol. 7, no. 9, pp. 761–8, 2010.

[103] S. Singer and G. L. Nicolson, "The fluid mosaic model of the structure of cell membranes," *Membranes and Viruses in Immunopathology; Day, SB, Good, RA, Eds*, pp. 7–47, 1972.

[104] C. Danilo and P. G. Frank, "Cholesterol and breast cancer development," *Curr Opin Pharmacol*, vol. 12, no. 6, pp. 677–82, 2012.

[105] S. K. Patra, "Dissecting lipid raft facilitated cell signaling pathways in cancer," *Biochim Biophys Acta*, vol. 1785, no. 2, pp. 182–206, 2008.

[106] Z. Liao, L. M. Cimakasky, R. Hampton, D. H. Nguyen, and J. E. Hildreth, "Lipid rafts and hiv pathogenesis: host membrane cholesterol is required for infection by hiv type 1," *AIDS Res Hum Retroviruses*, vol. 17, no. 11, pp. 1009–19, 2001.

[107] M. Leslie, "Mysteries of the cell. do lipid rafts exist?," *Science*, vol. 334, no. 6059, pp. 1046–7, 2011.

[108] S. H. Wu and H. M. McConnell, "Phase separations in phospholipid membranes," *Biochemistry*, vol. 14, no. 4, pp. 847–854, 1975.

[109] E. London, "Insights into lipid raft structure and formation from experiments in model membranes," *Current Opinion in Structural Biology*, vol. 12, no. 4, pp. 480–486, 2002.

[110] X. Xu and E. London, "The effect of sterol structure on membrane lipid domains reveals how cholesterol can induce lipid domain formation," *Biochemistry*, vol. 39, no. 5, pp. 843–849, 2000.

[111] H. J. Risselada and S. J. Marrink, "The molecular face of lipid rafts in model membranes," *Proc Natl Acad Sci U S A*, vol. 105, no. 45, pp. 17367–72, 2008.

[112] I. Casuso, J. Khao, M. Chami, P. Paul-Gilloteaux, M. Husain, J. P. Duneau, H. Stahlberg, J. N. Sturgis, and S. Scheuring, "Characterization of the motion of membrane proteins using high-speed atomic force microscopy," *Nat Nanotechnol*, vol. 7, no. 8, pp. 525–9, 2012.

[113] I. V. Ionova, V. A. Livshits, and D. Marsh, "Phase diagram of ternary cholesterol/palmitoylsphingomyelin/palmitoyloleoyl-phosphatidylcholine mixtures: spin-label epr study of lipid-raft formation," *Biophys J*, vol. 102, no. 8, pp. 1856–65, 2012.

[114] S. L. Veatch and S. L. Keller, "Miscibility phase diagrams of giant vesicles containing sphingomyelin," *Phys Rev Lett*, vol. 94, no. 14, p. 148101, 2005.

[115] K. Simons and W. L. Vaz, "Model systems, lipid rafts, and cell membranes," *Annu Rev Biophys Biomol Struct*, vol. 33, pp. 269–95, 2004.

[116] D. M. Owen, A. Magenau, D. Williamson, and K. Gaus, "The lipid raft hypothesis revisited–new insights on raft composition and function from super-resolution fluorescence microscopy," *Bioessays*, vol. 34, no. 9, pp. 739–47, 2012.

[117] L. J. Pike, "Rafts defined: a report on the keystone symposium on lipid rafts and cell function," *J Lipid Res*, vol. 47, no. 7, pp. 1597–8, 2006.

[118] T. Friedrichson and T. V. Kurzchalia, "Microdomains of gpi-anchored proteins in living cells revealed by crosslinking," *Nature*, vol. 394, no. 6695, pp. 802–5, 1998.

[119] K. G. Suzuki, T. K. Fujiwara, F. Sanematsu, R. Iino, M. Edidin, and A. Kusumi, "Gpi-anchored receptor clusters transiently recruit lyn and g alpha for temporary cluster immobilization and lyn activation: single-molecule tracking study 1," *J Cell Biol*, vol. 177, no. 4, pp. 717–30, 2007.

[120] K. G. Suzuki, T. K. Fujiwara, M. Edidin, and A. Kusumi, "Dynamic recruitment of phospholipase c gamma at transiently immobilized gpi-anchored receptor clusters induces ip3-ca2+ signaling: single-molecule tracking study 2," *J Cell Biol*, vol. 177, no. 4, pp. 731–42, 2007.

[121] B. Leitinger and N. Hogg, "The involvement of lipid rafts in the regulation of integrin function," *J Cell Sci*, vol. 115, no. Pt 5, pp. 963–72, 2002.

[122] M. L. Dustin and J. A. Cooper, "The immunological synapse and the actin cytoskeleton: molecular hardware for t cell signaling," *Nat Immunol*, vol. 1, no. 1, pp. 23–9, 2000.

[123] M. K. Doeven, J. H. Folgering, V. Krasnikov, E. R. Geertsma, G. van den Bogaart, and B. Poolman, "Distribution, lateral mobility and function of membrane proteins incorporated into giant unilamellar vesicles," *Biophys J*, vol. 88, no. 2, pp. 1134–42, 2005.

[124] K. Weise, G. Triola, L. Brunsveld, H. Waldmann, and R. Winter, "Influence of the lipidation motif on the partitioning and association of n-ras in model membrane subdomains," *J Am Chem Soc*, vol. 131, no. 4, pp. 1557–64, 2009.

[125] K. Bacia, C. G. Schuette, N. Kahya, R. Jahn, and P. Schwille, "Snares prefer liquid-disordered over "raft" (liquid-ordered) domains when reconstituted into giant unilamellar vesicles," *J Biol Chem*, vol. 279, no. 36, pp. 37951–5, 2004.

[126] C. Wan, V. Kiessling, and L. K. Tamm, "Coupling of cholesterol-rich lipid phases in asymmetric bilayers," *Biochemistry*, vol. 47, no. 7, pp. 2190–8, 2008.

[127] M. Lucky, *Chapter 1: Introduction*. New York, Ny: Cambridge University Press, 2013.

[128] F. X. Contreras, A. M. Ernst, F. Wieland, and B. Brugger, "Specificity of intramembrane protein-lipid interactions," *Cold Spring Harb Perspect Biol*, vol. 3, no. 6, 2011.

[129] H. Palsdottir, C. G. Lojero, B. L. Trumpower, and C. Hunte, "Structure of the yeast cytochrome bc1 complex with a hydroxyquinone anion qo site inhibitor bound," *J Biol Chem*, vol. 278, no. 33, pp. 31303–11, 2003.

[130] J. Deisenhofer and H. Michel, "Nobel lecture. the photosynthetic reaction centre from the purple bacterium rhodopseudomonas viridis," *EMBO J*, vol. 8, no. 8, pp. 2149–70, 1989.

[131] M. A. Hanson, V. Cherezov, M. T. Griffith, C. B. Roth, V. P. Jaakola, E. Y. Chien, J. Velasquez, P. Kuhn, and R. C. Stevens, "A specific cholesterol binding site is established by the 2.8 a structure of the human beta2-adrenergic receptor," *Structure*, vol. 16, no. 6, pp. 897–905, 2008.

[132] J. Gomez, B. and N. C. Robinson, "Phospholipase digestion of bound cardiolipin reversibly inactivates bovine cytochrome bc1," *Biochemistry*, vol. 38, no. 28, pp. 9031–8, 1999.

[133] C. Lange, J. H. Nett, B. L. Trumpower, and C. Hunte, "Specific roles of protein-phospholipid interactions in the yeast cytochrome bc1 complex structure," *EMBO J*, vol. 20, no. 23, pp. 6591–600, 2001.

[134] P. Marius, M. Zagnoni, M. E. Sandison, J. M. East, H. Morgan, and A. G. Lee, "Binding of anionic lipids to at least three nonannular sites on the potassium channel kcsa is required for channel opening," *Biophys J*, vol. 94, no. 5, pp. 1689–98, 2008.

[135] T. J. Pucadyil and A. Chattopadhyay, "Cholesterol modulates ligand binding and g-protein coupling to serotonin(1a) receptors from bovine hippocampus," *Biochim Biophys Acta*, vol. 1663, no. 1-2, pp. 188–200, 2004.

[136] A. Bist, P. E. Fielding, and C. J. Fielding, "Two sterol regulatory element-like sequences mediate up-regulation of caveolin gene transcription in response to low density lipoprotein free cholesterol," *Proceedings of the National Academy of Sciences*, vol. 94, no. 20, pp. 10693–10698, 1997.

[137] A. Regina Todeschini and S. I. Hakomori, "Functional role of glycosphingolipids and gangliosides in control of cell adhesion, motility, and growth, through glycosynaptic microdomains," *Biochim Biophys Acta*, vol. 1780, no. 3, pp. 421–33, 2008.

[138] H. Li and V. Papadopoulos, "Peripheral-type benzodiazepine receptor function in cholesterol transport. identification of a putative cholesterol recognition/interaction amino acid sequence and consensus pattern," *Endocrinology*, vol. 139, no. 12, pp. 4991–7, 1998.

[139] A. G. Lee, "Biological membranes: the importance of molecular detail," *Trends Biochem Sci*, vol. 36, no. 9, pp. 493–500, 2011.

[140] O. S. Andersen and n. Koeppe, R. E., "Bilayer thickness and membrane protein function: an energetic perspective," *Annu Rev Biophys Biomol Struct*, vol. 36, pp. 107–30, 2007.

[141] D. Marsh, "Protein modulation of lipids, and vice-versa, in membranes," *Biochim Biophys Acta*, vol. 1778, no. 7-8, pp. 1545–75, 2008.

[142] A. G. Lee, "Lipidprotein interactions in biological membranes: a structural perspective," *Biochimica et Biophysica Acta (BBA) - Biomembranes*, vol. 1612, no. 1, pp. 1–40, 2003.

[143] A. G. Lee, "How lipids affect the activities of integral membrane proteins," *Biochim Biophys Acta*, vol. 1666, no. 1-2, pp. 62–87, 2004.

[144] A. P. Starling, K. A. Dalton, J. M. East, S. Oliver, and A. G. Lee, "Effects of phosphatidylethanolamines on the activity of the ca2+-atpase of sarcoplasmic reticulum," *Biochemical Journal*, vol. 320, no. 1, pp. 309–314, 1996.

[145] Y. Song, A. K. Kenworthy, and C. R. Sanders, "Cholesterol as a co-solvent and a ligand for membrane proteins," *Protein Sci*, vol. 23, no. 1, pp. 1–22, 2014.

[146] F. A. Nezil and M. Bloom, "Combined influence of cholesterol and synthetic amphiphillic peptides upon bilayer thickness in model membranes," *Biophysical Journal*, vol. 61, no. 5, pp. 1176–1183, 1992.

[147] P. R. Maulik and G. G. Shipley, "Interactions of n-stearoyl sphingomyelin with cholesterol and dipalmitoylphosphatidylcholine in bilayer membranes," *Biophysical Journal*, vol. 70, no. 5, pp. 2256–2265, 1996.

[148] O. F. Kuzu, M. A. Noory, and G. P. Robertson, "The role of cholesterol in cancer," *Cancer Res*, vol. 76, no. 8, pp. 2063–70, 2016.

[149] A. R. Koudinov, "Essential role for cholesterol in synaptic plasticity and neuronal degeneration," *The FASEB Journal*, 2001.

[150] R. Nussinov, H. Jang, and C. J. Tsai, "Oligomerization and nanocluster organization render specificity," *Biol Rev Camb Philos Soc*, vol. 90, no. 2, pp. 587–98, 2015.

[151] A. Fink, N. Sal-Man, D. Gerber, and Y. Shai, "Transmembrane domains interactions within the membrane milieu: principles, advances and challenges," *Biochim Biophys Acta*, vol. 1818, no. 4, pp. 974–83, 2012.

[152] B. P. Head, H. H. Patel, and P. A. Insel, "Interaction of membrane/lipid rafts with the cytoskeleton: impact on signaling and function: membrane/lipid rafts, mediators of cytoskeletal arrangement and cell signaling," *Biochim Biophys Acta*, vol. 1838, no. 2, pp. 532–45, 2014.

[153] F. X. Zhou, H. J. Merianos, A. T. Brunger, and D. M. Engelman, "Polar residues drive association of polyleucine transmembrane helices," *Proc Natl Acad Sci U S A*, vol. 98, no. 5, pp. 2250–5, 2001.

[154] H. Gratkowski, J. D. Lear, and W. F. DeGrado, "Polar side chains drive the association of model transmembrane peptides," *Proc Natl Acad Sci U S A*, vol. 98, no. 3, pp. 880–5, 2001.

[155] S. Paladino, S. Lebreton, S. Tivodar, F. Formiggini, G. Ossato, E. Gratton, M. Tramier, M. Coppey-Moisan, and C. Zurzolo, "Golgi sorting regulates organization and activity of gpi proteins at apical membranes," *Nat Chem Biol*, vol. 10, no. 5, pp. 350–7, 2014.

[156] M. Ploug, "Structure-driven design of radionuclide tracers for non-invasive imaging of upar and targeted radiotherapy. the tale of a synthetic peptide antagonist," *Theranostics*, vol. 3, no. 7, pp. 467–76, 2013.

[157] O. Cunningham, A. Andolfo, M. L. Santovito, L. Iuzzolino, F. Blasi, and N. Sidenius, "Dimerization controls the lipid raft partitioning of upar/cd87 and regulates its biological functions," *EMBO J*, vol. 22, no. 22, pp. 5994–6003, 2003.

[158] S. Zorman, M. Botte, Q. Jiang, I. Collinson, and C. Schaffitzel, "Advances and challenges of membrane-protein complex production," *Curr Opin Struct Biol*, vol. 32, pp. 123–30, 2015.

[159] J. J. Lacapere, E. Pebay-Peyroula, J. M. Neumann, and C. Etchebest, "Determining membrane protein structures: still a challenge!," *Trends Biochem Sci*, vol. 32, no. 6, pp. 259–70, 2007.

[160] N. Wettschureck and S. Offermanns, "Mammalian g proteins and their cell type specific functions," *Physiol Rev*, vol. 85, no. 4, pp. 1159–204, 2005.

[161] S. Paladino, D. Sarnataro, R. Pillich, S. Tivodar, L. Nitsch, and C. Zurzolo, "Protein oligomerization modulates raft partitioning and apical sorting of gpi-anchored proteins," *J Cell Biol*, vol. 167, no. 4, pp. 699–709, 2004.

[162] H. J. Kaiser, A. Orlowski, T. Rog, T. K. Nyholm, W. Chai, T. Feizi, D. Lingwood, I. Vattulainen, and K. Simons, "Lateral sorting in model membranes by cholesterol-mediated hydrophobic matching," *Proc Natl Acad Sci U S A*, vol. 108, no. 40, pp. 16628–33, 2011.

[163] F. G. Giancotti, "Integrin signaling," *Science*, vol. 285, no. 5430, pp. 1028–1033, 1999.

[164] K. Ley, J. Rivera-Nieves, W. J. Sandborn, and S. Shattil, "Integrin-based therapeutics: biological basis, clinical use and new drugs," *Nat Rev Drug Discov*, vol. 15, no. 3, pp. 173–83, 2016.

[165] C. V. Carman and T. A. Springer, "Integrin avidity regulation: are changes in affinity and conformation underemphasized?," *Current Opinion in Cell Biology*, vol. 15, no. 5, pp. 547–556, 2003.

[166] N. J. Anthis and I. D. Campbell, "The tail of integrin activation," *Trends Biochem Sci*, vol. 36, no. 4, pp. 191–8, 2011.

[167] R. Li, R. Gorelik, V. Nanda, P. B. Law, J. D. Lear, W. F. DeGrado, and J. S. Bennett, "Dimerization of the transmembrane domain of integrin alphaiib subunit in cell membranes," *J Biol Chem*, vol. 279, no. 25, pp. 26666–73, 2004.

[168] D. V. Iwamoto and D. A. Calderwood, "Regulation of integrin-mediated adhesions," *Curr Opin Cell Biol*, vol. 36, pp. 41–7, 2015.

[169] N. Arora, A. Syed, S. Sander, and E. A. Smith, "Single particle tracking with sterol modulation reveals the cholesterol-mediated diffusion properties of integrin receptors," *Phys Biol*, vol. 11, no. 6, p. 066001, 2014.

[170] X. Wang, P. Sun, A. Al-Qamari, T. Tai, I. Kawashima, and A. S. Paller, "Carbohydrate-carbohydrate binding of ganglioside to integrin alpha(5) modulates alpha(5)beta(1) function," *J Biol Chem*, vol. 276, no. 11, pp. 8436–44, 2001.

[171] G. Eden, M. Archinti, F. Furlan, R. Murphy, and B. Degryse, "The urokinase receptor interactome," *Current Pharmaceutical Design*, vol. 17, no. 19, pp. 1874–1889, 2011.

[172] R. A. Alexander, G. W. Prager, J. Mihaly-Bison, P. Uhrin, S. Sunzenauer, B. R. Binder, G. J. Schutz, M. Freissmuth, and J. M. Breuss, "Vegf-induced endothelial cell migration requires urokinase receptor (upar)-dependent integrin redistribution," *Cardiovasc Res*, vol. 94, no. 1, pp. 125–35, 2012.

[173] B. Geiger and K. M. Yamada, "Molecular architecture and function of matrix adhesions," *Cold Spring Harb Perspect Biol*, vol. 3, no. 5, 2011.

[174] N. G. Kan, M. P. Stemmler, D. Junghans, B. Kanzler, W. N. de Vries, M. Dominis, and R. Kemler, "Gene replacement reveals a specific role for e-cadherin in the formation of a functional trophectoderm," *Development*, vol. 134, no. 1, pp. 31–41, 2007.

[175] W. Engl, B. Arasi, L. L. Yap, J. P. Thiery, and V. Viasnoff, "Actin dynamics modulate mechanosensitive immobilization of e-cadherin at adherens junctions," *Nat Cell Biol*, vol. 16, no. 6, pp. 587–94, 2014.

[176] C. G. Galbraith, K. M. Yamada, and M. P. Sheetz, "The relationship between force and focal complex development," *J Cell Biol*, vol. 159, no. 4, pp. 695–705, 2002.

[177] Z. Liu, J. L. Tan, D. M. Cohen, M. T. Yang, N. J. Sniadecki, S. A. Ruiz, C. M. Nelson, and C. S. Chen, "Mechanical tugging force regulates the size of cell-cell junctions," *Proc Natl Acad Sci U S A*, vol. 107, no. 22, pp. 9944–9, 2010.

[178] Y. Kametani and M. Takeichi, "Basal-to-apical cadherin flow at cell junctions," *Nat Cell Biol*, vol. 9, no. 1, pp. 92–8, 2007.

[179] T. Lecuit and L. Le Goff, "Orchestrating size and shape during morphogenesis," *Nature*, vol. 450, no. 7167, pp. 189–92, 2007.

[180] T. Lecuit, P. F. Lenne, and E. Munro, "Force generation, transmission, and integration during cell and tissue morphogenesis," *Annu Rev Cell Dev Biol*, vol. 27, pp. 157–84, 2011.

[181] J. Kafer, T. Hayashi, A. F. Maree, R. W. Carthew, and F. Graner, "Cell adhesion and cortex contractility determine cell patterning in the drosophila retina," *Proc Natl Acad Sci U S A*, vol. 104, no. 47, pp. 18549–54, 2007.

[182] M. L. Manning, R. A. Foty, M. S. Steinberg, and E. M. Schoetz, "Coaction of intercellular adhesion and cortical tension specifies tissue surface tension," *Proc Natl Acad Sci U S A*, vol. 107, no. 28, pp. 12517–22, 2010.

[183] A. S. Yap, W. M. Brieher, and B. M. Gumbiner, "Molecular and functional analysis of cadherin-based adherens junctions," *Annu Rev Cell Dev Biol*, vol. 13, pp. 119–46, 1997.

[184] W. W. Franke, "Discovering the molecular components of intercellular junctions–a historical view," *Cold Spring Harb Perspect Biol*, vol. 1, no. 3, p. a003061, 2009.

[185] R. M. Mege, J. Gavard, and M. Lambert, "Regulation of cell-cell junctions by the cytoskeleton," *Curr Opin Cell Biol*, vol. 18, no. 5, pp. 541–8, 2006.

[186] B. Ladoux, W. J. Nelson, J. Yan, and R. M. Mege, "The mechanotransduction machinery at work at adherens junctions," *Integr Biol (Camb)*, vol. 7, no. 10, pp. 1109–19, 2015.

[187] D. Cai, S. C. Chen, M. Prasad, L. He, X. Wang, V. Choesmel-Cadamuro, J. K. Sawyer, G. Danuser, and D. J. Montell, "Mechanical feedback through e-cadherin promotes direction sensing during collective cell migration," *Cell*, vol. 157, no. 5, pp. 1146–59, 2014.

[188] N. Borghi, M. Sorokina, O. G. Shcherbakova, W. I. Weis, B. L. Pruitt, W. J. Nelson, and A. R. Dunn, "E-cadherin is under constitutive actomyosin-generated tension that is increased at cell-cell contacts upon externally applied stretch," *Proc Natl Acad Sci U S A*, vol. 109, no. 31, pp. 12568–73, 2012.

[189] D. E. Conway, M. T. Breckenridge, E. Hinde, E. Gratton, C. S. Chen, and M. A. Schwartz, "Fluid shear stress on endothelial cells modulates mechanical tension across ve-cadherin and pecam-1," *Curr Biol*, vol. 23, no. 11, pp. 1024–30, 2013.

[190] M. Yao, W. Qiu, R. Liu, A. K. Efremov, P. Cong, R. Seddiki, M. Payre, C. T. Lim, B. Ladoux, R. M. Mege, and J. Yan, "Force-dependent conformational switch of alpha-catenin controls vinculin binding," *Nat Commun*, vol. 5, p. 4525, 2014.

[191] C. D. Buckley, J. Tan, K. L. Anderson, D. Hanein, N. Volkmann, W. I. Weis, W. J. Nelson, and A. R. Dunn, "Cell adhesion. the minimal cadherin-catenin complex binds to actin filaments under force," *Science*, vol. 346, no. 6209, p. 1254211, 2014.

[192] Q. le Duc, Q. Shi, I. Blonk, A. Sonnenberg, N. Wang, D. Leckband, and J. de Rooij, "Vinculin potentiates e-cadherin mechanosensing and is recruited to actin-anchored sites within adherens junctions in a myosin ii-dependent manner," *J Cell Biol*, vol. 189, no. 7, pp. 1107–15, 2010.

[193] S. Yonemura, Y. Wada, T. Watanabe, A. Nagafuchi, and M. Shibata, "alpha-catenin as a tension transducer that induces adherens junction development," *Nat Cell Biol*, vol. 12, no. 6, pp. 533–42, 2010.

[194] K. Ludtke, R. Jordan, P. Hommes, O. Nuyken, and C. A. Naumann, "Lipopolymers from new 2-substituted-2-oxazolines for artificial cell membrane constructs," *Macromol Biosci*, vol. 5, no. 5, pp. 384–93, 2005.

[195] Y. Ge, A. P. Siegel, R. Jordan, and C. A. Naumann, "Ligand binding alters dimerization and sequestering of urokinase receptors in raft-mimicking lipid mixtures," *Biophysical journal*, vol. 107, no. 9, pp. 2101–2111, 2014.

[196] K. T. Applegate, S. Besson, A. Matov, M. H. Bagonis, K. Jaqaman, and G. Danuser, "plustiptracker: Quantitative image analysis software for the measurement of microtubule dynamics," *J Struct Biol*, vol. 176, no. 2, pp. 168–84, 2011.

[197] A. M. Seddon, P. Curnow, and P. J. Booth, "Membrane proteins, lipids and detergents: not just a soap opera," *Biochim Biophys Acta*, vol. 1666, no. 1-2, pp. 105–17, 2004.

[198] Q. Huai, A. Zhou, L. Lin, A. P. Mazar, G. C. Parry, J. Callahan, D. E. Shaw, B. Furie, B. C. Furie, and M. Huang, "Crystal structures of two human vitronectin, urokinase and urokinase receptor complexes," *Nat Struct Mol Biol*, vol. 15, no. 4, pp. 422–3, 2008.

[199] B. Zhao, S. Gandhi, C. Yuan, Z. Luo, R. Li, H. Gardsvoll, V. de Lorenzi, N. Sidenius, M. Huang, and M. Ploug, "Stabilizing a flexible interdomain hinge region harboring the smb binding site drives upar into its closed conformation," *J Mol Biol*, vol. 427, no. 6 Pt B, pp. 1389–403, 2015.

[200] J. Schlessinger, "Ligand-induced, receptor-mediated dimerization and activation of egf receptor," *Cell*, vol. 110, no. 6, pp. 669–672, 2002.

[201] P. Mellroth, J. Karlsson, J. Hakansson, N. Schultz, W. E. Goldman, and H. Steiner, "Ligand-induced dimerization of drosophila peptidoglycan recognition proteins in vitro," *Proc Natl Acad Sci U S A*, vol. 102, no. 18, pp. 6455–60, 2005.

[202] J. F. Arthur, Y. Shen, M. L. Kahn, M. C. Berndt, R. K. Andrews, and E. E. Gardiner, "Ligand binding rapidly induces disulfide-dependent dimerization of glycoprotein vi on the platelet plasma membrane," *J Biol Chem*, vol. 282, no. 42, pp. 30434–41, 2007.

[203] H. Gardsvoll, B. Jacobsen, M. C. Kriegbaum, N. Behrendt, L. Engelholm, S. Ostergaard, and M. Ploug, "Conformational regulation of urokinase receptor function: impact of receptor occupancy and epitope-mapped monoclonal antibodies on lamellipodia induction," *J Biol Chem*, vol. 286, no. 38, pp. 33544–56, 2011.

[204] N. Sidenius, C. F. M. Sier, and F. Blasi, "Shedding and cleavage of the urokinase receptor (upar): identification and characterisation of upar fragments in vitro and in vivo," *FEBS Letters*, vol. 475, no. 1, pp. 52–56, 2000.

[205] T. Plesner, N. Behrendt, and M. Ploug, "Structure, function and expression on blood and bone marrow cells of the urokinase-type plasminogen activator receptor, upar," *Stem Cells*, vol. 15, no. 6, pp. 398–408, 1997.

[206] J. H. Benting, A. G. Rietveld, and K. Simons, "N-glycans mediate the apical sorting of a gpi-anchored, raft-associated protein in madin-darby canine kidney cells," *J Cell Biol*, vol. 146, no. 2, pp. 313–20, 1999.

[207] T. Harder, P. Scheiffele, P. Verkade, and K. Simons, "Lipid domain structure of the plasma membrane revealed by patching of membrane components," *The Journal of Cell Biology*, vol. 141, no. 4, pp. 929–942, 1998.

[208] M. Gandhavadi, D. Allende, A. Vidal, S. A. Simon, and T. J. McIntosh, "Structure, composition, and peptide binding properties of detergent soluble bilayers and detergent resistant rafts," *Biophysical Journal*, vol. 82, no. 3, pp. 1469–1482, 2002.

[209] I. D. Campbell and M. J. Humphries, "Integrin structure, activation, and interactions," *Cold Spring Harb Perspect Biol*, vol. 3, no. 3, 2011.

[210] D. S. Harburger and D. A. Calderwood, "Integrin signalling at a glance," *J Cell Sci*, vol. 122, no. Pt 2, pp. 159–63, 2009.

[211] R. O. Hynes, "Integrins," *Cell*, vol. 110, no. 6, pp. 673–687, 2002.

[212] L. Seguin, J. S. Desgrosellier, S. M. Weis, and D. A. Cheresh, "Integrins and cancer: regulators of cancer stemness, metastasis, and drug resistance," *Trends Cell Biol*, vol. 25, no. 4, pp. 234–40, 2015.

[213] B. H. Luo, C. V. Carman, and T. A. Springer, "Structural basis of integrin regulation and signaling," *Annu Rev Immunol*, vol. 25, pp. 619–47, 2007.

[214] J. A. Lundbk, O. S. Andersen, T. Werge, and C. Nielsen, "Cholesterol-induced protein sorting: An analysis of energetic feasibility," *Biophysical Journal*, vol. 84, no. 3, pp. 2080–2089, 2003.

[215] R. Wang, J. Bi, K. K. Ampah, C. Zhang, Z. Li, Y. Jiao, X. Wang, X. Ba, and X. Zeng, "Lipid raft regulates the initial spreading of melanoma a375 cells by modulating beta1 integrin clustering," *Int J Biochem Cell Biol*, vol. 45, no. 8, pp. 1679–89, 2013.

[216] K.-E. Gottschalk and H. Kessler, "The structures of integrins and integrin–ligand complexes: Implications for drug design and signal transduction," *Angewandte Chemie International Edition*, vol. 41, no. 20, pp. 3767–3774, 2002.

[217] K. E. Gottschalk, P. D. Adams, A. T. Brunger, and H. Kessler, "Transmembrane signal transduction of the alpha(iib)beta(3) integrin," *Protein Sci*, vol. 11, no. 7, pp. 1800–12, 2002.

[218] S. L. Veatch, O. Soubias, S. L. Keller, and K. Gawrisch, "Critical fluctuations in domain-forming lipid mixtures," *Proc Natl Acad Sci U S A*, vol. 104, no. 45, pp. 17650–5, 2007.

[219] T. Idema, J. M. van Leeuwen, and C. Storm, "Phase coexistence and line tension in ternary lipid systems," *Phys Rev E Stat Nonlin Soft Matter Phys*, vol. 80, no. 4 Pt 1, p. 041924, 2009.

[220] U. Coskun, M. Grzybek, D. Drechsel, and K. Simons, "Regulation of human egf receptor by lipids," *Proc Natl Acad Sci U S A*, vol. 108, no. 22, pp. 9044–8, 2011.

[221] E. G. Lundius, V. Vukojevic, E. Hertz, N. Stroth, A. Cederlund, M. Hiraiwa, L. Terenius, and P. Svenningsson, "Gpr37 protein trafficking to the plasma membrane regulated by prosaposin and gm1 gangliosides promotes cell viability," *J Biol Chem*, vol. 289, no. 8, pp. 4660–73, 2014.

[222] L. Botto, D. Cunati, S. Coco, S. Sesana, A. Bulbarelli, E. Biasini, L. Colombo, A. Negro, R. Chiesa, M. Masserini, and P. Palestini, "Role of lipid rafts and gm1 in the segregation and processing of prion protein," *PLoS One*, vol. 9, no. 5, p. e98344, 2014.

[223] S. Hakomori, "Organization and function of glycosphingolipids in membrane," *Proceedings of the Japan Academy, Series B*, vol. 81, no. 6, pp. 189–203, 2005.

[224] D. K. Sharma, J. C. Brown, Z. Cheng, E. L. Holicky, D. L. Marks, and R. E. Pagano, "The glycosphingolipid, lactosylceramide, regulates beta1-integrin clustering and endocytosis," *Cancer Res*, vol. 65, no. 18, pp. 8233–41, 2005.

[225] C. Eich, C. Manzo, S. de Keijzer, G. J. Bakker, I. Reinieren-Beeren, M. F. Garcia-Parajo, and A. Cambi, "Changes in membrane sphingolipid composition modulate dynamics and adhesion of integrin nanoclusters," *Sci Rep*, vol. 6, p. 20693, 2016.

[226] X. Wang, P. Sun, A. Al-Qamari, T. Tai, I. Kawashima, and A. S. Paller, "Carbohydrate-carbohydrate binding of ganglioside to integrin α5 modulates α5β1function," *Journal of Biological Chemistry*, vol. 276, no. 11, pp. 8436–8444, 2001.

[227] D. Lingwood, B. Binnington, T. Rog, I. Vattulainen, M. Grzybek, U. Coskun, C. A. Lingwood, and K. Simons, "Cholesterol modulates glycolipid conformation and receptor activity," *Nat Chem Biol*, vol. 7, no. 5, pp. 260–2, 2011.

[228] Y. Itokazu, R. E. Pagano, A. S. Schroeder, S. M. O'Grady, A. H. Limper, and D. L. Marks, "Reduced gm1 ganglioside in cftr-deficient human airway cells results in decreased beta1-integrin signaling and delayed wound repair," *Am J Physiol Cell Physiol*, vol. 306, no. 9, pp. C819–30, 2014.

[229] P. Hadaczek, G. Wu, N. Sharma, A. Ciesielska, K. Bankiewicz, A. L. Davidow, Z. H. Lu, J. Forsayeth, and R. W. Ledeen, "Gdnf signaling implemented by gm1 ganglioside; failure in parkinson's disease and gm1-deficient murine model," *Exp Neurol*, vol. 263, pp. 177–89, 2015.

[230] M. Takahashi, Y. Kizuka, K. Ohtsubo, J. Gu, and N. Taniguchi, "Disease-associated glycans on cell surface proteins," *Mol Aspects Med*, vol. 51, pp. 56–70, 2016.

[231] G. Wu, Z. H. Lu, N. Kulkarni, and R. W. Ledeen, "Deficiency of ganglioside gm1 correlates with parkinson's disease in mice and humans," *J Neurosci Res*, vol. 90, no. 10, pp. 1997–2008, 2012.

[232] H. Noh, S. Hong, and S. Huang, "Role of urokinase receptor in tumor progression and development," *Theranostics*, vol. 3, no. 7, pp. 487–95, 2013.

[233] P. Chaurasia, J. A. Aguirre-Ghiso, O. D. Liang, H. Gardsvoll, M. Ploug, and L. Ossowski, "A region in urokinase plasminogen receptor domain iii controlling a functional association with alpha5beta1 integrin and tumor growth," *J Biol Chem*, vol. 281, no. 21, pp. 14852–63, 2006.

[234] H. W. Smith, P. Marra, and C. J. Marshall, "upar promotes formation of the p130cas-crk complex to activate rac through dock180," *J Cell Biol*, vol. 182, no. 4, pp. 777–90, 2008.

[235] V. P. Hytonen and B. Wehrle-Haller, "Protein conformation as a regulator of cell-matrix adhesion," *Phys Chem Chem Phys*, vol. 16, no. 14, pp. 6342–57, 2014.

[236] M. L. Tang, A. Vararattanavech, and S. M. Tan, "Urokinase-type plasminogen activator receptor induces conformational changes in the integrin alphambeta2 headpiece and reorientation of its transmembrane domains," *J Biol Chem*, vol. 283, no. 37, pp. 25392–403, 2008.

[237] S. B. Ahn, A. Mohamedali, S. Anand, H. R. Cheruku, D. Birch, G. Sowmya, D. Cantor, S. Ranganathan, D. W. Inglis, R. Frank, M. Agrez, E. C. Nice, and M. S. Baker, "Characterization of the interaction between heterodimeric alphavbeta6 integrin and urokinase plasminogen activator receptor (upar) using functional proteomics," *J Proteome Res*, vol. 13, no. 12, pp. 5956–64, 2014.

[238] W. Xue, I. Mizukami, r. Todd, R. F., and H. R. Petty, "Urokinase-type plasminogen activator receptors associate with 1 and 3 integrins of fibrosarcoma cells: Dependence on extracellular matrix components," *Cancer Res*, vol. 57, no. 9, pp. 1682–9, 1997.

[239] Y. Wei, J. A. Eble, Z. Wang, J. A. Kreidberg, and H. A. Chapman, "Urokinase receptors promote beta 1 integrin function through interactions with integrin alpha 3beta 1," *Molecular Biology of the Cell*, vol. 12, no. 10, pp. 2975–2986, 2001.

[240] G. M. Ferraris, C. Schulte, V. Buttiglione, V. De Lorenzi, A. Piontini, M. Galluzzi, A. Podesta, C. D. Madsen, and N. Sidenius, "The interaction between upar and vitronectin triggers ligand-independent adhesion signalling by integrins," *EMBO J*, vol. 33, no. 21, pp. 2458–72, 2014.

[241] M. J. Elices, L. Osborn, Y. Takada, C. Crouse, S. Luhowskyj, M. E. Hemler, and R. R. Lobb, "Vcam-1 on activated endothelium interacts with the leukocyte integrin vla-4 at a site distinct from the vla-4/fibronectin binding site," *Cell*, vol. 60, no. 4, pp. 577–584, 1990.

[242] A. Merk, A. Bartesaghi, S. Banerjee, V. Falconieri, P. Rao, M. I. Davis, R. Pragani, M. B. Boxer, L. A. Earl, J. L. Milne, and S. Subramaniam, "Breaking cryo-em resolution barriers to facilitate drug discovery," *Cell*, vol. 165, no. 7, pp. 1698–707, 2016.

[243] Y. Chen, M. Tekmen, L. Hillesheim, J. Skinner, B. Wu, and J. D. Muller, "Dual-color photon-counting histogram," *Biophys J*, vol. 88, no. 3, pp. 2177–92, 2005.

[244] Y. Ge, Y. H. Lin, L. A. Lautscham, W. H. Goldmann, B. Fabry, and C. A. Naumann, "N-cadherin-functionalized polymer-tethered multi-bilayer: a cell surface-mimicking substrate to probe cellular mechanosensitivity," *Soft Matter*, 2016.

[245] S. F. Fenz, R. Merkel, and K. Sengupta, "Diffusion and intermembrane distance: case study of avidin and e-cadherin mediated adhesion," *Langmuir*, vol. 25, no. 2, pp. 1074–85, 2009.

[246] M. Causeret, N. Taulet, F. Comunale, C. Favard, and C. Gauthier-Rouviere, "N-cadherin association with lipid rafts regulates its dynamic assembly at cell-cell junctions in c2c12 myoblasts," *Mol Biol Cell*, vol. 16, no. 5, pp. 2168–80, 2005.

[247] M. Arnold, E. A. Cavalcanti-Adam, R. Glass, J. Blummel, W. Eck, M. Kantlehner, H. Kessler, and J. P. Spatz, "Activation of integrin function by nanopatterned adhesive interfaces," *Chemphyschem*, vol. 5, no. 3, pp. 383–8, 2004.

[248] I. Bravata, M. Allocca, G. Fiorino, and S. Danese, "Integrins and adhesion molecules as targets to treat inflammatory bowel disease," *Curr Opin Pharmacol*, vol. 25, pp. 67–71, 2015.

[249] P. V. Escriba, X. Busquets, J. Inokuchi, G. Balogh, Z. Torok, I. Horvath, J. L. Harwood, and L. Vigh, "Membrane lipid therapy: Modulation of the cell membrane composition and structure as a molecular base for drug discovery and new disease treatment," *Prog Lipid Res*, vol. 59, pp. 38–53, 2015.

[250] A. P. Mazar, "Urokinase plasminogen activator receptor choreographs multiple ligand interactions: implications for tumor progression and therapy," *Clin Cancer Res*, vol. 14, no. 18, pp. 5649–55, 2008.

[251] P. Heftberger, B. Kollmitzer, A. A. Rieder, H. Amenitsch, and G. Pabst, "In situ determination of structure and fluctuations of coexisting fluid membrane domains," *Biophys J*, vol. 108, no. 4, pp. 854–62, 2015.

VITA

VITA

Yifan Ge was born in Zhenjiang, Jiangsu, China. In 2010, Yifan received her B.S. in Pharmacy from Nanjing Medical University with honor. Then she became a research assistant in Nanjing University under the supervision of Dr.Yu Qin. In Aug. 2011, she pursued her graduate study as a PhD candidate in the Department of Chemistry and Chemical Biology at Indiana University-Purdue University Indianapolis under the direction of Professor Christoph Naumann. In 2014, Yifan enrolled in a graduate associate program in Kelley School of Business at Indiana University and obtained her graduate associate certificate in Business of Life Science.

As of December 2016, Yifan has published six peer-reviewed Journal papers, two of them are related to this Thesis work. Her work has also been reported in several international meetings.

This is Yifan's first and last dissertation.